



THE UNIVERSITY OF QUEENSLAND
A U S T R A L I A

**Trajectory Optimisation of a Partially-Reusable
Rocket-Scramjet-Rocket Small Satellite Launch System**

Sholto O. Forbes-Spyratos

B.Eng. (Mechanical and Aerospace) (Hons. I) & B.Sc. (Physics) UQ

A thesis submitted for the degree of Doctor of Philosophy at
The University of Queensland in 2018

School of Mechanical Engineering

Abstract

Declaration by author

This thesis is composed of my original work, and contains no material previously published or written by another person except where due reference has been made in the text. I have clearly stated the contribution by others to jointly-authored works that I have included in my thesis.

I have clearly stated the contribution of others to my thesis as a whole, including statistical assistance, survey design, data analysis, significant technical procedures, professional editorial advice, and any other original research work used or reported in my thesis. The content of my thesis is the result of work I have carried out since the commencement of my research higher degree candidature and does not include a substantial part of work that has been submitted to qualify for the award of any other degree or diploma in any university or other tertiary institution. I have clearly stated which parts of my thesis, if any, have been submitted to qualify for another award.

I acknowledge that an electronic copy of my thesis must be lodged with the University Library and, subject to the policy and procedures of The University of Queensland, the thesis be made available for research and study in accordance with the Copyright Act 1968 unless a period of embargo has been approved by the Dean of the Graduate School.

I acknowledge that copyright of all material contained in my thesis resides with the copyright holder(s) of that material. Where appropriate I have obtained copyright permission from the copyright holder to reproduce material in this thesis.

Publications during candidature

Journal papers

Sholto O. Forbes-Spyratos, Michael P. Kearney, Michael K. Smart, and Ingo H. Jahn. “Trajectory Design of a Rocket-Scramjet-Rocket Multi-Stage Launch System”. In: *Journal of Spacecraft and Rockets - Under Consideration* TBD (2018)

Conference papers

S.O. Forbes-Spyratos, M.P. Kearney, M.K. Smart, and I.H. Jahn. “Trajectory design of a rocket-scramjet-rocket multi-stage launch system”. In: *21st AIAA International Space Planes and Hypersonics Technologies Conference, Hypersonics 2017*. Xiamen, China, 2017. ISBN: 9781624104633

Publications included in this thesis

This thesis comprises partly of publications, as allowed by University of Queensland Policy PPL 4.60.07. The papers that have been included have all been published in peer reviewed journals at the time of submission.

Sholto O. Forbes-Spyratos, Michael P. Kearney, Michael K. Smart, and Ingo H. Jahn. “Trajectory Design of a Rocket-Scramjet-Rocket Multi-Stage Launch System”. In: *Journal of Spacecraft and Rockets - Under Consideration* TBD (2018)

Contributor	Contribution
Sholto O. Forbes-Spyratos	Performed simulations (%)
	Analysis of results (%)
	Wrote and edited paper (%)
Ingo H. Jahn	Analysis of results (%)
Michael P. Kearney	Analysis of results (%)
Michael K. Smart	Analysis of results (%)
	Wrote and edited paper (%)

Contributions by Others to the Thesis

Except for the contributions by others to publications above, there are no contributions by others to this thesis.

Statement of Parts of the Thesis Submitted to Qualify for the Award of Another Degree

None.

Acknowledgements

Keywords

keyword, keyword, keyword, keyword, keyword

Australian and New Zealand Standard Research Classification (ANZSRC)

ANZSRC code: 090107 Hypersonic Propulsion and Hypersonic Aerodynamics, 20%

ANZSRC code: 090106 Flight Dynamics, 20%

ANZSRC code: 090108, Satellite, Space Vehicle and Missile Design and Testing, 20%

ANZSRC code: 090104 Aircraft Performance and Flight Control Systems , 20%

ANZSRC code: 010303 Optimisation , 20%

Fields of Research (FoR) Classification

FoR code: 0901, Aerospace Engineering, 100%

CONTENTS

List of figures	xv
List of tables	xvii
1 Introduction	1
1.1 Research aims	2
1.2 Thesis outline	3
2 Literature review	5
2.1 Small Satellite Launchers	5
2.2 Airbreathing Access to Space Systems	8
2.3 Scramjets	9
2.4 The SPARTAN	10
2.4.1 Scramjet Engine Model	11
2.5 First Stage Rocket Booster	11
2.6 Exoatmospheric Rocket Engines	12
2.7 Partially-Airbreathing Launch Vehicle Ascent Trajectories	14
2.7.1 Single-Stage Vehicles	15
2.7.2 Multi-Stage Vehicles	16
2.8 Hypersonic Vehicle Flyback Trajectories	18
2.8.1 Examples of Optimised Fly-Back Trajectories	19
2.9 Optimal Control	22
2.9.1 The Single Shooting Method	24
2.9.2 The Multiple Shooting Method	24
2.9.3 The Pseudospectral Method	26

CONTENTS

2.9.4	Pseudospectral Examples	29
2.9.5	Available Solvers	30
2.10	Aerodynamic Analysis	31
2.10.1	HYPAERO	32
2.10.2	CART3D	32
2.10.3	Missile DATCOM	33
2.11	Summary	33
3	Launch Vehicle Baseline Design	35
3.1	First Stage Rocket	35
3.2	Second Stage Scramjet	36
3.2.1	Baseline Vehicle	36
3.2.2	Aerodynamics	36
3.2.3	Propulsion Modelling	37
3.3	Third Stage Rocket - Baseline	43
3.3.1	Heat Shield Sizing	43
3.3.2	Fuel Tank Sizing	44
3.3.3	Aerodynamics	45
3.3.4	Thrust Vectoring	45
4	LODESTAR	47
4.1	Optimal Control	48
4.1.1	GPOPS-2 Example - Brachistochrone Problem	49
4.2	The Trajectory Optimal Control Problems	50
4.2.1	Dynamic Model	50
4.2.2	Trajectory Connection Points	51
4.2.3	First Stage Trajectory	52
4.2.4	Second Stage Trajectory	53
4.2.5	Second Stage Return Trajectory	56
4.2.6	Third Stage Trajectory	57
4.2.7	Combined Second Stage Ascent & Return Trajectory	57
4.2.8	Validation	57
5	Ascent Trajectory	59
5.1	Third Stage trajectory	60
5.1.1	Third Stage Optimisation Methodology	60
5.1.2	Third Stage Optimisation Results	61
5.2	SPARTAN trajectory	62

5.2.1	Constant Dynamic Pressure - Minimum Pull-up	64
5.2.2	Optimal Payload	64
5.2.3	Maximum Dynamic Pressure Variation	66
5.2.4	Drag Sensitivity Study	68
5.3	First Stage Trajectory	68
5.3.1	First Stage Optimised Trajectory Result	70
6	Trajectories Involving Flyback	75
6.1	Flyback trajectories	75
6.2	Sensitivity Analysis	75
7	Full Trajectory Optimisation	77
8	Third Stage Sizing Study	79
9	Conclusions	81
9.1	Recommendations for future work	81
References		83
A	CART3D Results	91
A.1	Engine-On Plume Check	91
A.2	CART3D Results	91

LIST OF FIGURES

2.1	The SKYLON spaceplane [70].	8
2.2	The airbreathing vehicle flight corridor [57].	9
2.3	An early design of the socket-scramjet-rocket launch system incorporating the SPARTAN [26].	10
2.4	The C-RESTM10 propulsion database, specific impulse.	12
2.5	An example of a constant gain PID controller, controlling the SPARTAN trajectory around a 50kPa dynamic pressure design point [46].	14
2.6	15
2.7	Powell	15
2.8	16
2.9	Wilhite	16
2.10	a) Airbreathing b) Airbreathing/Rocket	17
2.11	The trajectory of the launch system developed by Tsuchiya and Mori [68]	17
2.12	17
2.13	The trajectory of the launch system developed by Mehta and Bowles [37].	17
2.14	The flight path of a glide-back booster, developed by Tetlow et al. CITEXX.	20
2.15	The flight path of a powered fly-back booster, developed by Tetlow et al. CITEXX. .	20
2.16	22
2.17	An illustration of the subdivision associated with multiple shooting [38]. Dashed lines illustrate the initial trajectory guess and the solid line indicates the final trajectory once the joining conditions are met.	25
2.18	30
2.19	HYPERO analysis surface grid [26].	32
2.20	SPARTAN aerodynamics, developed using HYPERO [48].	33

LIST OF FIGURES

2.21 The Skylon spaceplane, simulated using CART3D at Mach 12.189, $\alpha = 7.512^\circ$ [36]. Cell distribution produced by mesh adaption is shown.	34
3.1 The rocket-scramjet-rocket launch system, top view, showing the SPARTAN and first stage.	35
3.2 The rocket-scramjet-rocket launch system, side view, showing the SPARTAN and fuel tanks, along with the third and first stages.	36
3.3 CART3D result for the SPARTAN and first stage vehicles at Mach 2, -1° angle of attack.	37
3.4 CART3D flow result for the SPARTAN, at Mach 1.1, 6° angle of attack.	38
3.5 CART3D flow result for the SPARTAN, at Mach 3, 6° angle of attack.	38
3.6 CART3D flow result for the SPARTAN, at Mach 7, 6° angle of attack.	38
3.7 Coefficients of lift of the SPARTAN, calculated using CART3D.	39
3.8 Coefficients of drag of the SPARTAN, calculated using CART3D.	39
3.9 L/D of the SPARTAN.	40
3.10 Coefficient of lift of the SPARTAN with the C-REST engines powered-on. This is obtained by removing the engines and boat-tail from the CART3D simulation results.	40
3.11 Coefficient of drag of the SPARTAN with the C-REST engines powered-on. This is obtained by removing the engines and boat-tail from the CART3D simulation results.	41
3.12 L/D of the SPARTAN with the C-REST engines powered on.	41
3.13	42
3.14	43
3.15 [64]	44
4.1	50
4.2	51
4.3	53
4.4	54
4.5	55
5.1	61
5.2	62
5.3	63
5.4	65
5.5	66
5.6	67
5.7	68
5.8	69
5.9	70

LIST OF FIGURES

5.10	71
5.11	71
5.12	72
5.13	72
5.14	73
5.15	73
A.1	92
A.2	Mesh generated by CART3D around the SPARTAN and first stage vehicles.	92

LIST OF TABLES

2.1	Comparison of upper stage rocket engines.	13
2.2	Summary of programs capable of pseudospectral optimisation.	31
4.1	52
5.1	Summary of Simulation Results	60

CHAPTER 1

INTRODUCTION

The market for small satellites is increasing rapidly, driven primarily by the rapidly decreasing size of electronic components. Many of these small satellites are currently launched with multiple small satellites piggybacking onto the launch of larger satellites, comanifesting on a single launch to share costs. This has the result of smaller payloads being subject to the schedule of the other parties involved, and being delivered into an orbit determined by the requirements of the main payload. This dependence on a predetermined mission plan often has detrimental effects on the small satellite mission. Small satellites are often used in missions which require specific orbital and scheduling needs. Satellites to be used as part of constellations are especially sensitive to the orbit in which they are placed. Small satellites may be able to change orbits slightly, however larger changes mean additional fuel mass and potentially additional system mass if a larger drive is necessary. The production of a cheap and flexible small satellite delivery system would enable more small satellites to be delivered into customised orbits within relatively short time periods.

Airbreathing engines are an ideal candidate for producing the next generation of space access systems, producing higher specific impulse than rockets and requiring much less fuel to be carried enabling the design of a reusable second stage vehicle. A three stage design utilising a scramjet second stage with rocket powered first and third stages is being developed by The University of Queensland. In previous studies it has been assumed that the optimal trajectory for a scramjet powered vehicle is at its maximum dynamic pressure and all other trajectory stages have conformed to this assumption. This study will aim to produce an optimal trajectory plan which may be applied to any rocket-airbreathing-rocket system for delivering small satellites to Earth orbit. The SPARTAN vehicle being developed by the university of Queensland will be used as a model for simulations.

1.1 Research aims

The overall aim of this thesis is to apply state of the art numerical optimisation techniques to the trajectory of a rocket-scramjet-rocket small satellite launch system. The purpose of this optimised trajectory is to maximise the payload-to-orbit capabilities of the launch system, thereby also maximising the cost efficiency of the system.

This will be achieved through the following objectives:

1. *Third stage redesign.*

To ensure that the simulated system is representative of an up-to-date, relevant design, the third stage of the rocket-scramjet-rocket launch system is to be redesigned to use the Kestrel pressure-fed engine. This redesign requires the third stage shape and internal layout to be changed considerably, as well as the second stage internal layout to be reconfigured.

2. *First stage design.*

The first stage has not yet been studied previously, and as such a representative design of a first stage rocket is created.

3. *Launch system simulation.*

A thorough numerical simulation of the launch system is created, which fits into the format required by the optimisation algorithm.

4. *Optimisation integration*

1.2 Thesis outline

Edit this as required. This thesis is organised in eight chapters which are outlined below. The appendices included at the end of this document contain further technical information and supplementary experimental details. **If you want to add colours to the text for some reason (supervisor reviewing etc.), use the `textcolor` command. Check the code here to see how.**

Chapter 2 - Literature review

This chapter presents a review of literature related to the different aspects of this thesis.

Chapter 3 - Methodology

This chapter provides details of the experimental facility, experimental model, and test conditions used in the completion of the experiments that form the majority of this thesis.

Conclusions

The body of this thesis concludes by summarising the most significant findings from Chapters ?? through 7. Recommendations for future studies on cavity flameholders in three-dimensional, hydrocarbon-fuelled scramjet engines, such as the REST engine, are provided.

CHAPTER 2

LITERATURE REVIEW

This chapter examines the relevant literature associated with the different aspects of the work conducted as part of this thesis.

Explain order of literature and what was examined.

2.1 Small Satellite Launchers

What point do I want to make in this section?

The rocket-scramjet rocket launch system under development at The University of Queensland will face competition from a number of private and public organisations. These organisations are currently developing small satellite launchers to offer bespoke launches with low costs and relatively rapid turn around times. A summary of the small satellite launchers currently in active development is shown in Table ?? . Many of these launchers are projected to be available within the next few years, and will offer cost-per-kg comparable to piggybacking on larger launches.

Much of the market niche fulfilled by each launch system is determined by the payload to orbit capabilities of the vehicle. Although the launchers shown are all classed as 'small satellite launchers', organisations seeking a launch service will choose a launcher which is designed to launch payloads of comparable size to their desired payload, for maximum cost efficiency. There is a large variation in the payload-to-orbit capabilities of the small satellite launchers in development, ranging between 50kg to 500kg. The rocket-scramjet-rocket system studied in this thesis will target approximately 150kg of payload to orbit, most similar to the Vector-H[71], Haas2CA[3], Bloostar[74] and Electron[51].

There are two distinct design method currently employed by small satellite launcher developers; cost efficiency through simplicity, and cost efficiency through reusability. The majority of the small satellite launchers in development are non-reusable. The non-reusable small satellite launch systems

CHAPTER 2. LITERATURE REVIEW

aim to reduce costs by creating a launch system which is as cost-efficient as possible to produce and launch. This generally entails making use of conventional, well-tested designs, combined with state of the art manufacturing techniques, such as 3-D printing. This method allows for rapid development, although it has an intrinsic cost limit due to the requirement of manufacturing a new launch system for each launch. The reusable small satellite launchers aim to reduce costs by virtue of much, or all, of the launch system being able to be used for multiple launches. This method of cost reduction has far higher initial development costs, but has the potential for greater cost savings in the long term. It is notable that the launchers with re-use capabilities are entirely within the early stages of development, with no currently projected completion dates.

The majority of the small satellite launch systems have projected launch costs between \$20000-\$40000USD/kg. The outlier is the Haas2CA[3], developed by ARCA, which has the ambitious target of \$10000USD/kg. The Haas2CA is a single stage to orbit launcher, powered by a hydrogen peroxide/kerosene aerospike engine.

Launcher	Company	Country	Payload Capacity	Cost/Kg (USD)	Availability	Stages & Propulsion	Reusability
Electron [51]	RocketLab	NZ/USA	150Kg to SSO	\$32,600	Available	Rocket-rocket	No
Lynx [1]	XCOR	USA	-	-	-	rocket-rocket	First stage
LauncherOne [72]	Virgin Orbit	UK	300kg to SSO	\$33,000	-	Aircraft-rocket-rocket	Aircraft
Bloostar [74]	Zero2Infinity	Spain	100kg to SSO	\$40,000	-	Balloon-rocket-rocket-rocket	No
XS-1 [42]	Boeing	USA	-	-	-	-	First Stage
Eris [21]	Gilmour Space Technologies	Aus/SG	380kg to LEO	\$23,000-38,000	Q4 2020		No
Black Arrow 2 [25]	Horizon	UK	350kg to SSO	-	2019	Rocket-rocket	No
Haas 2CA [3]	ARCA	USA	100Kg to LEO	\$10,000	2018	Rocket	No
Intrepid-1 [52]	Rocket Crafters	USA	376kg to SSO	\$23,936	Q1 2019	Rocket-rocket	No
KZ-1A [31]	CASIC	China	250kg to SSO	-	-	Rocket-rocket	No
500R [41]	Orbital Access	UK	500kg to SSO	-	-	Aircraft-Rocket	Fully Reusable
Vector-H [71]	Vector Space Systems	USA	160kg to LEO	\$21,875	2018	rocket-rocket-(third rocket optional)	No
SMILE [32]	NLR	EU	50kg	<\$50,000	-	-	-

2.2 Airbreathing Access to Space Systems

The possibility of using airbreathing stages in access to space systems has been studied in some detail. These systems have been investigated in various forms including; single stage[45, 73, 70], dual stage [68][37] and tri stage [48] designs. The most prominent of the airbreathing access to space systems currently in development is the SKYLON Spaceplane being developed by Reaction Engines Limited [69]. The SKYLON is a spaceplane which utilises SABRE, a combined cycle airbreathing rocket propulsion system potentially reusable for 200 flights, and is being developed to deliver payloads on the order of 2800kg to heliosynchronous orbit [24].



Figure 2.1: The SKYLON spaceplane [70].

A single stage design has the advantage of being fully contained within one vehicle, which is convenient for reusability and return trajectories however it has been suggested by Smart & Tetlow [59] that these designs suffer from severe limitations as they must contain multiple engines which add mass at later stages of the trajectory and decrease the efficiency of the vehicle. Smart & Tetlow suggest that multistage systems offer significant improvements in payload mass fractions, and have the advantage of using airbreathing stages only within their operable range. Dual stage designs have been investigated in some detail using the 'spaceplane' concept by Mehta & Bowles [37] using life cycle cost analysis in order to take flexibility and reusability into account. Mehta & Bowles conclude that a two stage design is the optimal configuration for reusable hypersonic space access systems, however this study is only based on comparison with single stage to orbit systems, and it is more useful to consider their conclusions as an endorsement of multi stage airbreathing designs in general. They find that multi stage vehicles have higher potential for payload than single stage to orbit (SSTO) systems and have less propellant requirements, partly due to a greater atmospheric cruise capability.

2.3 Scramjets

A Scramjet, or supersonic combustion ramjet, is an airbreathing engine design which combusts air at supersonic speeds and is capable of high Mach number operation. Scramjets were proposed in the 1940's [11] and found to be capable of positive net thrust in 1993 [43] but have yet to be developed to a level which would allow for commercial application. Scramjet powered vehicles are a potential candidate for small payload delivery systems, offering much higher specific impulse than rockets over their operating range [6] [10]. Scramjet engines exhibit this advantage within their operating range due to using atmospheric oxygen for reaction and only carrying fuel, increasing the payload mass that the scramjet vehicle is able to carry. Figure 2.2 shows the operating corridor for scramjet engines, indicating the point at which transition to rocket stage would occur, the lower dynamic pressure limit on engine operation and the upper dynamic pressure limit on the aircraft structure.

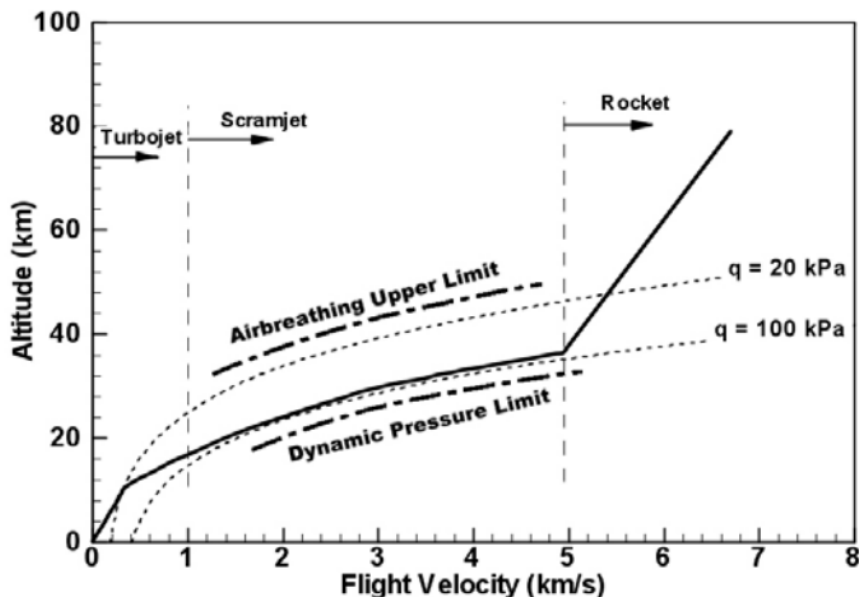


Figure 2.2: The airbreathing vehicle flight corridor [57].

Smart & Tetlow [59] have found that the fuel savings achieved by using a scramjet engine within these limits, coupled with small necessary payload mass, may enable the development of a partially or fully reusable space access system utilising a scramjet powered stage in the near future. Simulations carried out for three stage systems utilising scramjet and rocket engines for small payload delivery show favourable payload mass fractions with a reusable scramjet stage [59]. Scramjet powered vehicles may also offer the ability to put small payloads into orbit with greatly increased flexibility and launch window when compared to similarly sized rocket systems. This has been assessed in a study by Flaherty [18] comparing the United States Air Force's Reusable Military Launch System all-rocket launch vehicle RMLS102 against the Alliant Techsystems rocket/scramjet launch system ATK-RBCC. These vehicles are similarly sized and comparisons were made for payloads launched

to rendezvous with satellites in randomly generated orbits. These vehicles were compared using the range of orbital trajectories that each vehicle was able to rendezvous with within one day, determined by launch vehicle range. The rocket/scramjet ATK-RBCC was found to have a large advantage in trajectory flexibility over the rocket only vehicle, in a large part due to the scramjets ability to fly fuel efficiently over long distances. This means in general that a partially scramjet powered accelerator is able to fulfil the specific delivery needs of small payloads over a wider range of orbits within smaller time periods when compared to a fully rocket powered accelerator. This can be advantageous for time critical and orbit dependant payloads which have specific mission requirements to be met.

2.4 The SPARTAN

The three stage, partially reusable, access to space system under development at The University of Queensland utilises the SPARTAN[26] scramjet powered vehicle as the reusable second stage, shown in Figure 2.3. This system is considered in this study as a representative model for three stage, air-breathing access to space system designs. This launch system is designed for small payload deliveries to orbit and will in the future utilise a fly-back rocket booster to accelerate the SPARTAN stage to minimum Mach number required for stable burn, at which point separation occurs and the second stage uses a scramjet engine to accelerate to between approximately Mach 5-9. The first and second stages are to be reusable, the first stage via conversion into a propeller powered drone, and the second stage through either a glide or extra scramjet powered flight to a suitable landing site. However, the first stage booster considered in this study is a simple disposable design. The ascent profile is of interest to this study, however development of the fly-back trajectory profile requires detailed first stage vehicle design which is outside of the scope of this study.

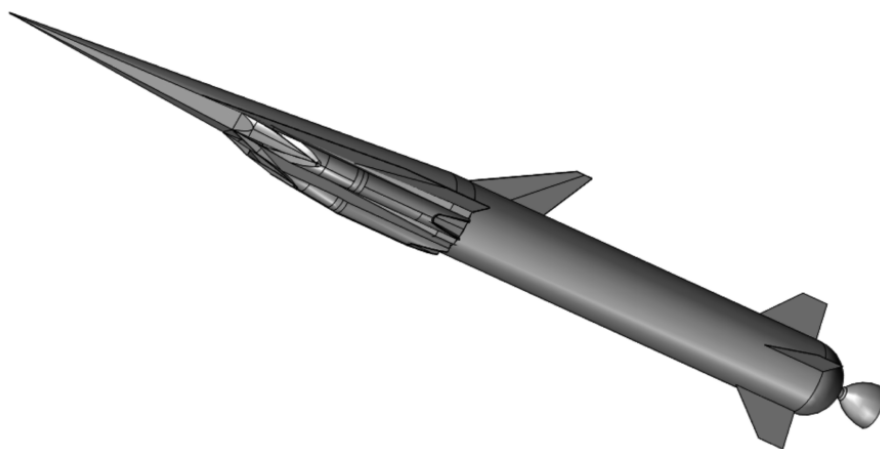


Figure 2.3: An early design of the socket-scramjet-rocket launch system incorporating the SPARTAN [26].

The third stage will be a disposable rocket stage, which will then deliver the payload to orbit,

exiting the atmosphere and performing a Hohmann transfer.

This system is in the preliminary design stage, with estimates of payload mass fraction indicating that 1.26% PMF is possible when delivering a 257.4kg payload to low earth orbit [47]. This compares well with existing space systems of similar size, with the advantage of being designed for reusability. The second stage vehicle has been designed to a detailed level, and optimised for payload delivery to heliosynchronous orbit.

The SPARTAN has been studied in some detail, simulated over a constant dynamic pressure trajectory with variation in the aerodynamic surface properties of the vehicle.

2.4.1 Scramjet Engine Model

To deliver a payload to orbit, the SPARTAN uses four Rectangular-to-Elliptical Shape Transition (REST) scramjet engines, with inlets configured to allow installation on a conical forebody. This study uses engines configured to fly between Mach 5 and 10, this type of engine is known as a C-RESTM10 engine[48]. The REST model has been studied experimentally for flight at off design conditions by Smart & Ruf [58]. The REST engine has been used as it has been proven to operate successfully at off-design conditions, an extremely important property for this study as the scramjet stage experiences a range of Mach number flight conditions, and significant variation in dynamic pressure.

A propulsion database of the C-RESTM10 has been provided for this study by Prof. Michael Smart.

2.5 First Stage Rocket Booster

The SPARTAN scramjet vehicle must be accelerated to its minimum operating speed by a first stage rocket booster. This booster must be capable of efficient operation from launch at sea level until staging. It is envisioned that the SPARTAN system will eventually use a reusable flyback booster[48]. However the flyback of the first stage is outside the scope of this study. Instead, a model of an existing first stage booster will be used, for which the Falcon-1e was chosen.

The SpaceX Falcon-1e launch system was a proposed small satellite launch system which would have entered use after 2010[61], but was discontinued and superseded by the Falcon-9 project. The Falcon-1e was designed to launch payloads between 600-900kg to low Earth orbit, with flexible orbit altitude and inclination. The Falcon-1e was to be the next generation of the Falcon-1[61], a launch tested, modern launch system. The Falcon-1e was chosen for its appropriate size and the proven flight effectiveness of the Falcon-1. The first stage of the Falcon-1e is powered by a Merlin 1C LOX/Kerosene turbopump engine. The first stage rocket is designed to be a Falcon-1e first stage scaled lengthwise to 50% of its original length.

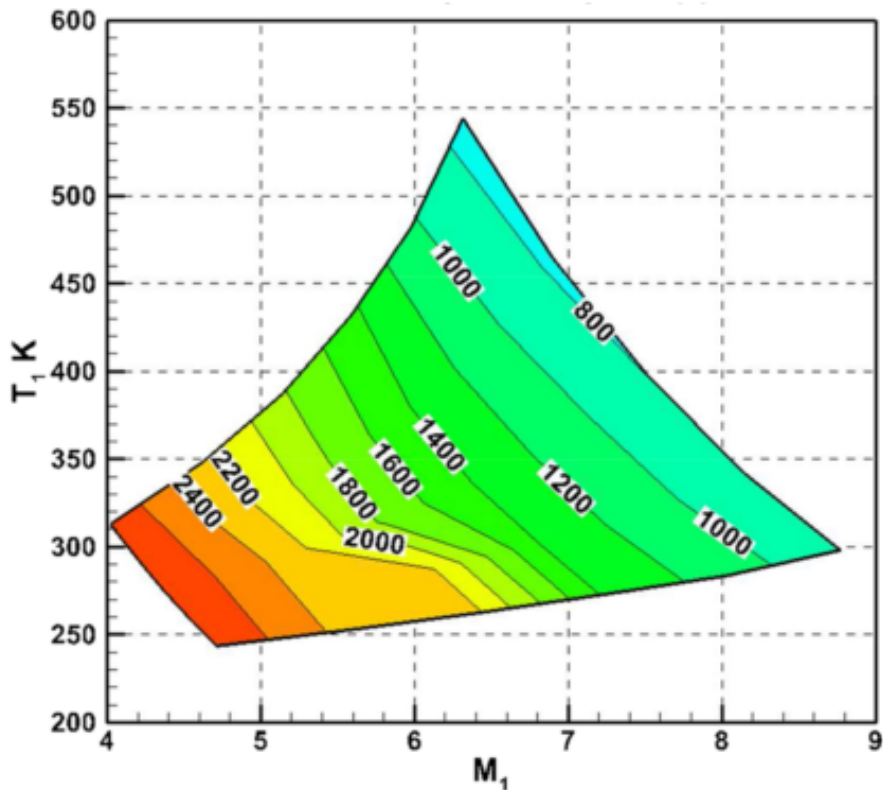


Figure 2.4: The C-RESTM10 propulsion database, specific impulse.

2.6 Exoatmospheric Rocket Engines

After scramjet stage burnout, the upper stage rocket must exit the atmosphere, and accelerate the payload to orbital velocity. This requires a rocket engine with sufficient thrust to accelerate the third stage rocket out of the atmosphere, and a diameter small enough to allow the rocket to fit within the fuselage of the SPARTAN. Table 2.1 shows a comparison study of upper stage rocket engines.

Engine	Fuel Supply	Fuel	Thrust	Isp	Mass	Diameter	Length	Thrust Vector Capability
Aestus	Pressure-fed	MMH/NTO	27.5kN	320s	110kg	1.27m	2.2m	4° & 4° by mechanical adjustment
OMS	Pressure-fed	MMH/NTO	26.7kN	316s	118kg	1.168m	1.956m	8°
Aestus II	Pump-fed	MMH/NTO	46kN	337.5s	148		2.2m	6°
RS-72	Pump-fed	MMH/NTO	55.4kN	338s	154kg		2.286	6°
ATE	Pump-fed	MMH/NTO	20kN	345s	57.9kg	0.38m	1.4m	15°
AJ10-118K	Pressure-fed	A-50/NTO	43.3kN	320.5s	124.5kg	1.53m	2.7m	Fixed
Kestrel	Pressure-fed	LOX/Kerosene	30.7kN	317	52kg	1.1m	1.9m	Yes, Unknown limits
R1-10-3A								

Table 2.1: Comparison of upper stage rocket engines.

2.7 Partially-Airbreathing Launch Vehicle Ascent Trajectories

Current simulations of the SPARTAN vehicle have been carried out with the assumption of a 50kPa dynamic pressure trajectory, a likely design point of the vehicle and scramjet engine. Constant dynamic pressure trajectories have been used for airbreathing vehicle simulation due to the trade-off between structural loading and engine performance for hypersonic vehicles [40]. As dynamic pressure increases so does the structural loading on the vehicle, however scramjet thrust is directly reliant on dynamic pressure ie. an increase in dynamic pressure directly means more air into the engine inlet. A constant dynamic pressure is viewed as being an acceptable compromise between these two factors. This form of trajectory has so far been simulated using proportional integral derivative (PID) feedback control, directly investigated since 1998 by Olds & Budianto [40]. This is a simple and effective form of control for systems being simulated over a constant dynamic pressure path [46]. This form of control utilises minimises an error function as the vehicle moves along its trajectory. This error function causes the controls of the vehicle to be modified by a feedback term which is a function of the error including proportional, integral and derivative terms. The result is a trajectory which is suitably close to the objective design point, with minimal overshoot and steady state error which can cause oscillations around the specified design value. Figure 2.5 shows an example of a constant gain PID controller as applied to the SPARTAN vehicle being simulated to a design point of 50kPa dynamic pressure. Oscillations can be observed around the design point due to overshoot and steady state error, factors which are prevalent in PID control systems.

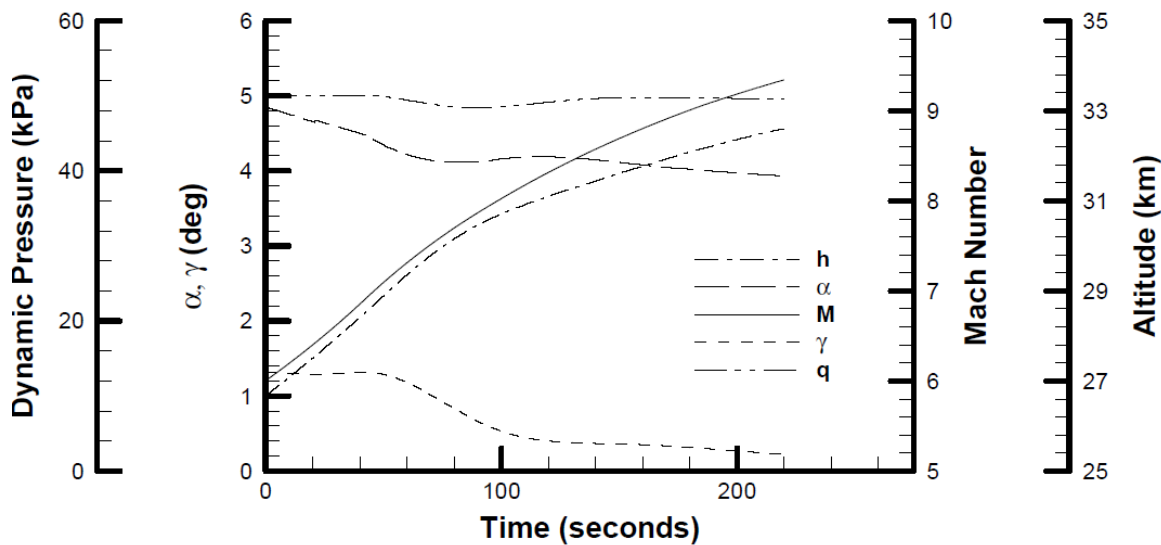


Figure 2.5: An example of a constant gain PID controller, controlling the SPARTAN trajectory around a 50kPa dynamic pressure design point [46].

It is possible that a constant dynamic pressure trajectory may not be the most appropriate trajectory for the second stage vehicle, as there is a variety of aerodynamic factors that must be considered

in designing optimal payload to orbit flight. It may be optimal for the vehicle to fly at less than maximum dynamic pressure at point throughout the trajectory, most likely at the first to second and second to third stage separation points. For a constant dynamic pressure trajectory the second-third stage transition will occur at a very low trajectory angle. This is suboptimal for the third stage rocket, which needs to perform a large pull up manoeuvre at high dynamic pressure. Launching this system at higher angle or altitude may improve third stage fuel usage greatly, at a small cost to the second stage fuel, allowing a greater payload to be delivered to orbit.

2.7.1 Single-Stage Vehicles

Optimal trajectories have previously been developed for launch systems integrating airbreathing and rocket propulsion within single-stage-to-orbit (SSTO) vehicles [45, 34, 67]. These optimal trajectory studies found unanimously that a pull-up manoeuvre before the end of the airbreathing engine cut-off was the optimal flight path for the SSTO airbreathing-rocket vehicles being investigated. A pull-up was found to be optimal for vehicles where the rocket engines are not ignited until circularization altitude [45, 34] as well as vehicles where the rocket engine is ignited immediately after airbreathing engine cut-off [67]. For SSTO vehicles a pull-up manoeuvre is a simple trade-off between the altitude at airbreathing engine cut-off and the velocity achievable at cut-off. Due to the entire vehicle being lifted into orbit, this becomes a relatively simple problem of engine efficiency. The airbreathing engine is used for its high efficiency, until the dynamic pressure drops below the operable limit of the airbreathing engine, or until the thrust provided by the airbreathing engine is significantly counteracted by the effects of drag and gravity.

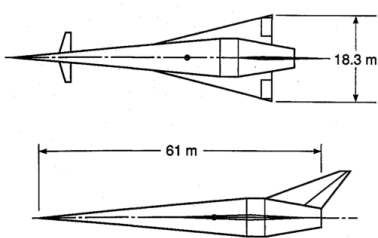


Figure 2.6

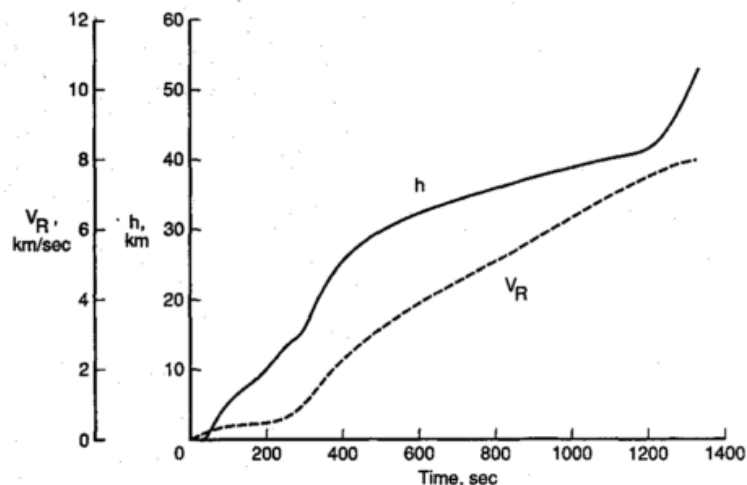


Figure 2.7: Powell

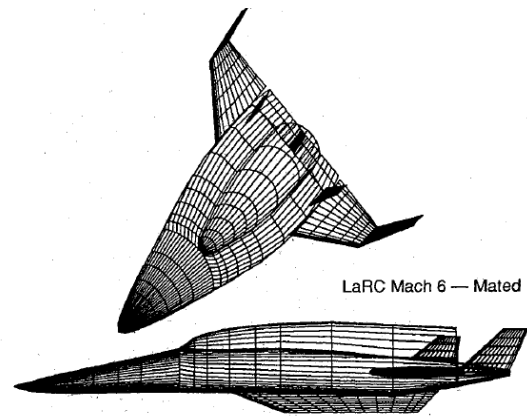


Figure 2.8

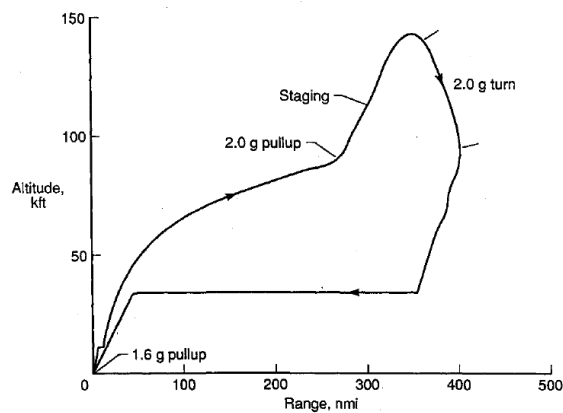


Figure 2.9: Wilhite

2.7.2 Multi-Stage Vehicles

For a multi-stage to orbit vehicle, calculating the optimal trajectory for maximum payload flight is significantly more difficult. A multi-stage vehicle has one or more stage transition points, where the vehicle separates a component which is discarded or reused later, and does not continue to orbit. At a stage transition point there is a large change in the mass and aerodynamics of the launch system. This change in flight dynamics makes finding the optimal stage transition point more complicated. To find the optimal separation point there is a trade-off between: I. The high efficiency of the scramjet engines, II. The thrust produced by the scramjet engines, III. The potential thrust of the rocket engines, IV. The energy necessary to increase the altitude of the scramjet stage, V. The aerodynamic efficiency when performing the required direction change. All of these factors must be considered in order to generate an optimal trajectory.

There has been a number of studies which have identified a pull-up manoeuvre as being advantageous for a multi-stage system [68, 73, 37]. However, in these studies a pull-up manoeuvre has been specified in order to decrease the dynamic pressure of the vehicle at airbreathing-rocket stage separation.

In the studies by Tsuchiya et al.[68] and Wilhite et al.[73], decreased dynamic pressure is necessary for the successful operation of the orbital rocket stages, of the systems under investigation. In these studies the airbreathing stages pull-up to the maximum allowable dynamic pressure for the rocket-powered orbital stages. When the orbital stages are able to operate, stage separation occurs. These pull-up manoeuvres demonstrate the advantages of a pull-up for the operation of the orbital stages, allowing the aerodynamic and thermal loading on the vehicle to be reduced. However these pull-up manoeuvres are not performed as part of optimal trajectories, instead they are designed to ensure that the performance constraints of the systems are met.

Mehta & Bowles [37] prescribe a 2g pull-up at flight conditions of Mach 10, 95000 ft for an airbreathing stage in order to "lower dynamic pressures and to achieve the optimal launching flight

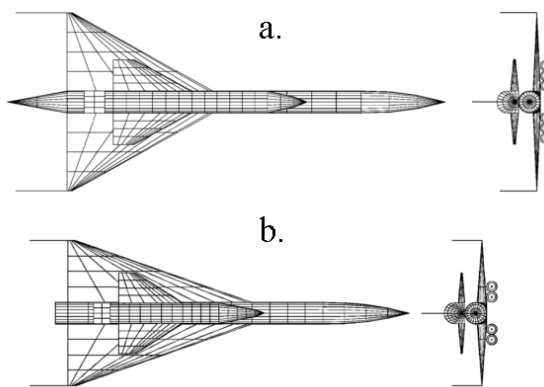


Figure 2.10: a) Airbreathing b) Airbreath- Rocket

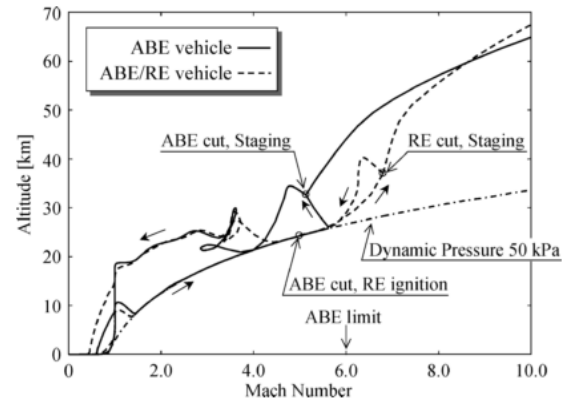


Figure 2.11: The trajectory of the launch system developed by Tsuchiya and Mori [68]



Figure 2.12

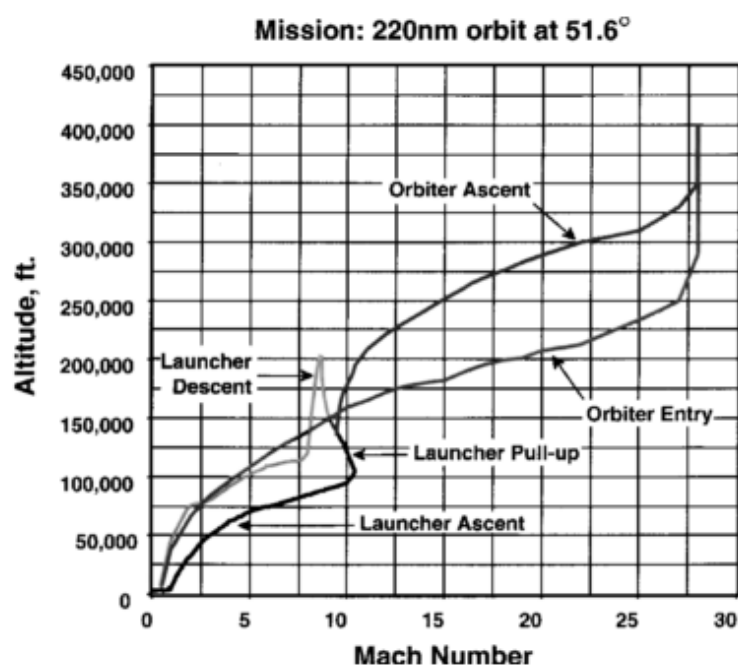


Figure 2.13: The trajectory of the launch system developed by Mehta and Bowles [37].

path angle for the orbiter vehicle”. This indicates that a pull-up manoeuvre before airbreathing-rocket transition is considered the optimal trajectory, however this study does not optimise the shape or magnitude of the pull-up manoeuvre, only considering the increased performance of the rocket vehicle.

2.8 Hypersonic Vehicle Flyback Trajectories

Past studies of the SPARTAN vehicle have assumed that a fly-back to launch site is possible after third stage separation[48]. However, this fly-back has not yet been simulated. A simulation of the fly-back of the SPARTAN is necessary in order to assess the viability of the SPARTAN concept. The fly-back of the SPARTAN is a crucial component to the viability of the rocket-scramjet-rocket launch system. The SPARTAN must return to the initial launch site to enable refurbishment to begin immediately, and so that there is no significant transportation of the SPARTAN required between launches. Due to the second-third stage staging velocity, it is complicated for the SPARTAN to cover the necessary fly-back distance. To maximise fuel efficiency, it is desirable for the SPARTAN to perform a minimum-fuel fly-back to the initial launch site, with the best-case scenario being for the fly-back to use no fuel at all.

There are three main methods that have been studied for potential hypersonic vehicle return; glide-back, cruise-back and boost-back. Glide-back involves the hypersonic vehicle returning to base and landing entirely using its aerodynamics. This requires sufficient lift to sustain the hypersonic vehicle over the entire return range, as well as the controllability to land the hypersonic vehicle in level flight. For a hypersonic trajectory a fully glide-back return flight is most likely unobtainable. This is due to the large downrange distance flown, and the large initial velocity at the beginning of the fly-back trajectory, when the vehicle is oriented away from the landing site. Multiple studies have investigated the maximum staging velocity allowable for the glide-back flight of a booster. In these studies, the maximum separation velocity for glide-back to be feasible has been found to be between Mach 3-4 at 30km-120km downrange distance, with higher initial velocities or longer downrange distances requiring fly-back under power[23, 65].

Cruise-back involves the inclusion of subsonic engines, which are used to power the fly-back of the hypersonic vehicle until landing similar to a conventional aircraft. These engines may be included solely for the fly-back[23], or used in the acceleration phase for low velocity acceleration[37, 65, 73]. The addition of subsonic engines powering a constant velocity cruise-back phase allows the accelerator to return to base with a similar trajectory to that of traditional aircraft, allowing the velocity and altitude of the accelerator to be precisely controlled. However, the addition of subsonic engines necessary for cruise-back increases the mass of the vehicle significantly, leading to decreased mass efficiency and increased design complexity[23].

A preferable mode of powered fly-back is to use the existing hypersonic airbreathing engines dur-

ing the return trajectory in a boost-back trajectory. Using the existing airbreathing engines allows for range to be added to the return trajectory, without the inclusion of additional engines. The hypersonic airbreathing engines can be operated at appropriate times during the fly-back, when they will be most impactful on the return trajectory range. However, the hypersonic airbreathing engines may only be used within their operating region, and vary in thrust and efficiency dependent on flight conditions. Hypersonic airbreathing engines have maximum efficiency at low Mach numbers[48], with the thrust produced depending on the dynamic pressure and inlet conditions, which vary with the trajectory path and angle of attack of the vehicle. This added complexity requires the use of trajectory optimisation methods to find the most efficient flight path for return to the launch site, and to ensure that the return of the vehicle under its own power is viable.

2.8.1 Examples of Optimised Fly-Back Trajectories

Tetlow et al. [65] compare powered cruise-back to glide-back flight for the return of the first stage booster of a rocket powered two-stage launch vehicle. The powered flyback vehicle uses airbreathing engines to cruise back to the launch site at relatively low speeds. The powered flyback and the glide-back cases are analysed separately to determine the difference in the optimal staging velocities. Figure 2 shows the optimised deceleration phase for the cruise-back vehicle, terminating at cruise-back conditions. This trajectory shows three distinct skips, with the minimum trajectory angle progressively decreasing between each. Tetlow et al. conclude that the 'skips' are due to the rate of density increase being greater than the deceleration rate 'causing increased lift and levelling out of the altitude profile'[65]. This trajectory was optimised for minimum cruise-back fuel mass, indicating that the 'skips' are the optimal trajectory shape to maximise range in high initial velocity fly-back. The powered cruise-back vehicle is able to stage at 3000m/s due to the ability to cover a large distance during cruise-back. The glide-back vehicle was optimised to find the maximum possible staging velocity at which a turn and glide-back is still possible. This was found to be at 1200m/. Figure 3 shows the corresponding optimal deceleration trajectory, terminating at sustainable glide conditions. This trajectory again shows multiple skips. The low allowable separation velocity of 1200m/s for the glide-back booster potentially suggests that the SPARTAN will require powered flyback. Tetlow et al. assume an admittedly optimistic L/D of 7 at Mach 0.9, and maximum angle of attack of 40 deg. However, the mass of the vehicle in this study is up to 1182 tons. A lower L/D may be acceptable for a lighter vehicle.

A maximum staging velocity at which glide-back is possible is also investigated by Hellman [23]. Hellman uses a suboptimal, scheduled trajectory simulation to investigate the flyback capabilities of a reusable rocket booster. Hellman finds that Mach 3 is the upper staging limit for a glide-back booster. This agrees with Tetlow et al. that high staging velocities are not possible for glide-back boosters, suggesting that the SPARTAN will require powered return flight.

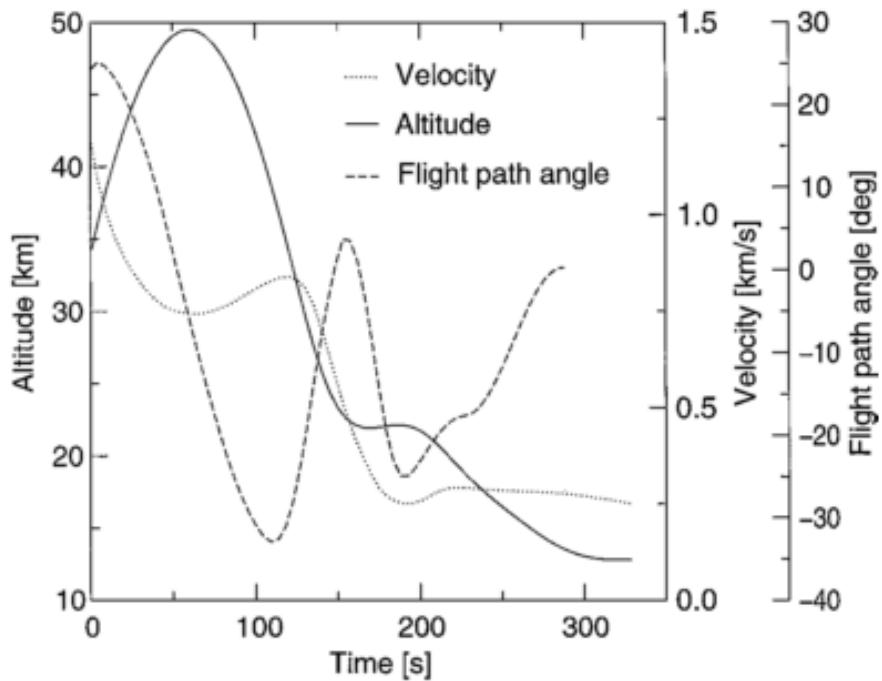


Figure 2.14: The flight path of a glide-back booster, developed by Tetlow et al. CITEXX.

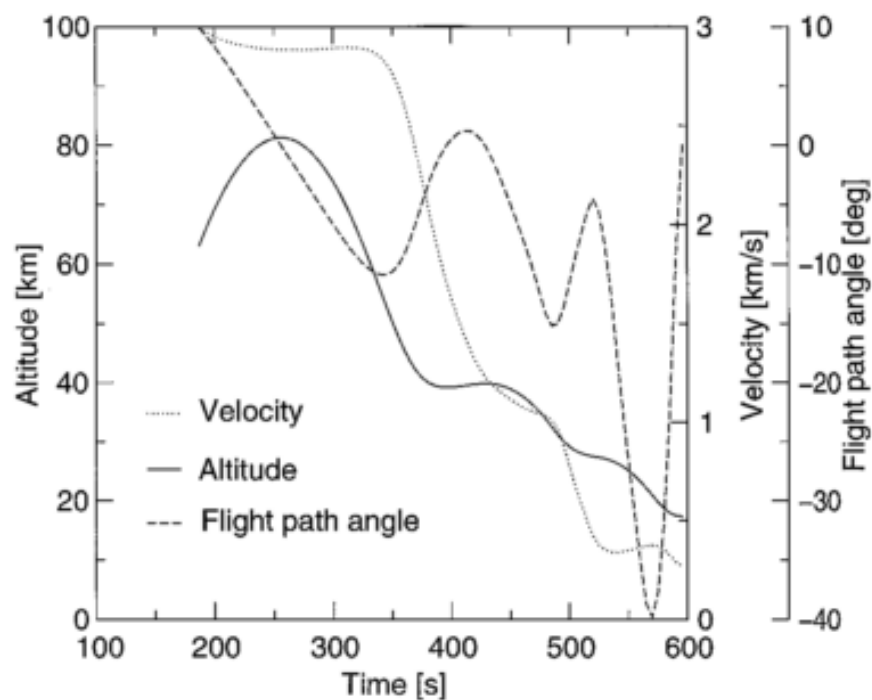


Figure 2.15: The flight path of a powered fly-back booster, developed by Tetlow et al. CITEXX.

The possibility of an airbreathing vehicle reigniting high speed airbreathing engines for short periods has been investigated by Tsuchiya and Mori [68]. Tsuchiya and Mori investigate two conceptual launch vehicles; a vehicle powered solely by airbreathing propulsion returning after separation of an orbital stage at Mach 5.1, and an airbreathing/rocket vehicle returning after a separation at Mach 6.8[68]. For the purposes of fly-back these vehicles are very similar, both using the high speed airbreathing engines during return flight. The optimal launch and return trajectories for these vehicles are shown in Figure 2.11. The separation for the airbreathing vehicle occurs at Mach 5.1, and the separation for the airbreathing/rocket vehicle at Mach 6.8. Both optimised return trajectories follow a relatively similar path. A long skip is performed, with both vehicles hitting the dynamic pressure limit. Both vehicles ignite the airbreathing engines at around Mach 3.5 for several tens of seconds to extend the range of the fly-back manoeuvres. After this, the vehicles descend and land at the launch site. The velocity at the landing point is not constrained, causing the airbreathing vehicle to land at slightly under Mach 1, and the airbreathing-rocket vehicle to land at approximately Mach 0.5. The latter is comparable with the landing velocity of the space shuttle [53]. These boosters fly to a downrange distance of 600-625km from the launch site, and separate from the orbital accelerator at a dynamic pressure of 15kPa[68]. At the start of their respective return trajectories, both boosters turn with a bank angle of 130-145°. Both the fully-airbreathing and partially-airbreathing vehicles ignite their airbreathing engines for 'several tens of seconds' at approximately Mach 3.5, in order to extend the flight range of the vehicles and return to the initial launch site[68]. Less than 5% of the vehicles initial propellant was required to return the vehicles to the initial launch sites[68].

These optimised return trajectories show three distinct sections; a turn manoeuvre, a skipping phase, and a high L/D descent. The skipping phase is similar to the boost-skip trajectory of the space shuttle CITEXX, which uses repeated entries into the atmosphere, and skips out, to extend the range of an atmospheric entry. A skipping trajectory has been shown to be range optimal for hypersonic vehicles able to skip out of the atmosphere [39], as well as vehicles flying entirely within the atmosphere[39, 12]. A skipping trajectory has also been shown to be optimal for an air-breathing hypersonic vehicle thrusting throughout the trajectory[9]. The range optimal operation of the air breathing engine is shown to be repeated ignitions at the trough of each skip. The scramjets are ignited as the vehicle climbs after the through, as the Mach number decreases to the minimum operable conditions of the scramjet engines. Minimising the Mach number during operation in this way maximises the efficiency of the scramjet engines.

When compared to the vehicles investigated by Tsuchiya and Mori[68], the SPARTAN separates from its third stage rocket at a considerably higher Mach number of Mach 9.1, as well as at a considerably higher dynamic pressure of 33.9kPa. The SPARTAN must also cover a longer fly-back range of 878km. In addition, the C-REST scramjet engines are limited to operating at hypersonic speeds of Mach 5.1 or higher. These design differences create substantially more challenging conditions than those studied by Tsuchiya and Mori. Consequently, it is necessary to investigate the ability of the

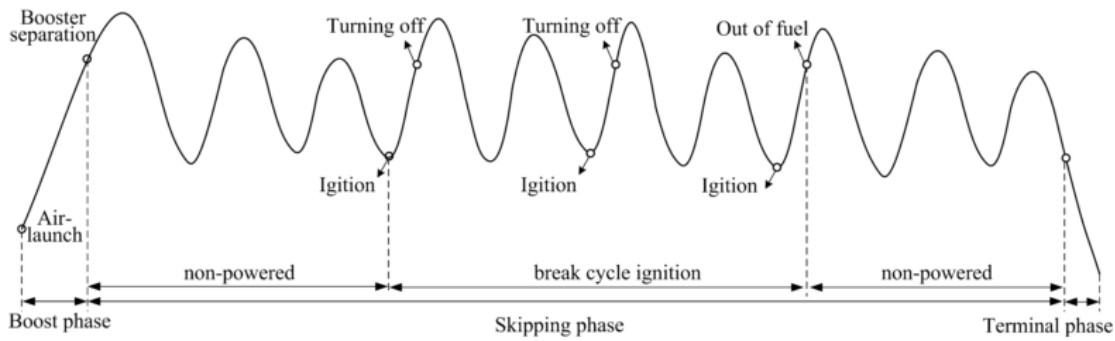


Figure 2.16

SPARTAN to return to the launch site following separation. From comparisons of the studies within this section it is evident that an optimisation of the return flight of the SPARTAN is required, and that a simply defined trajectory is not appropriate.

2.9 Optimal Control

To this point analysis of the SPARTAN trajectory has been performed using PID feedback control, assuming a constant dynamic pressure trajectory [46]. PID feedback control simulates the vehicle flight and manoeuvres the vehicle so that the trajectory conforms to a defined design point. Currently the trajectory of the SPARTAN has been simulated to align as closely as possible with 50kPa flight, a problem for which PID control is well suited.

This study aims to find the optimal trajectory path for the SPARTAN that will produce maximum payload to orbit capability for the three stage system. Feedback control is infeasible for finding an optimal trajectory shape as there is no single design point at each stage of the simulated trajectory to calibrate towards. A control method is required that can take into account all aerodynamic factors at every timestep in order to find an optimal trajectory. Defining the trajectory simulation as an optimisation problem allows the trajectory to be solved at every point simultaneously, producing an optimal trajectory over the entire simulation space. Optimal control theory is widely used in situations where an optimal trajectory path must be found, and has been used widely in aerospace applications. However a trajectory optimisation has not been attempted on a three stage airbreathing system, and is usually reserved for simpler systems as there can be issues with convergence and long computation times [13]. This does not rule out using an optimisation method on a complex aerodynamic system however it does reinforce that choosing the correct optimisation procedure and defining the problem in the correct way is integral to developing an accurate solution method. This study aims to find a method of optimisation that is applicable to a complex aerodynamic trajectory and to apply this to the SPARTAN vehicle to produce an optimal trajectory shape for maximum payload delivery to heliocentric orbit.

For an optimisation of a complex trajectory there are a variety of optimal control methods that are useful for specific problem types. These are separated into two categories: direct and indirect solution methods. Indirect methods are based on the calculus of variations or minimum principle model, and generally result in high accuracy solutions to optimisation problems [8]. However indirect models suffer from the drawbacks of small radii of convergence and the fact that the equations to be solved often exhibit strong nonlinearity and discontinuities. This means that indirect methods will not be solvable unless the problem is very well defined with a minimum of nonlinearity, making indirect methods unsuitable for many complex optimisation problems such as aerospace vehicle simulations which can exhibit strong nonlinear behaviour and have a wide solution space.

Direct methods transform an optimisation problem into a nonlinear programming (NLP) problem which can be solved computationally [62]. NLP solvers solve the optimisation problem defined as [4]:

$$\text{Minimise} \quad f(x) \quad (2.1)$$

$$\text{Subject to} \quad g_i(x) \leq 0 \quad \text{for } i = 1, \dots, m \quad (2.2)$$

$$\text{and} \quad h_j(x) = 0 \quad \text{for } j = 1, \dots, n \quad (2.3)$$

An optimisation problem that has been discretised in this form can thus be solved using any of a variety of NLP solvers. One of the most effective methods of solving twice differentiable NLP problems is sequential quadratic programming (SQP) [7] for which there is a variety of commercial solvers available such as NPSOL, SNOPT and packages within MATLAB.

In order for these packages to be able to solve an optimisation problem it must be presented in discretised form, and as such must be transformed using approximation techniques. The task of approximating a continuous optimisation problem in discrete NLP solvable form is not simple. SQP solvers can very easily run into convergence issues when provided with an optimisation problem which has not been well defined over a logical solution space. Also, any approximation must be carried out with care that the accuracy of the solution is not compromised. There are multiple ways to approximate a continuous optimisation problem directly as an NLP problem, the most common of which are shooting and collocation methods. The differences in the behaviour of each method are related to the interaction between the SQP solver and the discretisation method by which the problem is defined, and can affect the stability and accuracy of the solution as well as the solution time of the problem. For this study of in atmosphere trajectory optimisation with complex atmospheric and vehicle properties it was desired that a method be found with maximum stability and accuracy for a relatively large solution space, while solution time is a secondary priority.

2.9.1 The Single Shooting Method

The oldest and simplest method of approximating continuous optimisation problems as NLP problems is the direct single shooting method. Direct single shooting discretises the control function over the solution space, and solves this directly as an NLP by integrating the vehicle dynamics, or state variables, along the trajectory at each trajectory guess. Single shooting is simple to apply and has been used since the 1970s for rocket trajectory optimisation [27]. Single shooting methods suffer from nonlinearity problems, ie. an optimisation problem solved using the single shooting method will potentially struggle to solve if the problem exhibits even small nonlinearities, due to being unable to converge to an optimal solution. This makes the single shooting method unsuitable for complex problems such as a scramjet model, as there are many nonlinear factors inherent in atmosphere and airbreathing engine modelling.

2.9.2 The Multiple Shooting Method

Direct multiple shooting is a popular solution to trajectory optimisation problems. This method solves some of the instabilities of the single shooting method by splitting the trajectory into multiple shooting arcs, and collocating these at specific time points. This creates a system of discontinuities, illustrated in Figure 2.17, which are gradually removed by the solver algorithm until the trajectory is continuous. These discontinuities allow greater flexibility for the solver than is afforded by the single shooting method. The multiple shooting problem is solved as an NLP through discretisation of the state and control variables at each time node and integration for the state variables x over each shooting arc t_k [63]:

$$\dot{x} = v = f[x(t), u(t)] \quad (2.4)$$

With the state variables subject to the boundary conditions:

$$r[x(t_0), x(t_f)] = 0 \quad (2.5)$$

And solving for the unknown values s_i :

$$x(t_i) = s_i, \quad i = 1, 2, \dots, N \quad (2.6)$$

The control variables at the nodes are guessed and the state variables are integrated along the trajectory, with each node segment being considered separately. A matching condition is introduced that must be met between each segment; ie. the trajectory must be continuous. [38]

$$\mathbf{X}(\mathbf{s}) = \begin{Bmatrix} x(t_1; s_0, v_0) - s_1 \\ x(t_2; s_1, v_1) - s_2 \\ \vdots \\ x(t_N; s_{N-1}, v_{N-1}) - s_N \\ r[x(s_0), x(s_N)] \end{Bmatrix} = \mathbf{0} \quad (2.7)$$

This is now in the form of an NLP problem which may be solved in a standard NLP solver. ie. minimise:

$$\min J(s, v) = \sum_{i=0}^{N-1} J_i(s_i, v_i) \quad (2.8)$$

subject to:

$$x[t_{i+1}, s_i, v_i] - s_{i+1} = 0 \quad (2.9)$$

$$r[x(s_0), x(s_N)] = 0 \quad (2.10)$$

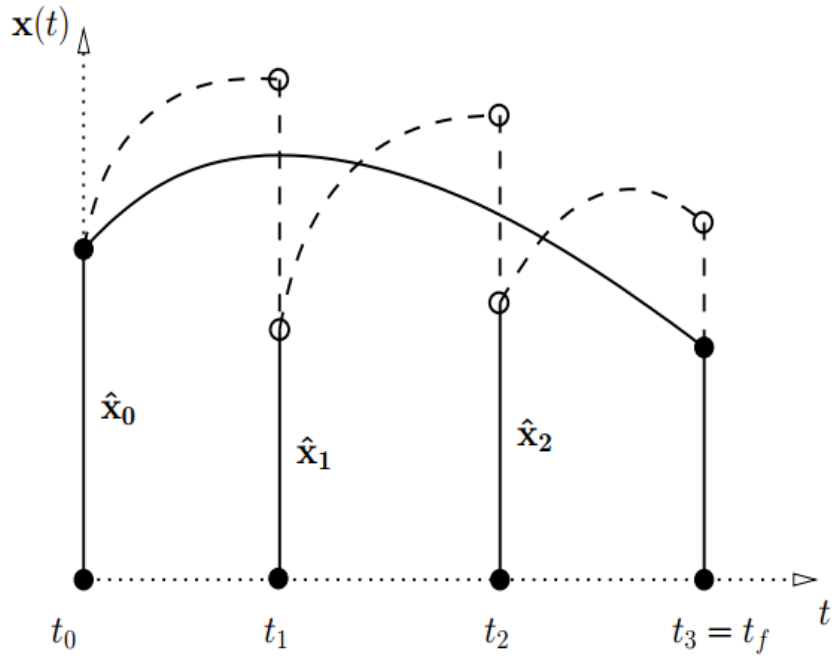


Figure 2.17: An illustration of the subdivision associated with multiple shooting [38]. Dashed lines illustrate the initial trajectory guess and the solid line indicates the final trajectory once the joining conditions are met.

The multiple shooting method has greatly improved convergence compared to the single shooting method, removing much of the susceptibility to instabilities resulting from nonlinear effects. How-

ever, the multiple shooting approach still suffers from a relatively small radius of convergence and slow computation times. Radius of convergence is extremely important to this study as the optimal solution cannot be approximated to a great degree of accuracy, and as such multiple shooting was deemed inappropriate for this study. It was desired to find a method with a global radius of convergence to apply to the optimisation problem being considered.

2.9.3 The Pseudospectral Method

check some of my claims about the pseudospectral method and cite GPOPS papers

GPOPS USES HP-ADAPTIVE GAUSS, WHICH HAS BEEN SHOWN TO improve(?) GAUSS
I should show the hp-adaptive gaussian method

Direct Trajectory Optimization and Costate Estimation via an Orthogonal Collocation Method - benson is quite a good paper (the first?) explaining gaussian ps method

also look at grops 1 manual

The most promising method found to address the issue of radius of convergence is the direct collocation approach, which provides global radius of convergence with the additional advantage of smaller computational time [17]. Direct collocation methods discretise the control and state equations of the optimal control problem, and use these as constraints in an NLP problem similarly to the multiple shooting approach. However the state functions in collocation methods are approximated by polynomial functions over the solution space, inherently being continuous at each collocation node rather than the state functions being integrated over each timestep. The derivative of the state functions then become a constraint within the NLP, being equated to the polynomial approximation functions by the solver algorithm. The method used to discretise the derivative functions is very important to the accuracy of the collocation method, with trapezoidal, Hermite-Simpson and pseudospectral methods being popular choices.

The most accurate form of collocation method is the pseudospectral, or orthogonal collocation method[14], which uses some elements of spectral method approximation to accurately approximate derivative terms. The pseudospectral method was first introduced in 1972 by Kreiss & Oliger [30] as an efficient way to compute meteorology and oceanography problems. The pseudospectral method is now garnering a large amount of attention for its ability to rapidly and accurately solve a wide variety of optimal control problems. The pseudospectral method employs the use of orthogonal polynomials such as Legendre or Chebychev polynomials to approximate the state and control functions at a specific set of collocation points[Huntington2007, 14]. The pseudospectral method has the property that when evaluated at the specific collocation points, the functions approximating approximate state and control are exactly equal to the continuous function being approximated at that point.

A large usability advantage of the pseudospectral method is the ability to generate Hamiltonian and costate values easily[22, 15]. The Hamiltonian and costate values allow a solution to easily and

quickly be checked to determine if some of the necessary conditions for optimality are being met. This is useful to determine initially if the optimal solution calculated by the pseudospectral solver is valid.

The pseudospectral method discretises the optimisation problem for application of an NLP solver. The initial form of the optimisation problem is that of a generic Bolza optimisation problem, described by a continuous Bolza cost function:

$$J(\mathbf{u}, \mathbf{x}, \tau_f) = M[\mathbf{x}(\tau_f), \tau_f] + \int_{\tau_0}^{\tau_f} L[\mathbf{x}(\tau), \mathbf{u}(\tau)] d\tau \quad (2.11)$$

Subject to a set of state dynamics, which describe the behaviour of the system over the solution space:

$$\dot{\mathbf{x}}(\tau) = f[\mathbf{x}(\tau), \mathbf{u}(\tau)] \quad (2.12)$$

These are constrained by boundary conditions of the system at the initial and final time points:

$$\psi_0[\mathbf{x}(\tau_0), \tau_0] = \mathbf{0} \quad (2.13)$$

$$\psi_f[\mathbf{x}(\tau_f), \tau_f] = \mathbf{0} \quad (2.14)$$

Three primary pseudospectral methods are described in this chapter. All of these methods make use of Lagrange interpolating polynomials. These methods use different collocation points.

The Legendre Pseudospectral Method

The Legendre polynomial method[16] uses Legendre-Gauss-Lobatto points for collocation. These create efficient and simple relationships for the evaluation of time-continuous optimisation problems [14]. The Legendre pseudospectral method uses the Legendre polynomial, defined as L_N :

$$L_N = \frac{1}{2^N N!} \frac{d^N}{dt^N} (t^2 - 1)^N \quad (2.15)$$

The Legendre-Gauss-Lobatto points, $t_l, l = 0, \dots, N$, are given by:

$$t_0 = 0$$

$$t_N = 1$$

and $t_l, l = 1 \leq l \leq N - 1$ are the zeros of \dot{L}_N .

The Legendre pseudospectral method transforms the problem to lie on the interval $t \in [-1, 1]$, so that the cost function (Equation 2.11) is discretised as follows:

$$J[\mathbf{x}(t_k), \mathbf{u}(t_k)] = \frac{\tau_f - \tau_0}{2} \sum_{k=0}^N L[\mathbf{x}(t_k), \mathbf{u}(t_k)] w_k + M(\mathbf{x}(t_N), \tau_f) \quad (2.16)$$

where w_k is a weighting function defined as:

$$w_k = \frac{2}{N(N+1)} \frac{1}{[L_N(t_k)]^2} \quad (2.17)$$

The state equations (Equation 2.12, in this case the system dynamics) are described at each LGL point by:

$$\frac{(\tau_f - \tau_0)}{2} \mathbf{f}[\mathbf{x}(t_k), \mathbf{u}(t_k)] - \sum_{l=0}^N D_{kl} \mathbf{x}(t_l) = \mathbf{0} \quad (2.18)$$

Where D is the differentiation matrix, defined at each entry k, l by:

$$k \neq l \quad D_{kl} = \frac{L_N(t_k)}{L_N(t_l)} \frac{1}{t_k - t_l} \quad (2.19)$$

$$k = l = 0 \quad D_{kl} = -\frac{N(N+1)}{4} \quad (2.20)$$

$$k = l = N \quad D_{kl} = \frac{N(N+1)}{4} \quad (2.21)$$

$$otherwise \quad D_{kl} = 0 \quad (2.22)$$

The boundary conditions are expressed analogously to the continuous problem:

$$\psi_0[\mathbf{x}(t_0), \tau_0] = \mathbf{0} \quad (2.23)$$

$$\psi_f[\mathbf{x}(t_N), \tau_f] = \mathbf{0} \quad (2.24)$$

The Chebychev Pseudospectral Method

The Gauss Pseudospectral Method

2.9.4 Pseudospectral Examples

need a six dof example, and a multiple state example

In order to assess the applicability of the pseudospectral method to an in atmosphere trajectory optimisation problem, the range of existing solutions utilising the pseudospectral method has been investigated. The pseudospectral method has been proven to be extremely effective for simulations in aerospace applications and has been proven in flight applications such as the zero propellant manoeuvre of the International Space Station in 2007, where the ISS was rotated 180 degrees without any propellant used following a pseudospectral method solution [5]. The pseudospectral method has been used successfully in a multitude of studies for the trajectory optimisation of hypersonic vehicles[33, 28, 75, 66, 12, 9, 50, 39].

The pseudospectral method has been used for the guidance of re-entry vehicles including in-atmosphere dynamics, to keep a vehicle on a desired three degree of freedom path in real-time in a study by Tian & Zong [66]. The pseudospectral method was found to generate an accurate trajectory around the desired reference trajectory, satisfying all necessary constraints in real-time for six state variables with minimal error. Nonlinear effects are an intrinsic part of simulating a complex aerodynamic system, and this study indicates that the pseudospectral method will be able to simulate the SPARTAN vehicle and is appropriate for use in this study.

Chai et al.[9] investigate the range optimal trajectory of a scramjet-powered hypersonic missile. Chai et. al successfully compute an optimal trajectory for an airbreathing hypersonic vehicle in three degrees of freedom[9]. The hp-adaptive pseudospectral method is compared to the Gauss pseudospectral method and the direct shooting method. Both pseudospectral methods show greater precision and robustness than the direct shooting method, and are reported to be much more computationally efficient. The direct shooting method takes 268.2s to complete, whereas the Gauss pseudospectral method completes optimisation in 12.7s, and the hp-adaptive pseudospectral method takes only 5.3s[9]. The pseudospectral methods produce similar results. The hp-adaptive pseudospectral method shows a slight range increase over the Gauss pseudospectral method due to its ability to redistribute the collocation points adaptively, which improves robustness.

These results indicate that the pseudospectral method does not exhibit instabilities with nonlinear effects such as atmospheric density varying the dynamics of the system being optimised, and that the pseudospectral method can be used for systems with at least up to six state variables.

Based on the proven track record of the pseudospectral method in simulation situations, it was decided that using the pseudospectral method for the optimisation of the rocket-scramjet-rocket system was a sound and feasible decision. It has been necessary to investigate the range of solvers available

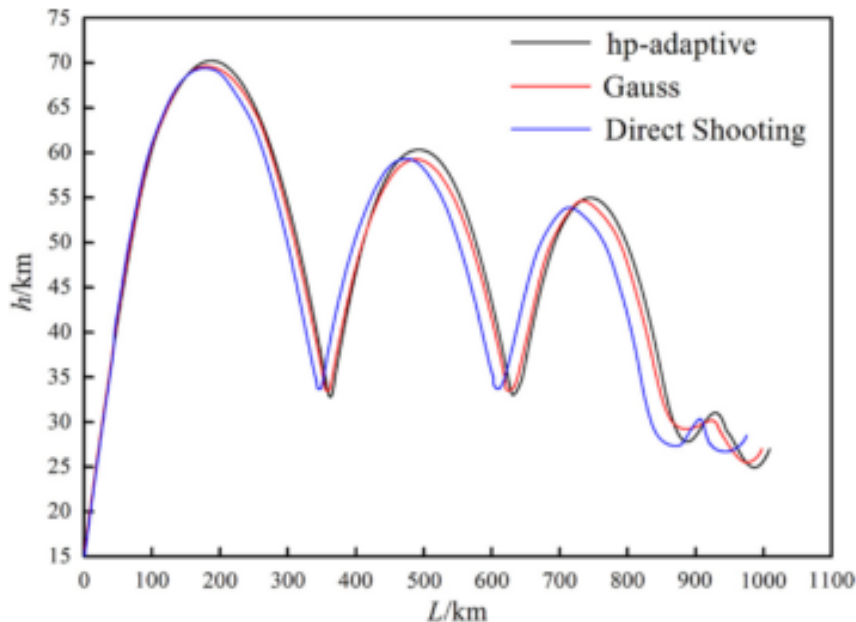


Figure 2.18

that will utilise a pseudospectral method to solve an optimisation problem with the desired capabilities and usability.

2.9.5 Available Solvers

change this section to reflect more current perspective

The pseudospectral method has a number of solvers available commercially, the foremost of which are DIDO, produced by Elissar Global [54], GPOPS II [49] and PROPT, a module integrated with TOMLAB [56]. These solvers utilise nonlinear programming techniques to solve optimal control problems in discretised form and are all similar in their operation. These have been investigated for a variety of considerations with details available in Section ??.

There are a number of existing programs that can complete optimisation problems using the pseudospectral method and as such creating an optimiser from scratch was considered to be overly time consuming and not a useful contribution. A number of programs were found, which are detailed in Table 2.2. An effort was made to find an open source program that could complete the desired optimisation however it was found that all open source programs studied were out of date or not well supported. Out of the premium packages available GPOPS II and DIDO were considered the best options, both being proven in aerospace applications, with available free trials and affordable price points. Free trials were requested from both, however the free trial for GPOPS II was not received while the free trial for DIDO was received with good customer service provided. On reception of the DIDO trial it was found that DIDO provides the required optimiser package in an easy to use form,

Software	Platform	Cost	Notes
DIDO	MATLAB	\$50 (Student)	Simple and automated with free trial available. Documentation readily available. Can perform required problem. Provides costates and Hamiltonian values.
GPOPS II	MATLAB	\$100	Free trial available, but was unable to obtain. Some documentation available. Can perform required problem.
ROC-HJ Solver	C++	Free	A basic solver for some specific optimal control problems. Does not perform collocation.
PROPT (IPOPT)	MATLAB	\$500	No free trial. Documentation available. Can perform required problem.
Imperial College OCS	MATLAB	Free	Documentation and download unavailable
PSOPT	C++	Free	Open source and can perform required problem. Not updated, many modules out of date.

Table 2.2: Summary of programs capable of pseudospectral optimisation.

with sufficient documentation and examples provided to streamline the simulation process. DIDO also provides costate and Hamiltonian values, used for verifying that the optimised solution is accurate and physically sound, as well as the lowest price point and benefit of being proven in both real space applications and in-atmosphere simulations. After weighing these considerations DIDO was selected as the best program to use for the pseudospectral optimisation and simulation.

2.10 Aerodynamic Analysis

- preliminary design requires fast and easy aerodynamics

Simulating the trajectory of access to space vehicles requires the aerodynamics of the launch vehicle to be characterised accurately. This entails the creation of large aerodynamic coefficient databases, which cover the operable region of the vehicle, and include the effect of control surface deflections. The liability of the vehicle design to change during the preliminary design phases renders highly accurate CFD or experimental studies expensive and inefficient CITATION. Instead, solutions are found which are able to approximate the aerodynamic characteristics to an appropriate accuracy, while providing fast set-up speeds as well as computation times.

2.10.1 HYPAERO

Hypaero is an aerodynamic calculation tool developed for the preliminary design of hypersonic vehicles. HYPAERO uses strip theory, dividing the surface of the vehicle into panels to calculate aerodynamic properties along the aircraft as illustrated in Figure 2.19. In strip theory two dimensional sections are created running the length of the vehicle, defining streamlines along the vehicle faces. Pressure, Mach number and skin friction are calculated along these streamlines to compute the aerodynamic coefficients of the vehicle. The Aerodynamic analysis of the SPARTAN has been performed using HYPAERO by Jazra et al. [26]. The aerodynamic coefficients of the SPARTAN vehicle have been provided for this study by Dawid Preller.

NEED TO CHANGE THIS to clarify where I'm using this

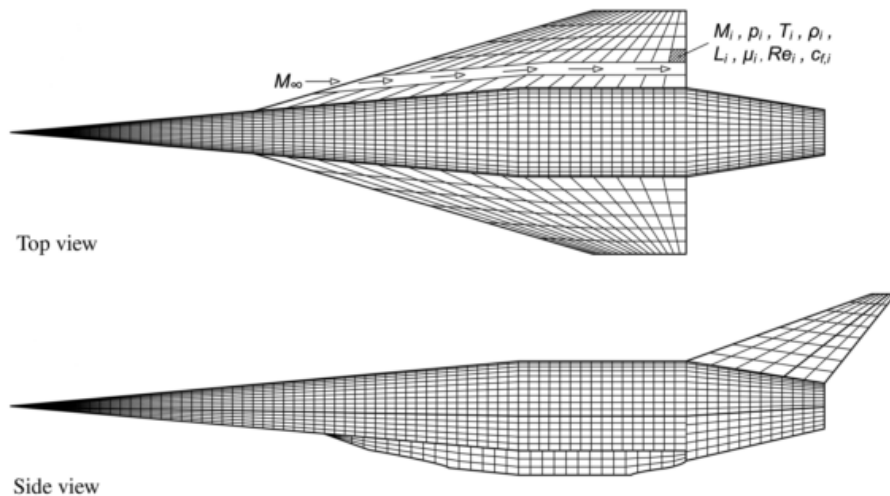


Figure 2.19: HYPAERO analysis surface grid [26].

2.10.2 CART3D

CART3D is an inviscid CFD package, designed for use during preliminary vehicle design and analysis CITATION. CART3D requires only a surface triangulation of the vehicle being analysed. CART3D features adjoint mesh adaption, and uses cartesian 'cut-cells' which intersect the surface, allowing complex geometries to be analysed. The mesh automatically refines as the simulation progresses, reducing error. The absence of a requirement for a user generated mesh allows CART3D to be easily applied to complex launch vehicle designs, as well as allowing for simple modification of control surface deflections and flight conditions. CART3D has been used extensively for aerodynamic simulations in preliminary design, including analysis of the Skylon spaceplane[36], HIFiRE-5[29], and in low sonic boom shape optimisations[2]. Mehta et al. used CART3D to analyse the Skylon spaceplane, in a study which investigated the aerodynamics of the vehicle as well as the plumes produced by the

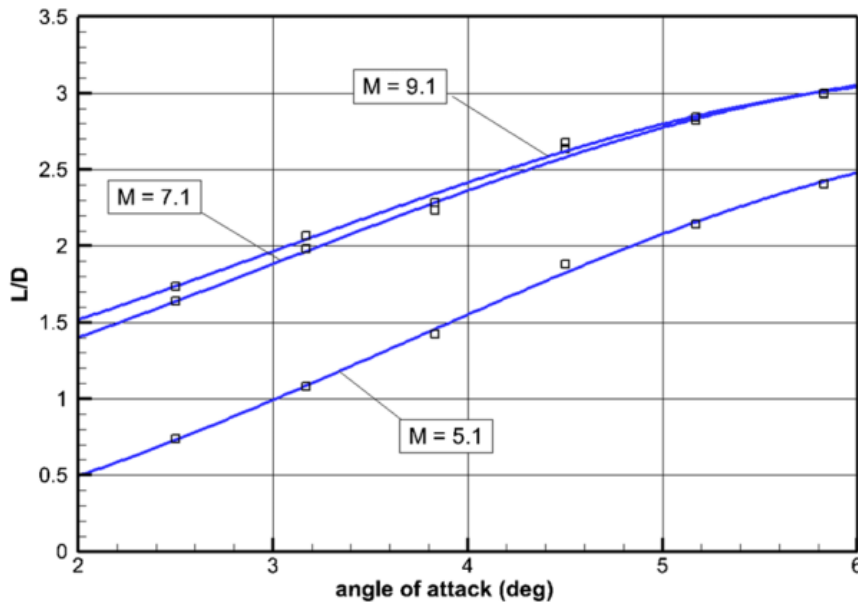


Figure 2.20: SPARTAN aerodynamics, developed using HYPAERO [48].

Reaction Engines LTD SABRE engines[36]. The Skylon was analysed at a range of mach numbers from 2.625 to 16.969, at altitudes from 15.326km to 75.771km. These results indicate the applicability of CART3D over a wide range of Mach numbers, which is of particular use to this study. During a study by Aftosmis & Nemec where CART3D was applied to low sonic boom shape optimisation, CART3D was shown to have good agreement with experimental results in tests at Mach 1.6.

The wide Mach number range of CART3D, along with its ease of use and demonstrated accuracy, makes CART3D a useful tool for this study.

2.10.3 Missile DATCOM

Missile DATCOM is a widely used, semi-empirical, aerodynamic prediction tool for missile configurations. Missile DATCOM is capable of calculating the aerodynamic forces, stability derivatives and moments over a range of angle of attack and Mach number values, allowing an aerodynamic database to be generated simply and rapidly. Missile DATCOM has been shown to produce close agreement with experimental wind tunnel data for normal force and pitching moment coefficients, and reasonable agreement for axial force coefficients [60].

2.11 Summary

This chapter has reviewed literature relevant to this thesis. Add more details.

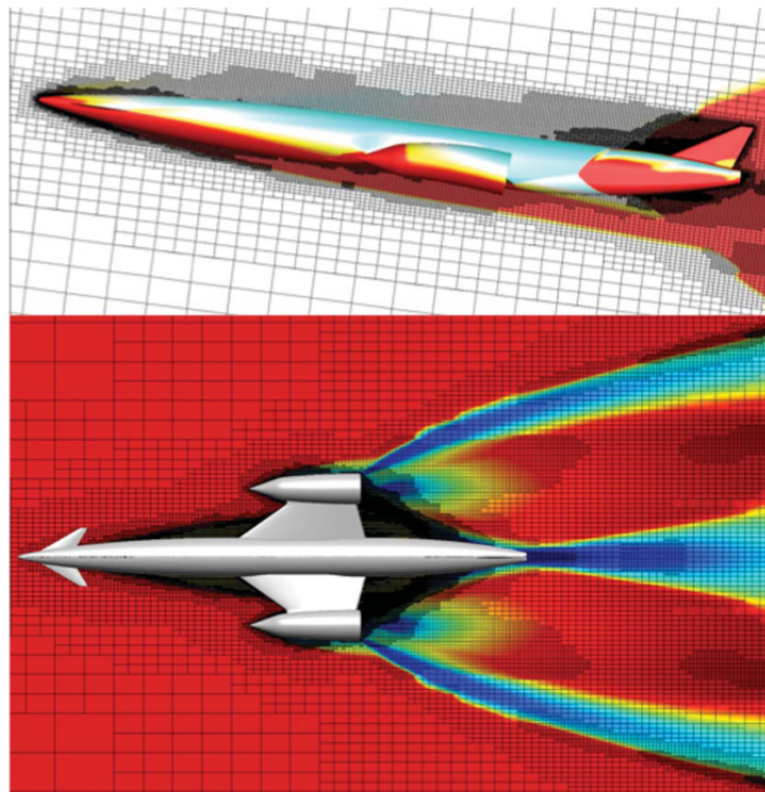


Figure 2.21: The Skylon spaceplane, simulated using CART3D at Mach 12.189, $\alpha = 7.512^\circ$ [36]. Cell distribution produced by mesh adaption is shown.

CHAPTER 3

LAUNCH VEHICLE BASELINE DESIGN

This chapter presents the baseline three stage small satellite launch system utilised in this thesis. The design for the first stage rocket-powered vehicle, second stage scramjet-powered vehicle (the SPARTAN), and third stage rocket-powered vehicle are presented. This baseline design is used for the initial trajectory analysis and optimisation in this study. The launch system has been designed based on the SPARTAN vehicle developed by Preller & Smart.

This chapter also describes the aerodynamic models of the vehicles used in this study, including the engine models.

3.1 First Stage Rocket

The first stage rocket-powered vehicle is based on the first stage of the SpaceX Falcon-1e. The Falcon-1e has been chosen due to its appropriate scale, and the proven flightworthiness of the Falcon-1.

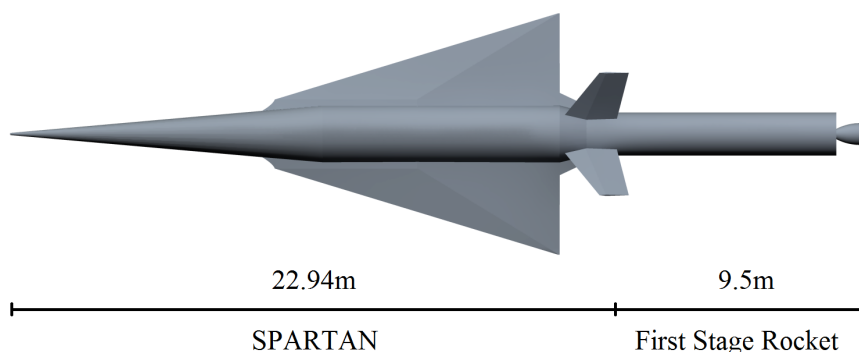


Figure 3.1: The rocket-scramjet-rocket launch system, top view, showing the SPARTAN and first stage.



Figure 3.2: The rocket-scramjet-rocket launch system, side view, showing the SPARTAN and fuel tanks, along with the third and first stages.

- detailed design
- First Stage aerodynamic coefficients calculated in CART3D
- details of CAD, pointwise mesh, and CART3D gridding settings

3.2 Second Stage Scramjet

3.2.1 Baseline Vehicle

The SPARTAN vehicle in this study has been designed based on the work by Preller & Smart CITATION.

The baseline SPARTAN has been designed to hold a 9 m long third stage. Two cylindrical tanks underneath the third stage and a conical tank situated in the nose have a total volume of 22.0m³ and hold a total of 1562kg of LH₂ fuel. This assumes an LH₂ density of 71kg/m³, slightly denser than LH₂ at phase transition point at 1 atm.

The fuel tanks are sized to fit around the kestrel-powered third stage, described in Section XX. The fuel tanks have a total tank volume of 22.0m³, containing a fuel mass of 1562kg. The mass of the fuel tanks is scaled from Dawid Prellers model of the SPARTAN, giving a total fuel tank mass of 179.41kg.

3.2.2 Aerodynamics

method of calculating aerodynamics for trim at required lift

-detail hypaero vs CART3D?

CG - determined using CREO. -detail CG positioning and shifting during flight as well as method for calculating trim

conical shock calculation

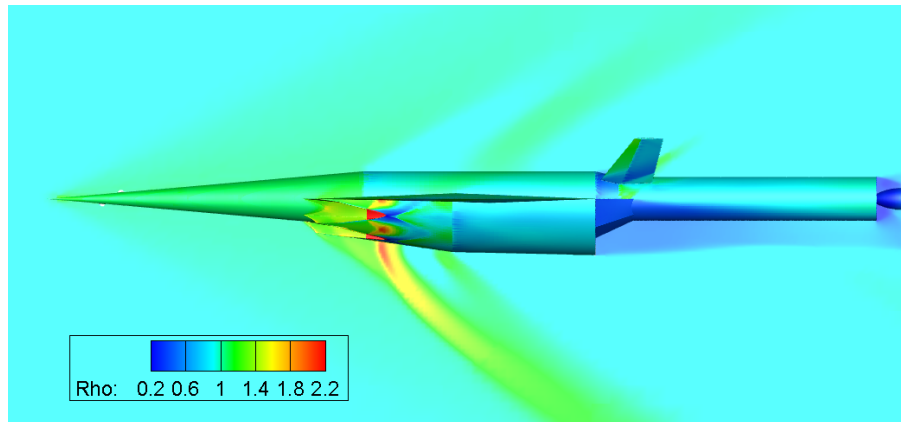


Figure 3.3: CART3D result for the SPARTAN and first stage vehicles at Mach 2, -1° angle of attack.

Aerodynamics Including First Stage

Aerodynamics of SPARTAN Alone

NOTE calculated SPARTAN aero using missile datcom (something close) and lift is very similar to CART3D, with drag being in between/a little lower than CART. Seems to support CART.

This section details the aerodynamics of the SPARTAN, calculated using CART3D. A SPARTAN model was provided for this study by Mr. Joseph Chai. A surface grid was created on this model using Pointwise[44]. This model includes engine flowpaths.

Images of pointwise mesh

CART3D lift/drag

Images of CART3D results for a range of Mach numbers

details of CART3D setup (no adapt levels / radius etc)

CART3D validation

-CG location and movement -moment of inertia

-show side and bottom results for $M=0.5, 1.1, 5, 9$ (appendix)

need engine off, engine on and flap deflection comparisons CHANGE THESE GRAPHICS

These results show a distinct maximum region in the L/D of the SPARTAN at high Mach numbers, within the hypersonic regime. Below Mach 5, the L/D of the SPARTAN decreases sharply.

For the engine-on case, the engines and boat tail are removed from the aerodynamics of the vehicle. In the engine-on case the drag is decreased for all conditions. The lift is increased at low angle of attack, and increased at high angle of attack.

-put in plots for moments, think about best way to present trim?

3.2.3 Propulsion Modelling

conical shock calcs

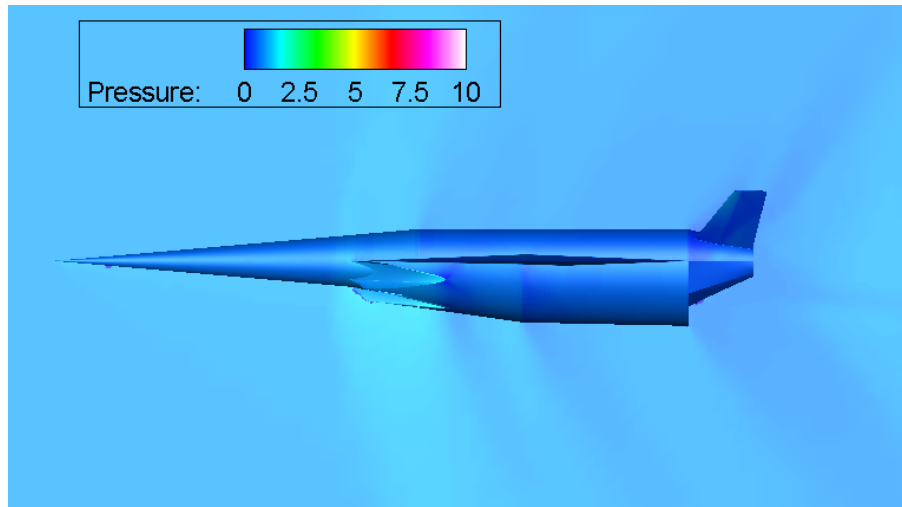


Figure 3.4: CART3D flow result for the SPARTAN, at Mach 1.1, 6° angle of attack.

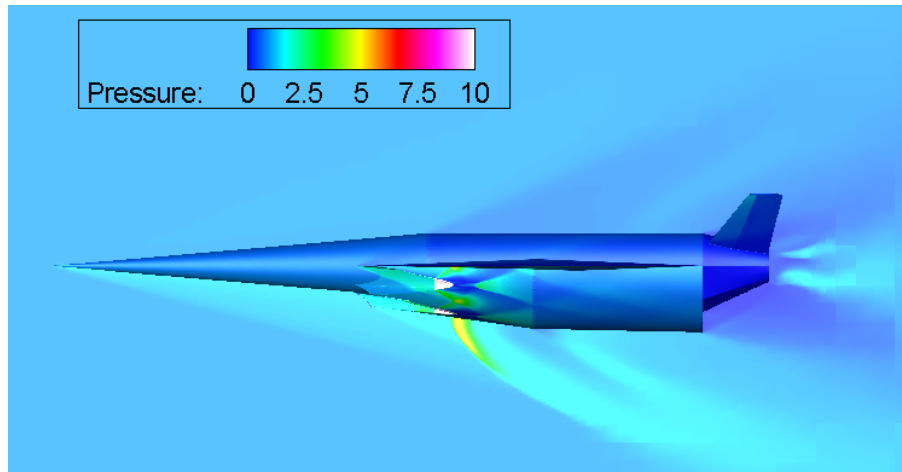


Figure 3.5: CART3D flow result for the SPARTAN, at Mach 3, 6° angle of attack.

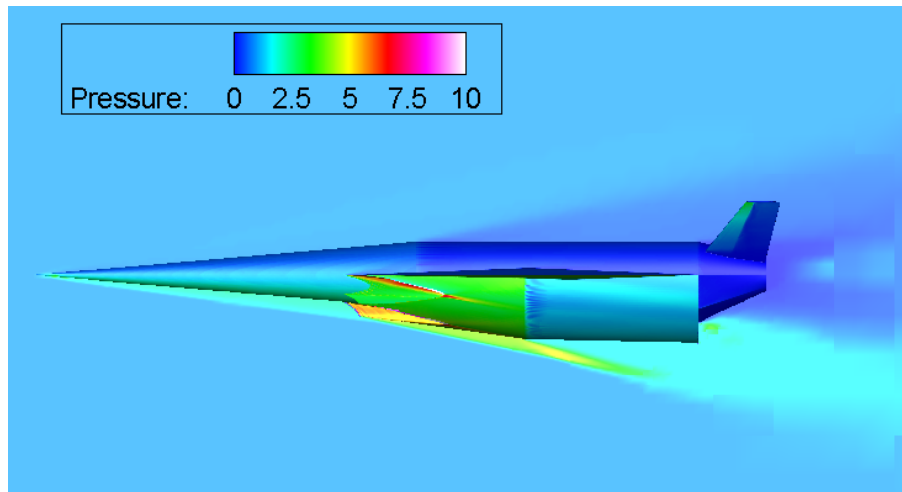


Figure 3.6: CART3D flow result for the SPARTAN, at Mach 7, 6° angle of attack.

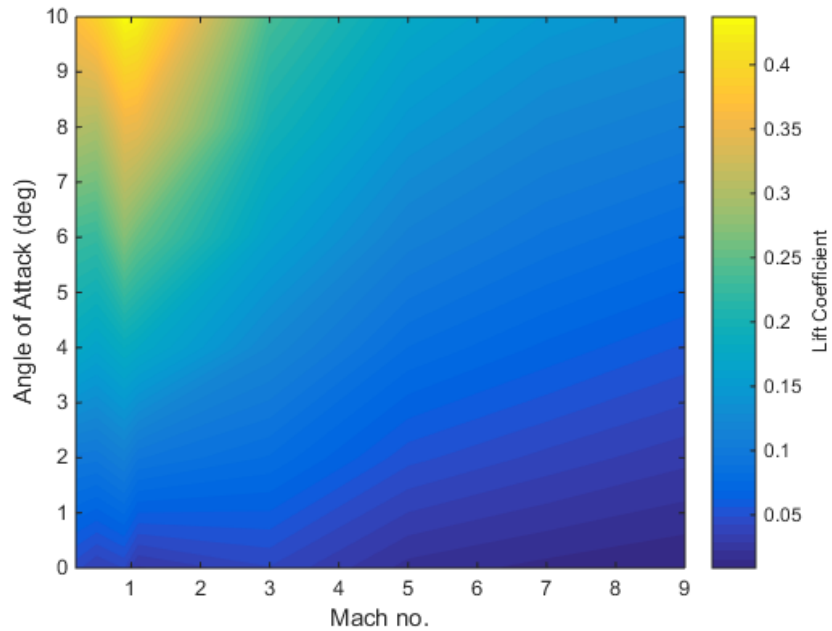


Figure 3.7: Coefficients of lift of the SPARTAN, calculated using CART3D.

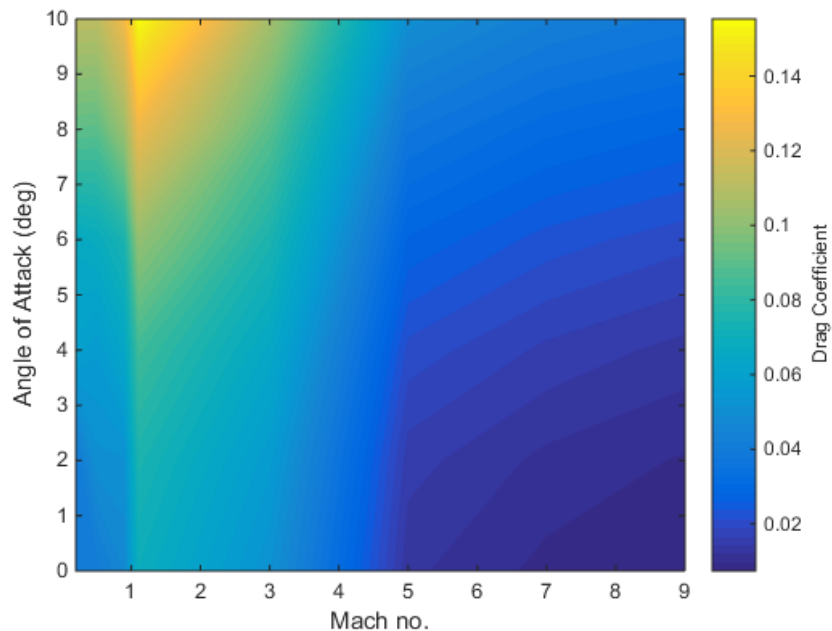


Figure 3.8: Coefficients of drag of the SPARTAN, calculated using CART3D.

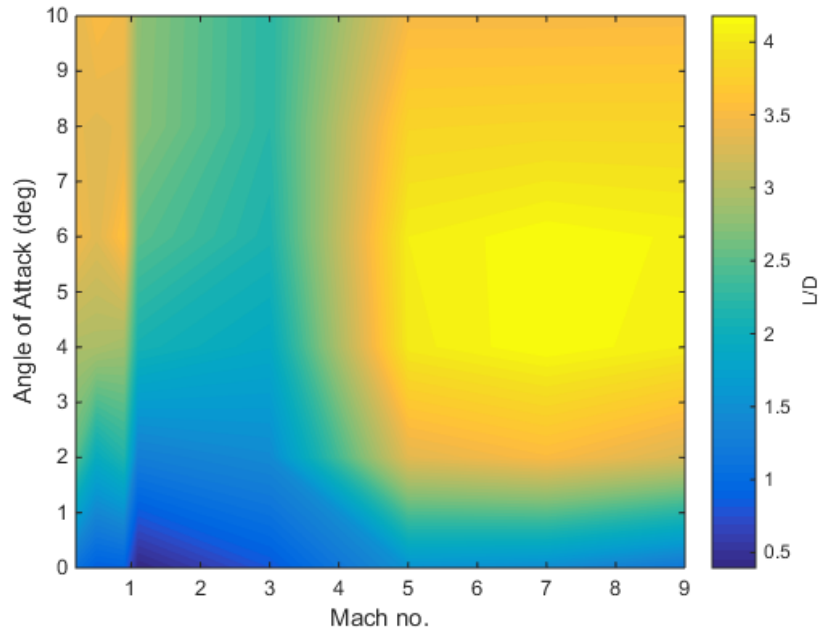


Figure 3.9: L/D of the SPARTAN.

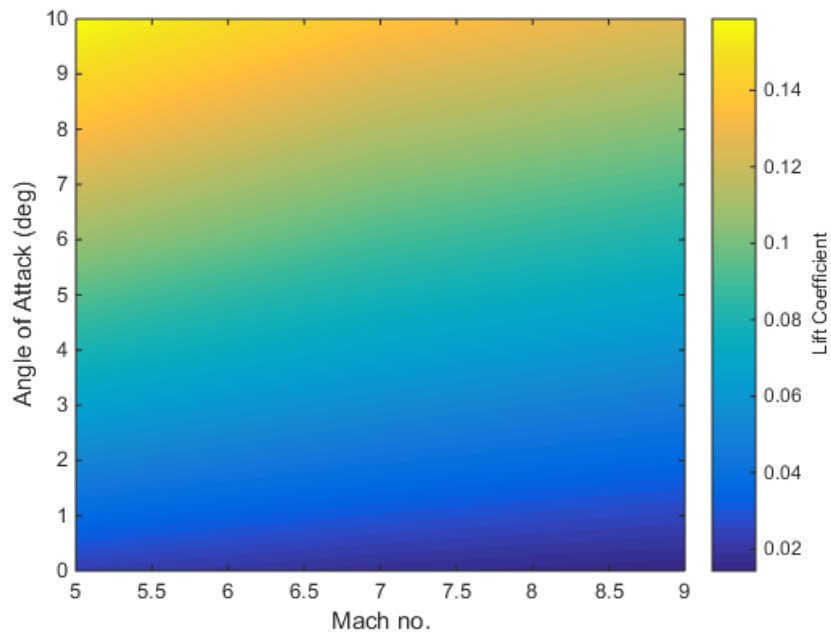


Figure 3.10: Coefficient of lift of the SPARTAN with the C-REST engines powered-on. This is obtained by removing the engines and boat-tail from the CART3D simulation results.

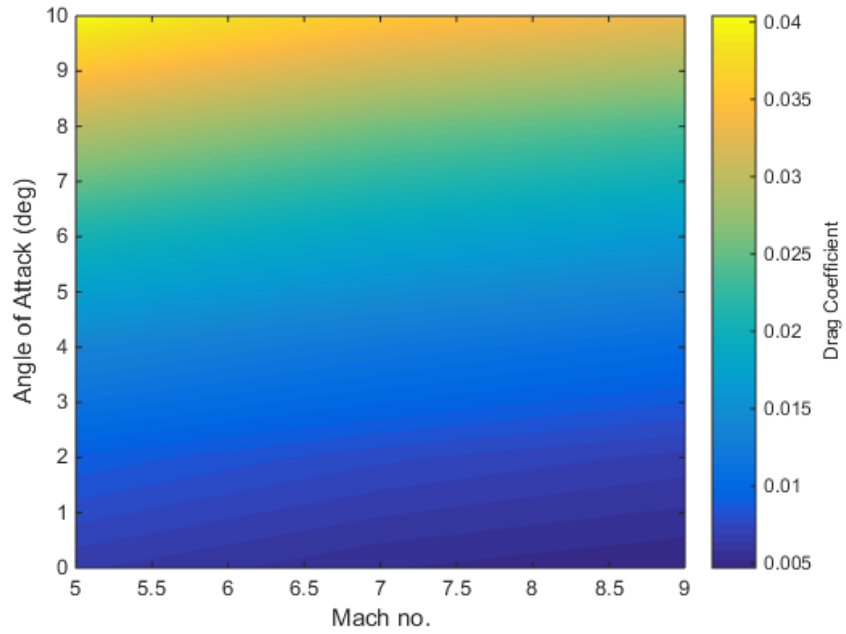


Figure 3.11: Coefficient of drag of the SPARTAN with the C-REST engines powered-on. This is obtained by removing the engines and boat-tail from the CART3D simulation results.

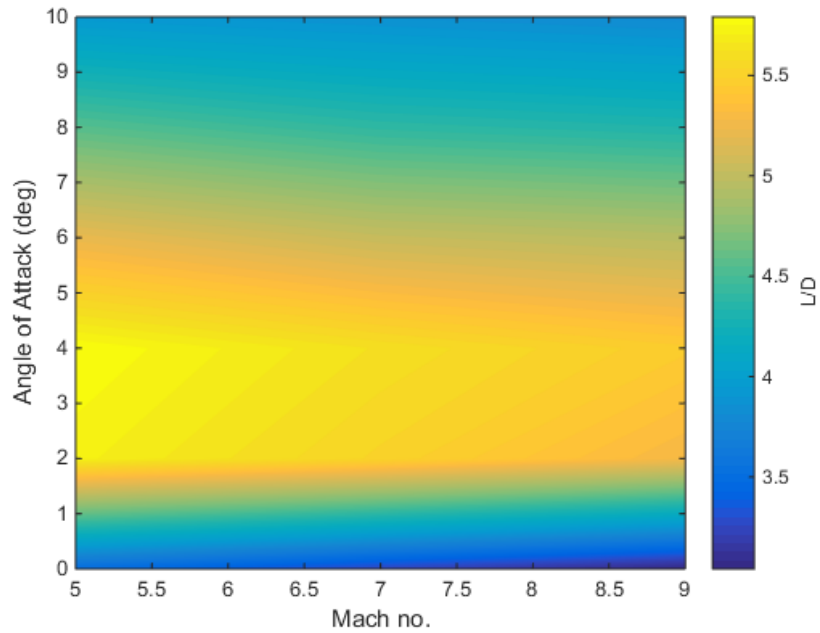


Figure 3.12: L/D of the SPARTAN with the C-REST engines powered on.

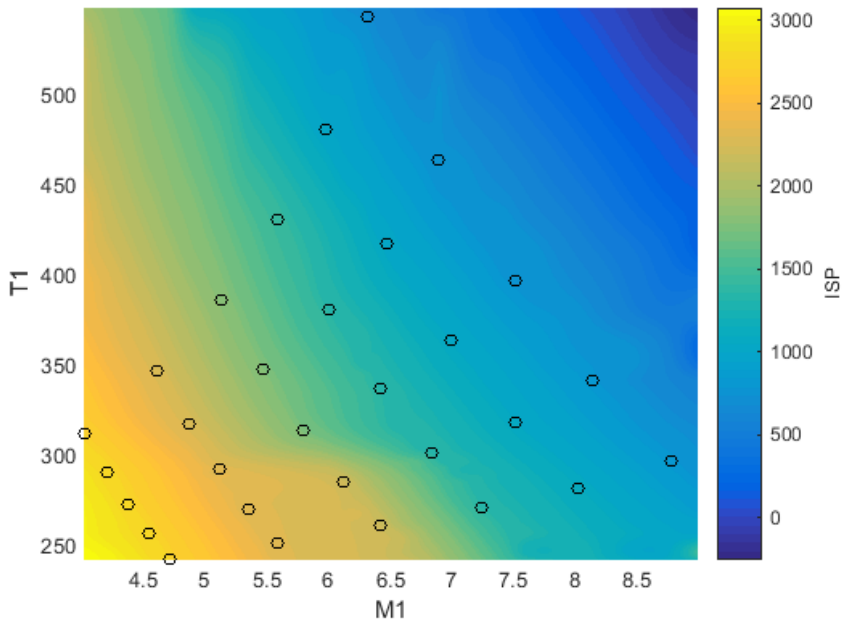


Figure 3.13

C-REST thrust calculator method?

The SPARTAN is powered by four underslung scramjet engines. These engines are Rectangular To Elliptical Shape Transition (REST) engines, configured to allow for a conical forebody (C-REST). The engine model used is a CRESTM10 database[48], analysed using quasi-1D simulation. This database provides data points of engine performance over inlet conditions within the operational range, at 50kPa dynamic pressure equivalent conditions. The specific impulse and equivalence ratio data sets are shown in Figure XXX. This data is interpolated for the given inlet conditions to calculate the exit conditions and the specific impulse produced by the engine. The specific impulse is obtained by spline interpolation. The thrust, T , is then obtained by inclusion of the mass flow rate (\dot{m}) obtained via the inlet conditions, ie. $T = g_0 \dot{m} I_{sp}$. The C-REST engine is a fixed geometry engine, designed for operability at high Mach numbers[48]. At lower Mach numbers, the addition of excessive fuel may cause the engine to choke and unstart, resulting in total loss of thrust[48]. To avoid unstart, an equivalence ratio (ϕ) of less than 1 is set at low Mach numbers. As the equivalence ratio is equal to 1 in the majority of the Mach number and temperature regime, only the regions in which it is less than 1 are used for the interpolation. The equivalence ratio interpolation is linear, as the number of data points available for interpolation is low.

During flight the C-REST inlet conditions will stay within the region bounded by the available data. However, for the purposes of the pseudospectral method solver, it is necessary for the vehicle model to be able to extrapolate for ISP and equivalence ratio data.

Put Plot of eq Here too



Figure 3.14

3.3 Third Stage Rocket - Baseline

In this study the third stage rocket has been designed to accommodate a SpaceX Kestrel engine. In previous studies, the third stage was designed to be powered by a Pratt & Whitney RL-10-3A pump-fed engine. The Kestrel has been used over the RL-10-3A for its cost effectiveness. As a pressure-fed engine, the Kestrel trades off specific impulse for weight and cost savings when compared to the RL-10-3A. As the only expendable portion of the system; the cost of the third stage is one of the main drivers of overall system cost. Reducing the cost of the third stage allows the cost of launch to be directly reduced.

The third stage rocket is released at the end of the scramjet accelerator burn, and lifts the payload out of the atmosphere and into the desired orbit. The third stage weighs a total of 3300kg. This was chosen as a design weight, to fit the fuel necessary to achieve orbit with an acceptable payload while also allowing for ample payload volume. The third stage has a structural mass fraction of 0.09, similar to the Falcon 1 second stage [61]. This gives a total structural mass of 285.7kg.

The kestrel engine has been modified to have 50% increased propellant mass flow rate, giving a mass flow rate of 14.8kg/s. The nozzle of the Kestrel engine has been kept at 1.1m diameter. This increase in mass flow results in a 2% loss of efficiency from the nozzle[64], due to the thrust coefficient decreasing as shown in Figure 3.15. The modified specific impulse of the engine is 310.7s.

The third stage has a total length of 9m, with a 3m long nose, 4.5m long centrebody and 1.5m long engine.

The centre of gravity is determined using CREO, and is at XXm from the nose. It is assumed that the mass of the structure of the rocket (excluding fuel tanks, heat shielding, engine and payload) is distributed homogeneously, for simplicity.

3.3.1 Heat Shield Sizing

The third stage rocket is separated from the SPARTAN at a high dynamic pressure, after which it spends a considerable amount of time accelerating in-atmosphere before reaching exoatmospheric conditions. This release into a high dynamic pressure environment creates a large amount of heating, which must be mitigated by heat shielding. The third stage is protected while in-atmosphere by a heat shield, weighting 130.9kg. This heat shield is constructed from a phenolic cork cylinder, a reinforced carbon-carbon nose cone, and a tungsten nose tip. The tungsten nose is 50mm diameter, at the end

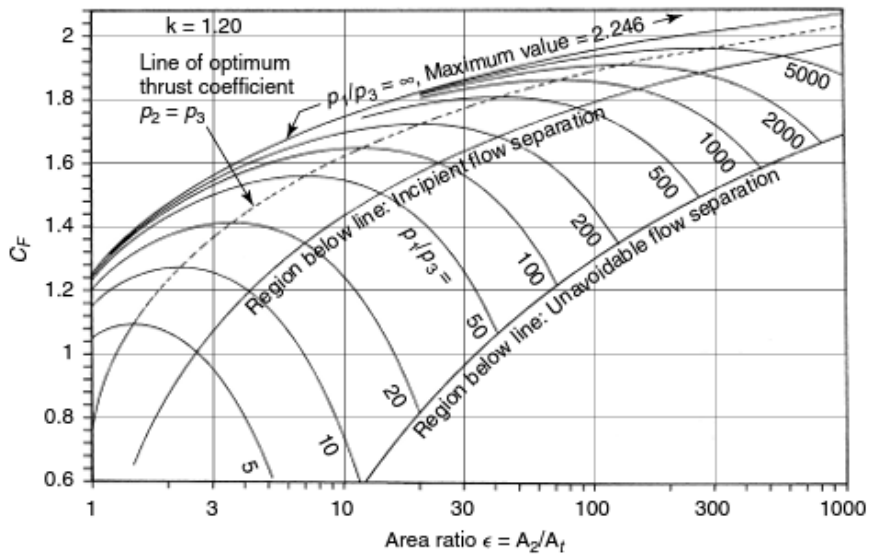


Figure 3.15: [64]

of a 50mm cylinder. The density of tungsten is $\rho_{Tungsten} = 19.25 \text{ g/cm}^3$, giving a total mass for the nose of $m = 12.6\text{kg}$. The carbon-carbon shell has a density of $\rho_{CC} = 1800 \text{ kg/m}^3$. The carbon-carbon shell has a thickness of 10mm. The mass of the carbon-carbon is 89.3kg. The cork cylinder has a density of $\rho_{Cork} = 320 \text{ kg/m}^3$, a thickness of 5mm and a total mass of 23.7kg. The total mass of the heat shield is 125.6kg.

3.3.2 Fuel Tank Sizing

The fuel tanks have been sized assuming 100kg of payload-to-orbit. Note that the method of calculating final payload-to-orbit relies on using left over 'fuel mass' as effective payload mass. Realistically this would cause the fuel tanks to be resized slightly. For the purposes of this study the fuel tanks have been assumed to be of constant size for simplicity. Currently this is a reasonable assumption as the internals of the rocket are very simplified. The structural mass is held constant at 9%. The third stage carries a total propellant mass of 2736.7kg. Table XX breaks shows the component break-down of the LOX oxidiser and RP1 fuel.

	LOX	RP1
Ratio	2.56	1
Density	1141kg/m ³	813kg/m ³ [35]
Volume	1.7248m ³	0.9455m ³
Mass	1968.0 kg	768.7 kg

3.3.3 Aerodynamics

The third stage aerodynamics have been calculated using Missile DATCOM [REFXX], a preliminary design tool for estimating the aerodynamic characteristics of missile and rocket vehicles. Missile DATCOM utilises empirical methods, along with various estimation techniques, to compute the aerodynamics of missile-like vehicles across the subsonic, supersonic and hypersonic regimes. The code used to compute the aerodynamics of the third stage rocket is detailed in Appendix XX.

Put plots of aerodynamics here

3.3.4 Thrust Vectoring

The third stage rocket is trimmed during the in-atmosphere portion of its ascent trajectory via thrust vectoring. The centre of pressure is calculated using missile DATCOM. The thrust vector is set so that the moment generated by the engine matches the lift force acting at the centre of pressure. The maximum thrust vector limit has been set to 8° . As no data on the maximum thrust vectoring capabilities of the kestrel engine was able to be found, this was set to the maximum gimbal range of the Aestus pressure-fed engine and OMS, similar pressure fed engines.

CHAPTER 4

LODESTAR

This chapter covers the optimal control program LODESTAR, which has been used to simulate the optimal trajectories of the rocket-scramjet-rocket system. The basics of optimal control and the optimal control methods used are presented, as well as the specific problem formulation used by LODESTAR.

The program LODESTAR (Launch Optimisation and Data Evaluation for Scramjet Trajectory Analysis Research) has been developed to aid with the simulation and trajectory optimisation of space launch systems. LODESTAR is a MATLAB based trajectory optimiser which utilises GPOPS-2, a proprietary pseudospectral method optimisation package as well as MATLAB's inbuilt SQP solver. LODESTAR optimises a trajectory towards a user-defined objective function, such as constant dynamic pressure or maximum payload-to-orbit. LODESTAR accurately models both rocket-powered and scramjet-powered vehicles in 5 degrees of freedom. LODESTAR contains multiple modules configured for the SPARTAN launch system, which are able to optimise trajectories for;

1. The ascent of the first stage rocket.
2. The ascent of the second stage scramjet-powered accelerator.
3. The flyback of the second stage scramjet-powered accelerator.
4. The ascent of the third stage rocket.

LODESTAR performs optimisation using four classes of variables, primals, controls, constraints and costs, which define the optimisation problem being solved. Primals are the variables which define the physical trajectory and are dependent on other primals and the control variable. The control variables are independent in the solution space and can be modified freely by the solver algorithm within the prescribed limits. Constraints bound the primal and control variables to a well defined solution space and events confine the primal and control values to a specified value at a specific point

in time. The cost variables define the target of the optimisation problem. A solution is found when the cost is minimised to a suitable accuracy.

GPOPS-II and DIDO require these variables to be precisely described. LODESTAR contains multiple modules that calculate the vehicle aerodynamic properties and run external simulations which then feed data back to the pseudospectral solver for evaluation. Modules calculate the vehicle aerodynamic and engine output at each point along the trajectory. The vehicle model module takes this data and calculates the mass of the vehicle as well as the 6 degree of freedom motion derivatives of the vehicle along the trajectory. As this is an iterative process, the calculated motion derivatives do not match the motion approximation exactly until convergence is achieved (This is a fundamental property of the pseudospectral method, see Section 2.9.3).

-XX define the iterative process here, include evaluation of the optimisation variables, and sequential quadratic programming

The cost is calculated using the primal variables. The trajectory is evaluated to produce the final cost of the trajectory. The final step of each iteration is updating the primal derivatives, which is performed by the dynamics file. The primal derivatives and cost are evaluated by DIDO to determine if the trajectory has produced a suitable result.

4.1 Optimal Control

The pseudospectral method and direct single shooting techniques used by LODESTAR are described in detail in sections XX. Practically, the implementation of these techniques involves the specification of the set of constraints and objectives which govern the optimisation problem. These constraints inform the optimiser of the bounds of the optimisation, and perform the functions of limiting the search space to the physically possible (eg. constraining altitude to be greater than ground level) as well as constraining the vehicle within its performance limits (eg. limiting the angle of attack). These constraints also come in the form of initial or terminal constraints, which define the initial conditions of the trajectory as well as any conditions which the trajectory must meet at termination.

The pseudospectral method requires the specification of a set of 'primal variables'. These primal variables describe the physical dynamics of the system. In the pseudospectral method, the dynamics of the system are used as constraints on the optimal control problem;

$$\dot{\mathbf{x}}(\tau) = f[\mathbf{x}(\tau), \mathbf{u}(\tau)]. \quad (4.1)$$

Implementing the dynamics as constraints allows the optimiser to explore each primal variable independently, greatly increasing the robustness of the optimal control problem. However, the constraints may be violated by the optimiser in the process of searching for an optimal solution. A violation of the physical dynamics constraints means that the dynamics of the system may not hold throughout the

Primal Variables	x Position y Position Velocity
Control Variables	Angle of Descent
Initial Constraints	Velocity x Position y Position
Terminal Constraints	x Position y Position
Path Constraints	None
Target Cost	Minimum Time

solution process, causing potential complications for the computational model of the vehicle. Much of the design of the vehicle simulation in this study is driven by the need for smooth, continuous interpolation schemes, and viable extrapolation regions ie. even if the solution is well within the range of all input data sets, the solver must be able to explore all regions within the set bounds.

4.1.1 GPOPS-2 Example - Brachistochrone Problem

This section describes a short example optimal control problem solved in GPOPS-II. The purpose of this example is to demonstrate the effectiveness of the pseudospectral method and GPOPS-II, and to provide a simple example case to establish the terminology of an optimal control problem.

The brachistochrone (from the Greek for 'shortest time') problem is a simple optimal control problem, which describes a ball rolling in two dimensions under gravity. The objective is to find the curve of descent which will minimise the time from point *a*, where the ball is at rest, to point *b*. It is assumed that gravity is constant and that there is no forces other than gravity acting on the ball.

The analytical solution of this problem can be computed using the Euler-Lagrange equation as the equations describing a cycloid:

$$x = A(\theta - \sin \theta),$$

$$y = A(1 - \cos \theta)$$

This problem has been solved using GPOPS-2. Table XX describes the set-up of the optimal control problem in GPOPS-2. The dynamic equations for the Brachistochrone problem are:

$$\dot{x} = v * \cos(u),$$

$$\dot{y} = v * \sin(u),$$

$$\dot{v} = -g * \sin(u).$$

The GPOPS-2 solution to the Brachistochrone problem is shown in Figure XX. This is overlaid with a plot of the optimal solution.

- xx put optimal solution in here **compare to analytical solution (dont include, just have plot)**

The dynamics of the basic Brachistochrone problem are very simple. As the dynamic become

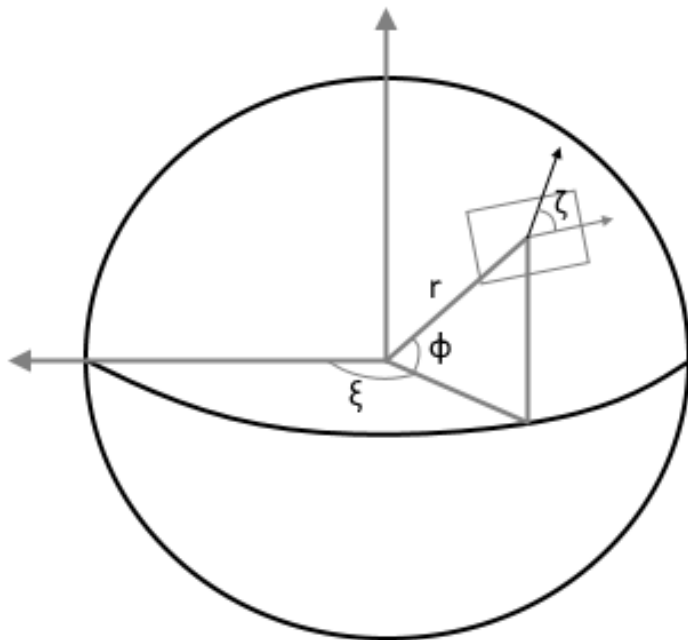


Figure 4.1

more complex, it is no longer possible to obtain an analytical solution.

4.2 The Trajectory Optimal Control Problems

4.2.1 Dynamic Model

The drag and lift produced by each stage of the vehicle are calculated using the standard definition of the aerodynamic coefficients:

$$F_d = \frac{1}{2} \rho c_d v^2 A, \quad (4.2)$$

$$F_L = \frac{1}{2} \rho c_L v^2 A. \quad (4.3)$$

The dynamics of the vehicle are calculated in six degrees of freedom, with pitch constrained to zero. The dynamics of all stages are calculated using an geodetic rotational reference frame, written in terms of the angle of attack α , bank angle η , radius from centre of Earth r , longitude ξ , latitude ϕ , flight path angle γ , velocity v and heading angle ζ . The equations of motion are [28]:

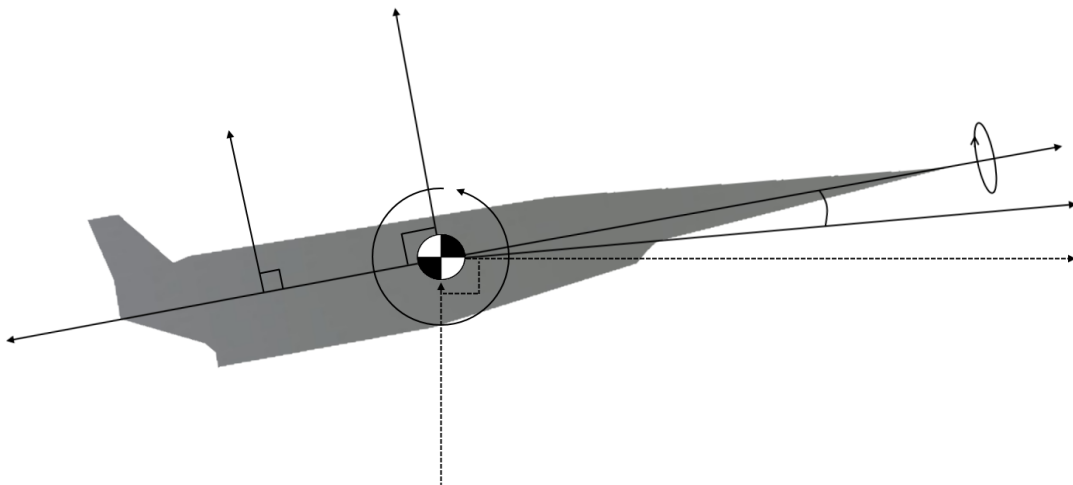


Figure 4.2

$$\dot{r} = v \sin \gamma \quad (4.4)$$

$$\dot{\xi} = \frac{v \cos \gamma \cos \zeta}{r \cos \phi} \quad (4.5)$$

$$\dot{\phi} = \frac{v \cos \gamma \sin \zeta}{r} \quad (4.6)$$

$$\dot{\gamma} = \frac{T \sin \alpha \cos \eta}{mv} + \left(\frac{v}{r} - \frac{\mu_E}{r^2 v} \right) \cos \gamma + \frac{L}{mv} + \cos \phi [2\omega_E \cos \zeta + \frac{\omega_E^2 r}{v} (\cos \phi \cos \gamma + \sin \phi \sin \gamma \sin \zeta)] \quad (4.7)$$

$$\dot{v} = \frac{T \cos \alpha}{m} - \frac{\mu_E}{r^2} \sin \gamma - \frac{D}{m} + \omega_E^2 r \cos \phi (\cos \phi \sin \gamma - \sin \phi \cos \gamma \sin \zeta) \quad (4.8)$$

$$\dot{\zeta} = \frac{T \sin \alpha \sin \eta}{mv} - \frac{v}{r} \tan \phi \cos \gamma \cos \zeta + 2\omega_E \cos \phi \tan \gamma \sin \zeta - \frac{\omega_E^2 r}{v \cos \gamma} \sin \phi \cos \phi \cos \zeta - 2\omega_E \sin \phi \quad (4.9)$$

Flow chart of modules details of simulation (5DOF geodetic rotational) details of limits

verification methods -hamiltonian/costates -complementary conditions -forward sim (for sanity checking, will need to detail deficiencies in this) -forward integration -logic check (ie solver is still a heuristic process, run multiple times with varying guess. Is solution logical?)

- outline the pseudospectral method, as implemented in GPOPS? ie with stage definitions

4.2.2 Trajectory Connection Points

The optimisation of a large, nonlinear system is a complex and time-consuming task. The optimisation of the trajectory of the rocket-scramjet-rocket launch system considered in this study is an extremely

Section	Initial Constraint	End Constraint
1 st Stage Vertical Ascent (I-II)	Constrained to start at a velocity of 0m/s.	Constrained to fly to 90m altitude and 30m/s velocity.
1 st Stage Pitching Ascent (II-III)	Constrained to start at 90m altitude and 30m/s velocity	Constrained entirely to 2 nd stage initial conditions
2 nd Stage Ascent (III-IV)	Constrained to 1520m/s velocity.	Constrained to 102.0° heading angle, the approximate angle which allows the third stage to reach sun synchronous orbit.
2 nd Stage Return (IV-VI)	Constrained entirely to 2 nd stage ascent end conditions.	Constrained to conditions approaching landing at the initial launch site.
3 rd Stage Ascent (IV-V)	Constrained entirely to 2 nd stage ascent end conditions.	Flight parallel with Earth's surface.
3 rd Stage Hohmann Transfer (V)	Constrained entirely to 3 rd stage ascent end conditions.	Constrained to sun synchronoud orbit.

Table 4.1

complex problem, if simulated in its entirety. It is a potentially unmanageable task to produce an optimised trajectory by considering the entire launch trajectory as a single nonlinear programming problem. To mitigate the complexity of the simulation, the trajectory of the rocket-scramjet-rocket launch system has been broken down into subsections, shown in Figure 4.3. These contiguous subsections are then able to be analysed and optimised independently. The subsections of the trajectory are connected through the use of initial and end constraints on the independent optimisation problems. These constraints are described in Table ??.

4.2.3 First Stage Trajectory

LODESTAR is able to optimise the first stage of a launch vehicle, for an angle of attack controlled trajectory, from launch to a pre-defined end point. LODESTAR is able to optimise for either a maximum velocity or minimum mass optimisation objective.

A maximum velocity case is desired when a specific first stage vehicle design is being investigated.

A minimum mass objective is applicable when the first stage trajectory has a pre-defined end goal. This is the case with the SPARTAN vehicle where the SPARTAN scramjet accelerator is to be released at its minimum operating conditions at close to horizontal flight. A variable mass for the first stage launch vehicle is desired as the mass has large effects on the dynamics of th vehicle, effecting the trajectory angle change rate, as well as the acceleration and time of flight of the vehicle. It is useful in the preliminary design stages to be able to optimise the mass of the first stage vehicle, allowing a less trial-and-error approach. In the minimum mass case, the launch altitude is slightly variable, as LODESTAR starts optimisation from a set pitchover altitude and velocity, and the pre-pitchover

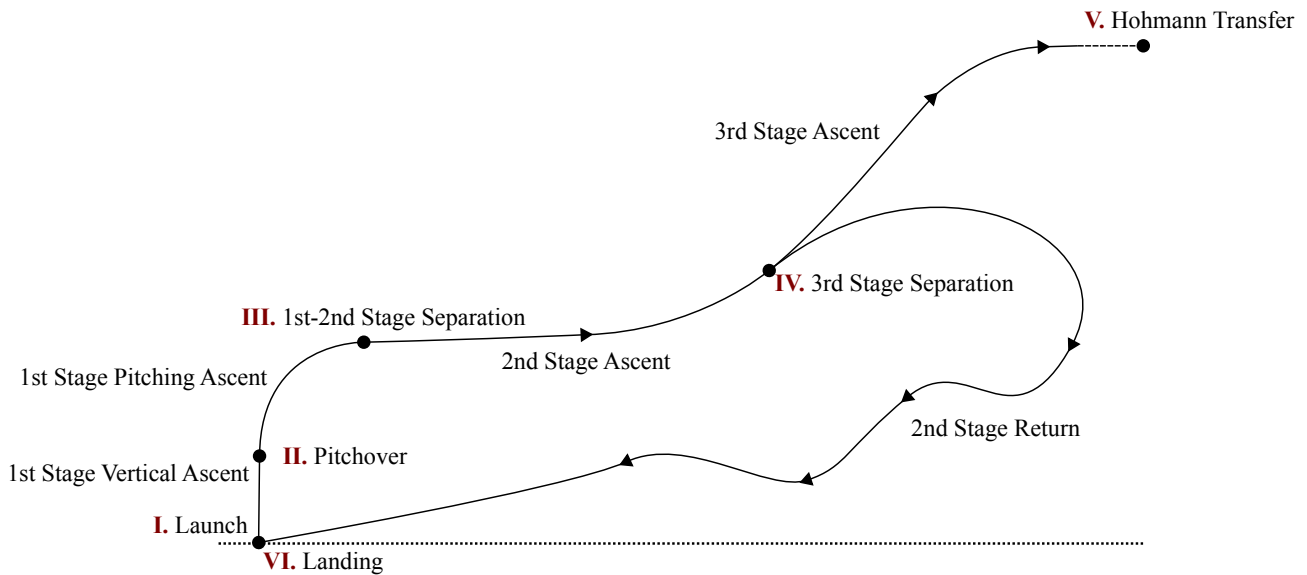


Figure 4.3

trajectory is calculated to match the pitchover mass.

Input	Contains
Aerodynamic Database	

The first stage is launched from an area in northern Queensland.

Initial Constraints	
Terminal Constraints	
Path Constraints	
Target Cost	

Control Variables

Primal Variables

4.2.4 Second Stage Trajectory

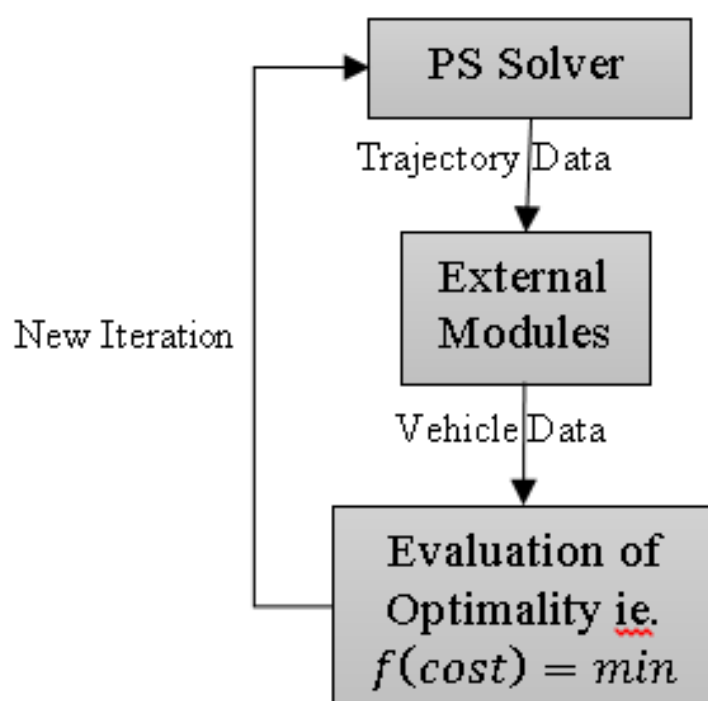


Figure 4.4

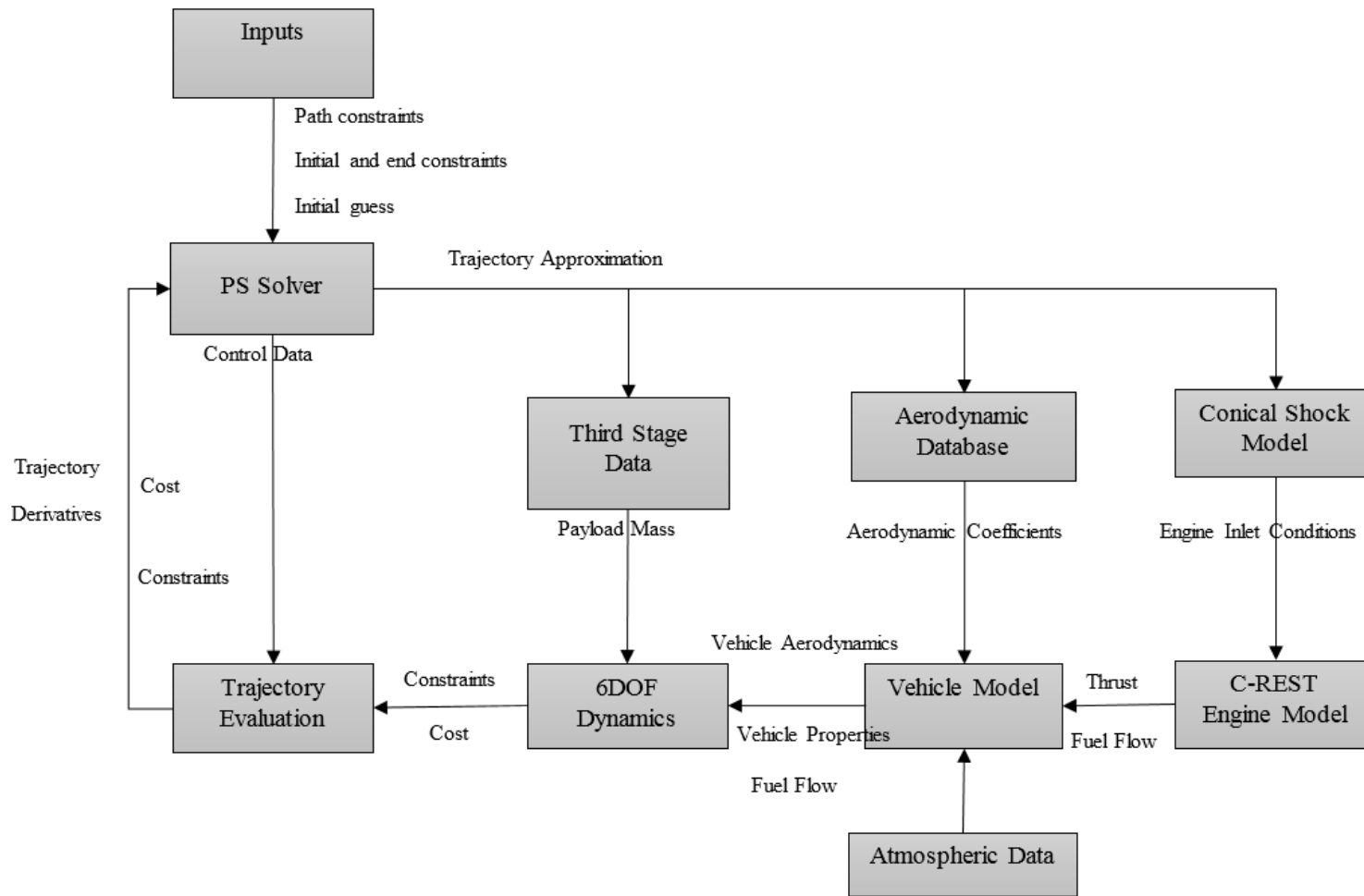


Figure 4.5

LODESTAR is able to optimise the trajectory of airbreathing accelerators in the supersonic or hypersonic regime. LODESTAR is able to optimise for a range of optimisation metrics, including a maximum payload-to-orbit and constant dynamic pressure. The trajectory of the SPARTAN scramjet-powered accelerator has been simulated in LODESTAR.

Initial Constraints	Velocity Fuel Mass Latitude Longitude
Terminal Constraints	Fuel mass Heading Angle
Path Constraints	Dynamic Pressure
Target Cost	Maximum Payload-to-Orbit

Control Variables

Primal Variables

primal variable limits:

4.2.5 Second Stage Return Trajectory

After releasing the third stage rocket, the scramjet-powered second stage must return back to an area close to the initial launch site. During the flyback, the SPARTAN cannot exceed its dynamic pressure limit of 50kPa. The SPARTAN must land on the ground with minimum velocity, within close proximity to the launch area. It is assumed that a landing strip is available at the spot where the SPARTAN lands. The SPARTAN is required to land within a set radius of the launch site. This constraint is;

$$(\phi_{end} - \phi_{launch})^2 + (\xi_{end} - \xi_{launch})^2 - r^2 \leq 0 \quad (4.10)$$

Summary Table

Initial Constraints	Altitude Velocity Flight Path Angle Heading Angle Latitude Longitude
Terminal Constraints	Distance From Launch Site
Path Constraints	Dynamic Pressure
Target Cost	Minimum End Velocity

Control Variables

4.2.6 Third Stage Trajectory

-detail the vehicle dynamics with a free body diagram

Input	Contains
Aerodynamic Database	Mach Number, AoA, CA, CN, CD, CL, cP
Output	Contains

The third stage is required to deliver the payload into heliosynchronous orbit. The heliosynchronous orbit chosen is 566.89km.

Initial Constraints	
Terminal Constraints	
Path Constraints	Angle of Attack
Target Cost	

The third stage trajectory angle is initiated at a heading angle of 102.0° . This is chosen as the heading angle which allows the third stage to closely match the required orbital inclination angle for sun synchronous orbit at 567km, of 97.63° .

-Detail the hohmann transfer

Control Variables

4.2.7 Combined Second Stage Ascent & Return Trajectory

4.2.8 Validation

Optimality Conditions

LODESTAR provides the capacity to partially validate the optimal solution provided by the pseudospectral method solver. This partial validation is used to determine whether the pseudospectral method solver has converged close to an optimal solution of the nonlinear programming problem. It is particularly useful to validate that the optimality and constraint tolerances which have been chosen are sufficiently small, or to check whether the pseudospectral method solver has approached an optimal solution in the case that the defined tolerances are not able to be reached. This partial validation is achieved through the examination of some of the necessary conditions for optimality. The necessary conditions

The control Hamiltonian is investigated to verify that the first order necessary conditions hold. Due to the unconstrained end time of the trajectory problems, $H \equiv 0$ [Pucci2007]. The Hamiltonian is defined as: $H(x(t), u(t), \lambda(t), t) = \lambda^T(t)f(x(t), u(t)) + L(x(t), u(t))$. Make sure this is consistent with format in lit review, link This is calculated using LODESTAR and the Hamiltonian condition

is able to be verified. The Hamiltonian will likely not be exactly equal to zero along the trajectory. This is due to the heuristic nature of the solver, which will approach close to an optimal solution, but never reach it exactly. A sufficiently small Hamiltonian indicates that the end solution approaches an optimal solution, and may be a candidate as an optimised trajectory case.

Costates Complementary conditions

To assess the quality of the optimisation problem solved using the pseudospectral method,

The primal feasibility of the solution is checked through a comparison of the state derivatives, $\dot{x} = f(x, u)$. \dot{x} is first determined through numerical differentiation of the primal variables over the solution time. Then $f(x, u)$ is determined using the dynamics of the system and vehicle model, in the same way that $f(x, u)$ is input to the pseudospectral solver. Examination of the error between the 'expected' state derivatives, and the numerical approximation of the derivatives, $\dot{x} - f(x, u)$, allows the accuracy of the system dynamics to be verified.

GPOPS - output.result.solution.phase.pathmultipliers I believe these should be 0, as they are the mu associated with path constraints (and the function C;0, meaning mu=0)

output.result.solution.phase.costate gives costates, not sure how to use these

include IPOPT infeasibilities infpr and infdu (need to mention GPOPS-2 is based on IPOPT)

Forward Simulations

-both the control check and derivative check

The pseudospectral method considers the dynamics of the system as constraints on the optimal control problem, and solves across the entire trajectory simultaneously. This causes the physical system dynamics to have an associated margin of error, ie. $\dot{x} = f(x)$ will only hold to a certain degree of accuracy. For a well converged solution, this margin of error will be negligibly small, and the dynamics of the system will be consistent with realistic Newtonian dynamics. However, when the problem is not well converged, the dynamics of the system may have a large error. It is possible to make a preliminary check of the system dynamics using the XX (complementary conditions?). However, to be certain that the system is behaving as it should be, a full forward simulation is necessary. This forward simulation starts at the initial conditions prescribed by the pseudospectral method solver, and propagates the dynamics of the system forward in time using numerical approximation. The forward simulation uses only inputs of the control sequence, as solved for by the pseudospectral method.

CHAPTER 5

ASCENT TRAJECTORY

- keep this DIDO and hypaero and direct shooting

-explain why I moved to other GPOPS and CART3D at the end of the chapter

This chapter presents an optimised ascent trajectory of the three stage rocket-scramjet-rocket system. First the third stage trajectory optimised for maximum payload-to-orbit, and results tabulated for a range of second-third stage release points. Then, the second stage trajectory is optimised for maximum payload-to-orbit. The third stage payload-to-orbit database is used as the optimisation cost for the second stage, by interpolating for the release point obtained at the end of the trajectory. The first stage trajectory is optimised last. The first stage is optimised for the minimum fuel required to reach the first to second stage release point defined by the second stage optimal trajectory. The reason for using a different objective for the first stage is that the first stage mass defines the ability of the first stage to turn, as well as the amount that it can accelerate. If the first stage design is set, it will define much of the optimal trajectory for the second stage.

The following trajectories are studied in this chapter:

1. : $q = 50\text{kPa}$ fixed SPARTAN trajectory with minimum pull-up

→ Verifies simulation and provides baseline trajectory.

2. : Trajectory optimised for payload-to-orbit, $q_{max} = 50\text{kPa}$

→ Demonstrates improved performance through coupled trajectory optimisation.

3. : Trajectory optimised for payload-to-orbit, $q_{max} = 45\text{kPa}$ & $q_{max} = 55\text{kPa}$

→ Comparison of these simulations allows investigation into the effect of q max on payload-to-orbit.

4. : Trajectory optimised for payload-to-orbit, $q_{max} = 50\text{kpa}$, 110% SPARTAN Drag

→ Comparison of optimal trajectories at 100% and 110% drag allows investigation of the robustness of the solution with variation in vehicle design.

Table 5.1 details key results for comparison.

Table 5.1: Summary of Simulation Results

Trajectory Condition	1 $q = 50\text{kPa}$ $\gamma_{2 \rightarrow 3} = 1.5^\circ$	2 $q \leq 50\text{kPa}$ Max $m_{Payload}$	3a $q \leq 45\text{kPa}$ Max $m_{Payload}$	3b $q \leq 55\text{kPa}$ Max $m_{Payload}$	4 $q \leq 50\text{kPa}$ Max $m_{Payload}$ 110% C_D
Payload to Orbit (kg)	156.8	169.9	163.9	176.4	161.8
Separation Alt, 1→2 (km)	24.4	25.0	25.6	24.0	25.3
1st Stage Structural Mass Fraction	.0737	.0732	.0728	.0744	.0735
Separation Alt, 2→3(km)	33.17	34.49	34.46	34.58	34.29
Separation v, 2→3(m/s)	2905	2881	2861	2893	2829
Separation γ, 2→3(deg)	1.50	2.91	2.31	3.39	2.97
Separation q, 2→3(kPa)	46.3	36.9	36.59	36.71	36.7
2nd Stage L/d, 2→3	3.21	3.24	3.35	3.34	2.94
2nd Stage Flight Time (s)	349.1	357.0	381.8	326.8	356.9
3rd Stage t, $q > 20\text{kpa}$ (s)	65	29	25	23	27

5.1 Third Stage trajectory

5.1.1 Third Stage Optimisation Methodology

-Details on methodology -outline the limits that I put on it (ie cant go below starting altitude) -I should maybe run a case without these limits to show the difference -outline necessity for differing guess (will need to cite this as a regularly used process)

The third stage rocket trajectory is optimised for maximum payload-to-orbit, so that the second stage scramjet and third stage rocket form a Bolza optimisation problem and maximise payload collectively. The cost function is configured to maximise payload at the end of the trajectory:

$$\min_{\mathbf{u}_3} C_{3 \rightarrow LEO}(\mathbf{x}_3(t_{3,f})) \quad (5.1)$$

where

$$C_{3 \rightarrow LEO}(\mathbf{x}_3(t_{3,f})) = -m_{payload}, \quad (5.2)$$

and $\mathbf{x}_3(t_{3,f})$ are the tabulated separation conditions of altitude, velocity, and trajectory angle. A direct shooting optimisation is performed with twenty angle of attack node points, interconnected by spline interpolation from separation, $t_{3,0}$, to a variable end time, $t_{AoA,f}$. At this time, the angle of attack is gradually reduced, so that it reaches 0 at the end of burn time, $t_{burn,f}$, also variable. A constraint is

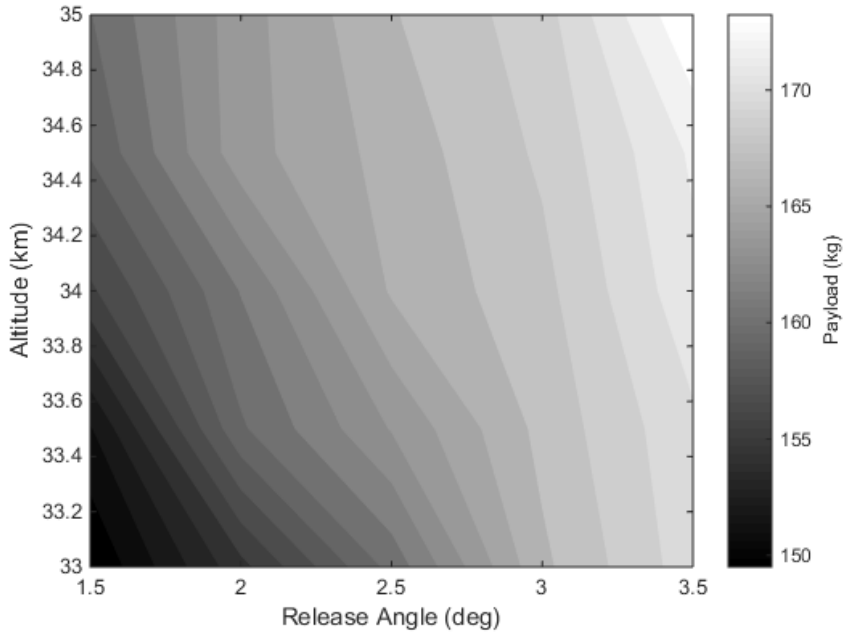


Figure 5.1

imposed so that the angle of attack must have at least 10 seconds to reduce to 0 at end of burn, ie. $t_{burn,f} - t_{AoA,f} \geq 10$, to allow time for manoeuvring.

The payload mass is calculated after the Hohmann transfer to the desired orbit, by taking the remaining fuel to be the effective payload capacity. Sequential quadratic programming (SQP) is used to find the optimal solution, utilising MATLAB's *fmincon* solver. As an example, tabulated optimal payload to orbit results for a 2875m/s third stage release velocity are shown in Figure 5.1. Payload increases with both altitude and release angle, however it is clear that the potential payload increase due to increasing the separation altitude lessens as release angle increases.

5.1.2 Third Stage Optimisation Results

Third stage trajectories for release angles of 1.50° and 2.91° are shown in Figures 5.2 and ???. These trajectories correspond to third stage release points at the end of a constant dynamic pressure trajectory with minimum pull-up (as shown in Section ??) and an optimised 50kPa limited trajectory (as shown in Section ??). These third stage trajectories show a pull-up to high altitude before the circularisation burn is performed.

The third stage released at 1.5° , shown in Figure 5.2, is limited by the maximum thrust vector angle for the first 47s of flight. This places significant limitations on the maximum allowable angle of attack. This angle of attack limitation reduces the lift of the rocket, causing it to spend a large amount of time at low altitude, in a high drag environment. The angle of attack increases gradually to a maximum of 17.6° at 66s before decreasing until burnout at 140s.

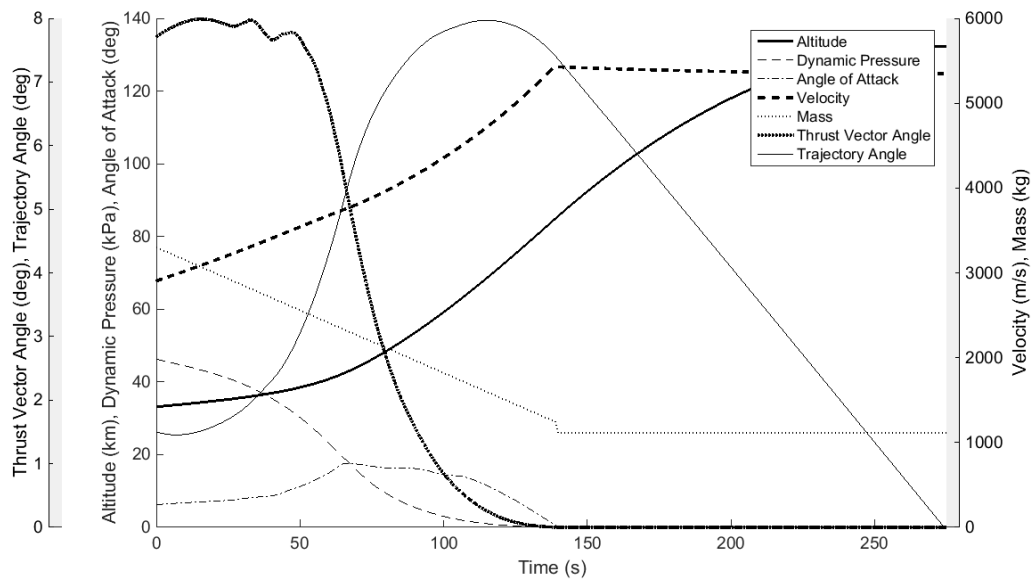


Figure 5.2

The release of the third stage rocket from an optimised scramjet trajectory is shown in Figure ???. Release at a higher, more optimal angle, mitigates the effects of the thrust vector angle limitation, so that the thrust vector limit is only reached during the first 10s flight time. After this, the angle of attack is limited by the maximum allowable normal force rather than the thrust vector limit, resulting in a higher maximum angle of attack. The rocket increases trajectory angle and gains altitude rapidly, resulting in less time spent in a high drag environment, and a larger payload to orbit. The angle of attack is increased gradually to 18.14° at 48s, before decreasing until burnout at 138s.

5.2 SPARTAN trajectory

- constant q -45kPa, 50kPa and 55kPa limited trajectories -high drag trajectory
- it might be interesting to compare different third stage rocket engines

Second Stage Optimisation - Constant Dynamic Pressure, Minimum Pull-Up

The constant dynamic pressure case with minimum pull-up optimises the trajectory to minimise variation from the desired dynamic pressure, with the third stage release angle constrained to 1.5° , approximately the minimum release angle necessary to reach orbit. This constraint results in a trajectory with the smallest possible pull-up manoeuvre. The trajectory is configured with a quadratic cost function centred around 50kPa dynamic pressure:

$$\min_{\mathbf{u}_2} C_2(\mathbf{x}_2(t_2), \mathbf{u}_2(t_2)) \quad (5.3)$$

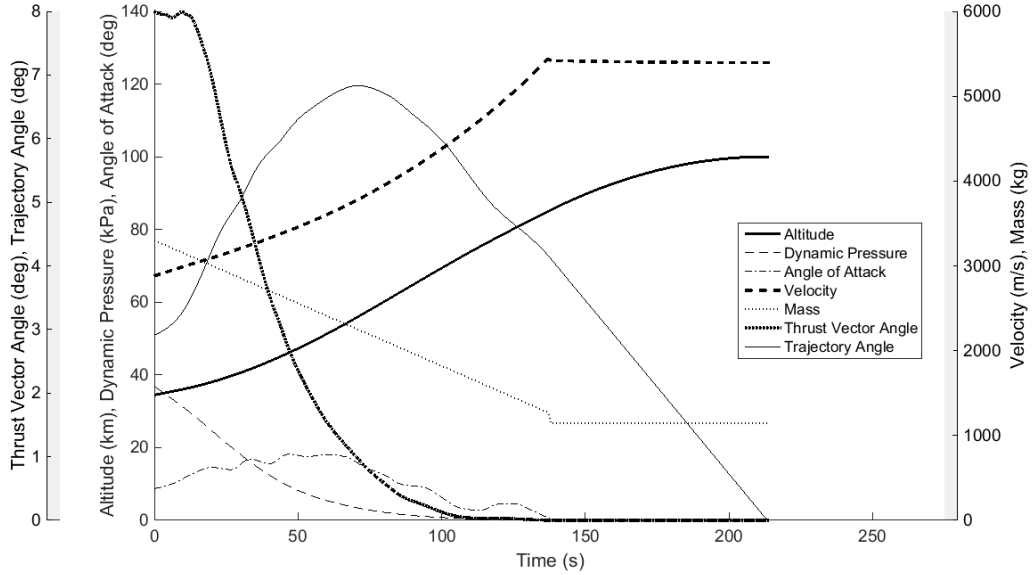


Figure 5.3

where

$$C_2(\mathbf{x}_2(t_2), \mathbf{u}_2(t_2)) = \int_{t_{2,0}}^{t_{2,f}} \frac{(\mathbf{q} - 50 \times 10^3)^2 + 10^5}{10^5} dt \quad (5.4)$$

This quadratic function provides a smooth, continuous function to increase solver stability and ensure uniform dynamic pressure. Second-third stage separation occurs when the scramjet has expended all of its fuel. The third stage is then optimised for maximum payload from the calculated second-third stage separation point.

Second Stage Optimisation - Maximised Payload

For the maximum payload optimisation, the second and third stages are considered using a dynamic programming approach. First, in order to increase the computational efficiency of the optimisation, optimal third stage payloads are tabulated over a 3 degree grid of separation conditions, $\mathbf{x}_2(t_{2,f})$, as described in Section ??, providing the optimal payload for a range of velocity, altitude and trajectory angles at separation as shown in Figure 5.1. Then, the interpolated third stage payload is used as the terminal cost $C_{2 \rightarrow 3}(\mathbf{x}_2(t_{2,f}))$ for the calculation of the second stage trajectory optimisation, which optimises both the second and third stages by setting the cost function to maximise payload:

$$\min_{\mathbf{u}_2} C_2(\mathbf{x}_2(t_2), \mathbf{u}_2(t_2)) + C_{2 \rightarrow 3}(\mathbf{x}_2(t_{2,f})) \quad (5.5)$$

where

$$C_2(\mathbf{x}_2(t_2), \mathbf{u}_2(t_2)) = 0.01 \int_{t_{2,0}}^{t_{2,f}} \dot{m}_{fuel} dt \quad (5.6)$$

$$C_{2 \rightarrow 3}(\mathbf{x}_2(t_{2,f})) = -m_{payload}. \quad (5.7)$$

$C_2(\mathbf{x}_2(t_2), \mathbf{u}_2(t_2))$ is included to improve numerical stability and is chosen to have negligible effect on the resultant trajectory. This problem is solved using the pseudospectral method [55]. The third stage is optimised for maximum payload from the calculated second-third stage separation point, as a check to ensure that the interpolation has provided an accurate payload-to-orbit result.

5.2.1 Constant Dynamic Pressure - Minimum Pull-up

A constant dynamic pressure trajectory with a pull-up to 1.5° trajectory angle at third stage release is produced as a baseline for comparison with a payload-optimised trajectory, and to verify that LODESTAR is able to optimise a complex airbreathing trajectory. A pull-up to 1.5° trajectory angle is the minimum necessary for the third stage to reach orbit. At release angles below 1.5° , the thrust vector limitations necessary to produce a trimmed trajectory constrain the angle of attack of the third stage so that the rocket does not generate the lift required to exit the atmosphere. This angle of attack limitation, imposed by the maximum thrust vector, necessitates a scramjet-stage pull-up manoeuvre in order for the third stage rocket to operate successfully.

The constant dynamic pressure, minimum pull-up trajectory for the SPARTAN stage is shown in Figures ??, ?? and ?? with key results summarised in Table 5.1. Due to the clear objective of a constant dynamic pressure trajectory, any deviations from the target dynamic pressure are readily apparent, allowing the efficacy of the optimiser to be verified. These results show very close adherence to 50kPa dynamic pressure (maximum 0.29% deviation) until pull-up at 336.4s. Third stage release occurs at 349.1s at 33.17km altitude. Over the trajectory the Mach no. increases from 5.10 to 9.52 and the velocity from 1520m/s to 2905m/s. The flap deflection shows an overall increase from -0.53° to 5.76° over the trajectory. The net specific impulse ($I_{sp,net} = \frac{T-F_d}{m_{fg}}$) generally decreases over the trajectory, as the efficiency of the scramjet engines decreases. However, at the beginning of the trajectory the equivalence ratio increases as the capture limitations are relaxed with increasing Mach number. This causes the net specific impulse to increase, to a maximum of 1739s, during the first 19.45s flight time.

Figure 5.2 shows the corresponding third stage atmospheric exit trajectory after release, evaluated as described in Section ???. After atmospheric exit, this trajectory is followed by a Hohmann transfer to a heliosynchronous orbit, resulting in a total payload to orbit of 156.8kg.

Optimality Validation

5.2.2 Optimal Payload

LODESTAR is configured to optimise the total payload mass to orbit. A maximum dynamic pressure limit of 50kPa is applied to the optimisation process to allow direct comparison with the constant q

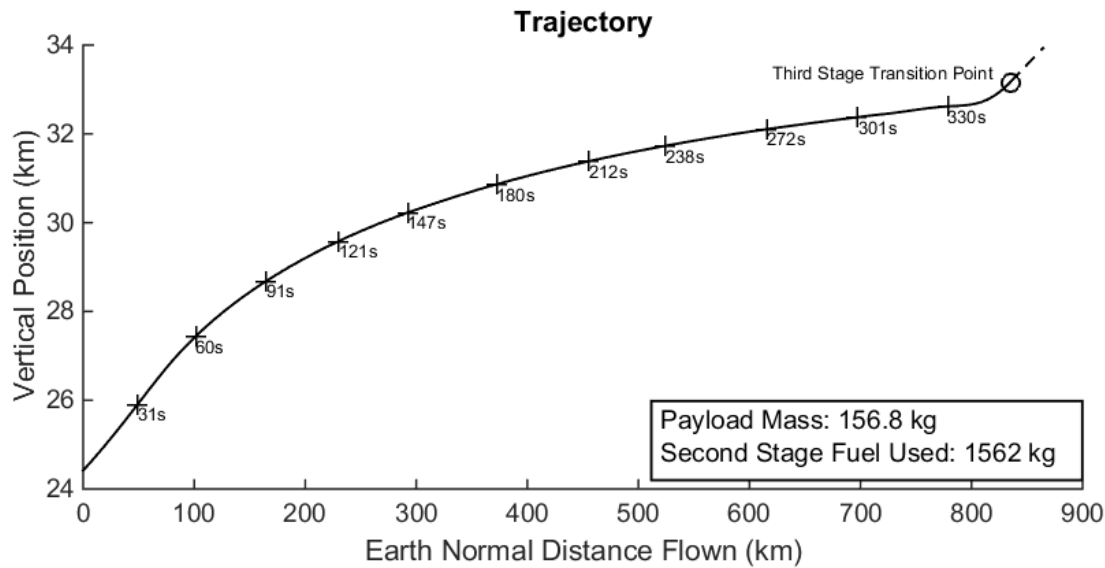


Figure 5.4

trajectory and so that an equivalent vehicle can be used.

The optimal trajectory shape for a $q = 50\text{kPa}$ limited, maximum payload to orbit trajectory is shown in Figures ??, ?? and ?? with key results summarised in Table 5.1. The equivalence ratio of the engine is less than 1 until 52.77s, causing the SPARTAN to fly under 50kPa in this region (to a minimum of 40.8kPa) in order to raise equivalence ratio by flying in a higher temperature region. This increase in equivalence ratio results in a corresponding increase in net specific impulse. After the equivalence ratio increases to 1, the trajectory follows a constant dynamic pressure path at 50kPa until 331.7s at which point a pull-up manoeuvre is performed, gaining altitude until rocket stage release at 357.0s flight time. This trajectory is able to deliver 169.9kg of payload to heliocentric orbit, an increase of 8.35% over the constant dynamic pressure result with minimum pull-up. The point at which the pull-up manoeuvre begins is the optimisation result that takes into account the best combination of velocity, altitude and release angle for scramjet stage performance and the release of the rocket stage. This pull-up indicates the region at which increasing altitude and release angle becomes more important than extracting maximum thrust from the scramjet (which is attained at high q and low flight angle at an equivalence ratio of 1). Flight in a lower dynamic pressure environment results in less thrust output from the scramjet engines, as well as an increase in angle of attack and flap deflection angle to compensate for the additional lift required. Due to this, less overall acceleration is obtained compared to the constant dynamic pressure result with minimum pull-up. Separation occurs at a velocity of 2881m/s, a decrease of 24m/s. However, at the same time separation altitude increases by 1.32km to 34.49km, resulting in a decrease in separation dynamic pressure to 36.9kPa.

The larger scramjet stage pull-up assists the rocket in manoeuvring to exoatmospheric altitude by increasing the altitude and angle at separation by virtue of the increased L/D ratio and manoeuvra-

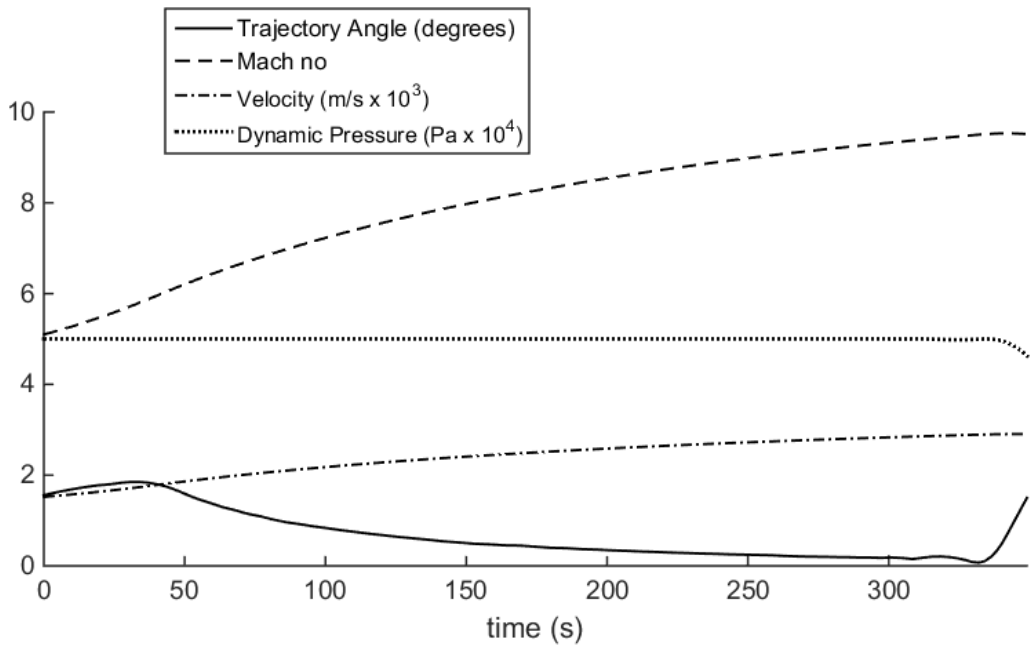


Figure 5.5

bility of the scramjet vehicle. Even a small increase in release angle, to the optimal angle of 2.91° , significantly reduces the turning that is required by the rocket as evident from comparing Fig 5.2 and ???. Further benefits are the reduced time that the rocket must spend in a high dynamic pressure environment, and a decrease in the maximum dynamic pressure that the rocket stage experiences by 20.3%, as shown in Table 5.1. This allows the structural mass and heat shielding, necessary to achieve exoatmospheric flight, to be decreased, enabling higher payload to orbit.

Compared to studies considering vehicles with a scramjet-rocket transition within a single stage [34][67], the maximum payload to orbit trajectory of the multi-stage system shows a scramjet-rocket transition point at much lower altitudes. This lower transition point is a consequence of the stage separation creating an energy trade-off, which does not occur in a single stage vehicle. Single-stage vehicles must necessarily transport all components to exoatmosphere, and so utilise the scramjet engines until higher altitude to take advantage of their high efficiency. A multi-stage vehicle is able to separate the scramjet stage. This separation occurs when the performance benefits provided by the superior aerodynamics and engine efficiency of the scramjet stage are offset by the energy required to lift the extra mass to higher altitude. The beneficial ability to separate the scramjet stage results in a lower altitude scramjet-rocket transition point, when compared to single stage vehicle designs.

5.2.3 Maximum Dynamic Pressure Variation

To investigate the sensitivity of the vehicle to changes in q_{max} , the maximum dynamic pressure is varied to 45kPa and 55kPa and the flight trajectory optimised, with results shown in Figures ???,

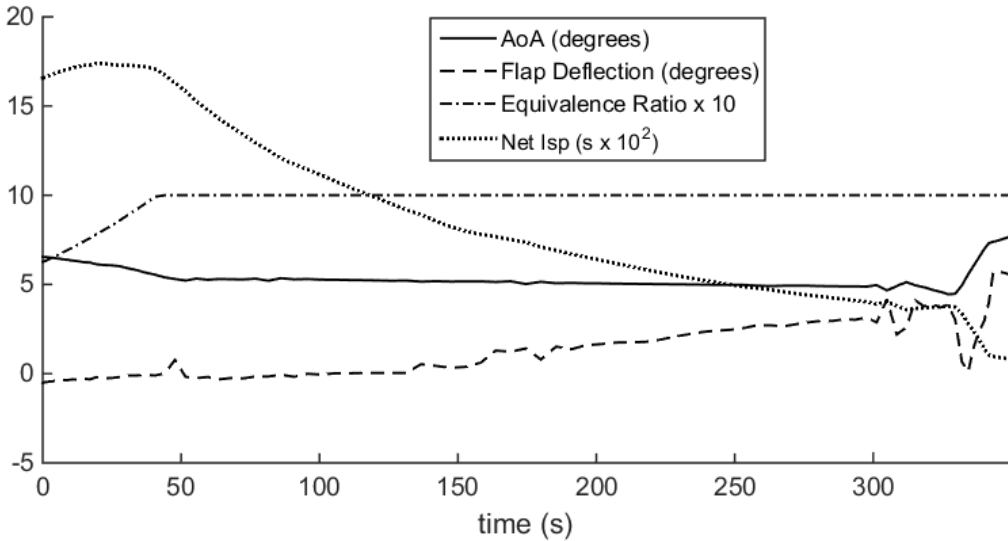


Figure 5.6

?? and ?? and summarised in Table 5.1. The $\pm 10\%$ variation in maximum dynamic pressure has very little effect on the payload mass delivered to heliocentric orbit. Varying the maximum dynamic pressure by $\pm 5\text{kPa}$ from 50kPa causes a variation of only $+6.5\text{kg}(+3.8\%)$ or $-6.0\text{kg}(-3.5\%)$ in payload to orbit. Separation altitudes of 34.46km and 34.58km are reached for 45kPa and 55kPa limited cases respectively, with separation velocities of 2861m/s and 2893m/s . The 45kPa limited case flies for 381.8s , significantly longer than the 55kPa case which flies for 326.8s . Both trajectories pull-up to similar altitudes, with relatively small variation in separation velocity -20m/s or $+12\text{m/s}$). This small variation in velocity is despite the increase in air density and decrease in angle of attack required for flight at 55kPa dynamic pressure, both of which increase the mass flow into the engine. Although the thrust output of the REST engines increases with dynamic pressure, so does the drag on the vehicle, and the net increase in performance is small.

Only small variation in optimal payload mass is observed, without modification of vehicle design to account for the dynamic pressure limit. This indicates that designing and operating a vehicle at lower dynamic pressures may be preferable. Flying at a lower maximum dynamic pressure allows reduction of the structural weight and heat shielding of the vehicle. However, as the 45kPa limited case has a higher first-second stage separation altitude, a larger first stage fuel mass is required, though this increase in fuel mass is small. Between 25.6km and 24.0km (45kPa and 55kPa optimal start points) there is only a 2.2% variation in the fuel mass required. This small variation in first stage fuel consumption would easily be offset by a decrease in second stage structural mass.

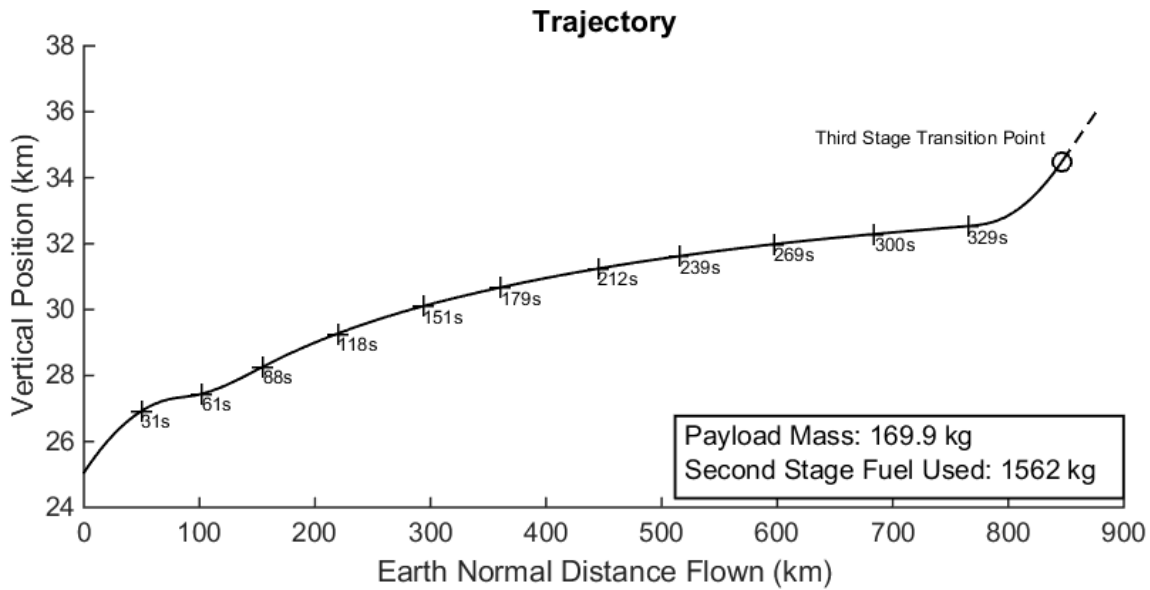


Figure 5.7

5.2.4 Drag Sensitivity Study

To investigate the effect of vehicle design and uncertainty in aerodynamic performance on the optimal trajectory the drag on the vehicle is increased by 10%, and an optimised trajectory calculated with dynamic pressure limited to 50kpa. Selected results are compared to the 100% drag result in Figures ?? and ???. These results show that when drag is increased (ie. L/d is decreased) the optimal trajectory shape is similar to the base-line case, though the high drag second stage follows a slightly slower and hence lower flight path, with a lower stage transition point. The similar flight path shape of the high drag case suggests that sacrificing velocity to increase separation altitude in a pull-up manoeuvre is optimal for multiple vehicle designs. Although the lower transition point indicates that the rocket is favoured at an earlier point in the climb manoeuvre, due to the decreased aerodynamic efficiency of the scramjet vehicle. The net result is a lower payload-to-orbit of 161.8kg (a decrease of 4.8%).

5.3 First Stage Trajectory

multiple release points -fixed mass, optimal velocity -fixed velocity, optimal mass

First Stage Optimisation

After launch, the first stage flies vertically until 100m altitude, when a pitchover is initiated. From pitchover, the first stage is optimised for the minimum fuel mass necessary to reach the first-second stage separation conditions, $\mathbf{x}_1(t_{1,f})$, of 1520m/s velocity, and altitude and flight path angle determined by the second stage trajectory.

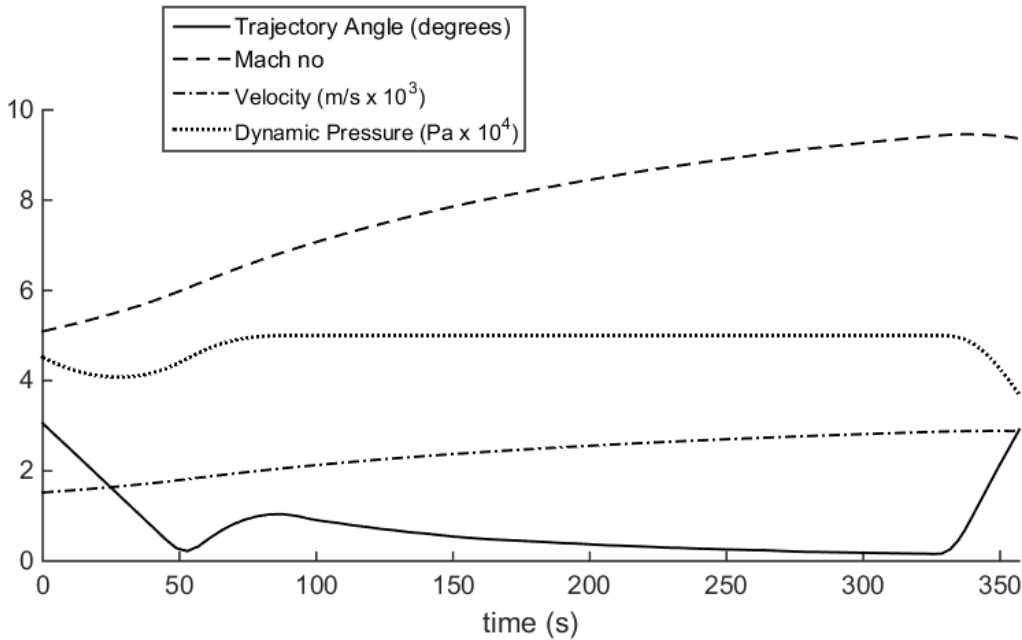


Figure 5.8

The separation velocity of 1520m/s corresponds to Mach 5.1 at 50kPa, the minimum operating point of the proposed scramjet[48]. Release at the minimum operable point is advantageous, as the scramjet specific impulse increases at low velocities[48]. The altitude and flight path angle at first-second stage separation is defined by the optimised second stage. This approach is used on account of the selected first stage being able to reach the required range of altitudes and flight angles at 1520m/s with small fuel mass variations. Nevertheless small variation in fuel mass can have an important effect on the capabilities of the first stage, determining the velocity achievable at first to second stage separation, as well as the rate at which the rocket is able to pitch, and consequentially, the altitude and flight path angle range of the first stage. The optimum (lowest fuel consumption) trajectory for the first stage stack that can reach first-second stage separation condition $\mathbf{x}_1(t_{1,f})$ is found by setting a cost function to minimise fuel mass:

$$\min_{\mathbf{u}_1} C_{1 \rightarrow 2}(\mathbf{x}_1(t_{1,f})) \quad (5.8)$$

where

$$C_{1 \rightarrow 2}(\mathbf{x}_1(t_{1,f})) = m_{fuel} \quad (5.9)$$

and the end point is fixed by the optimal second stage start conditions. The first stage is limited to -5° angle of attack to produce a conservative trajectory solution, within the capabilities of the vehicle. The optimal trajectory is determined using the pseudospectral method.

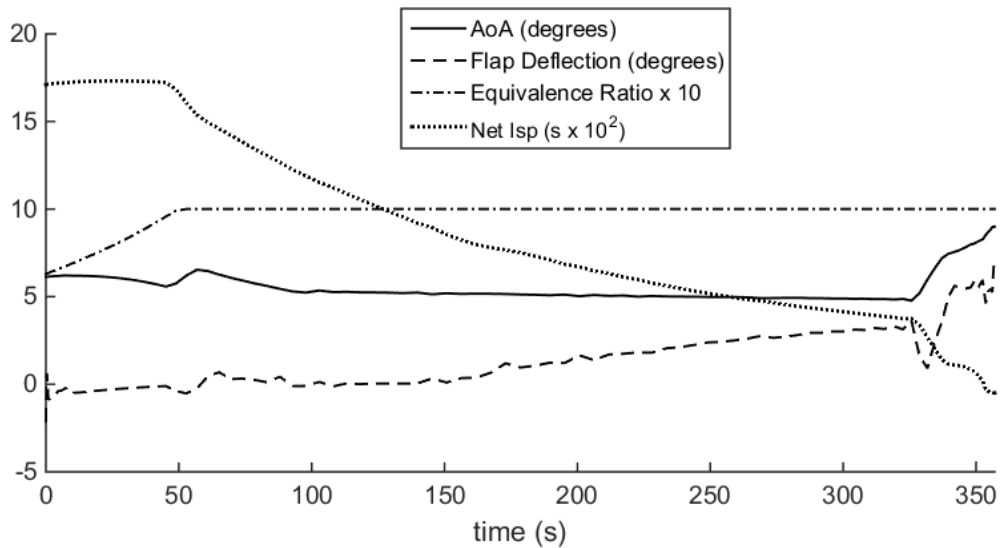


Figure 5.9

5.3.1 First Stage Optimised Trajectory Result

Figure 5.15 shows an example first stage trajectory, optimised for minimum mass, with end conditions of 24.4km altitude and 1.56° trajectory angle. These separation conditions correspond to the second stage separation conditions for a 50kpa dynamic pressure trajectory.

The first stage flies a fixed vertical trajectory for 3.74s, after which a pitchover is initiated. After pitchover the angle of attack reduces gradually to the minimum of -5°, adjusting in stages in order to reach the desired end conditions. An altitude of 24.4km is reached after a total flight time of 94.0s, with a total ground distance of 33.3km covered. This trajectory shape is very similar for all first stage simulation cases.

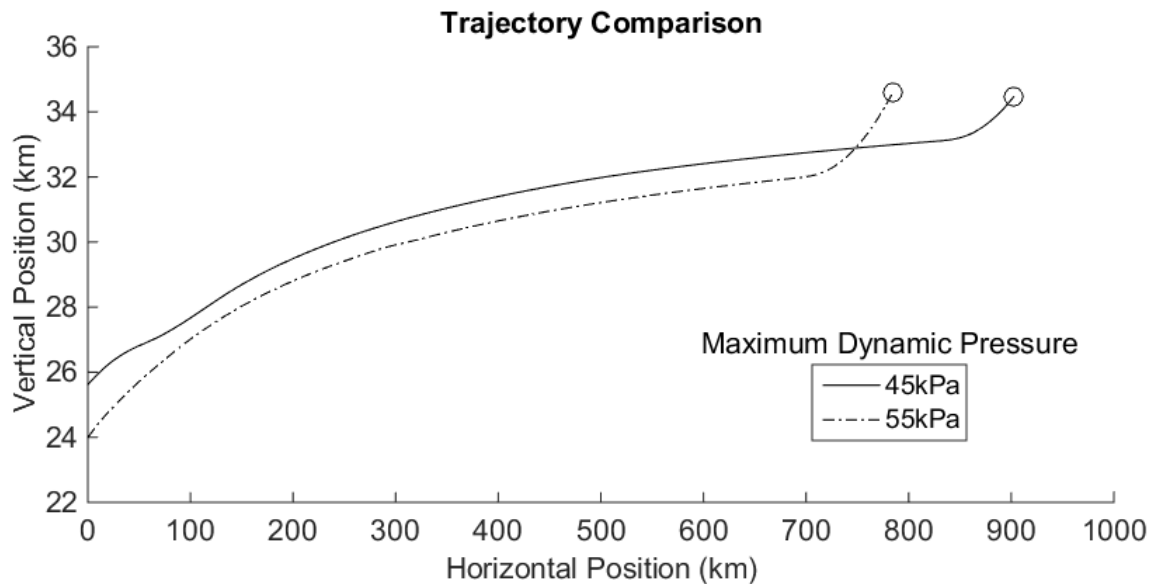


Figure 5.10

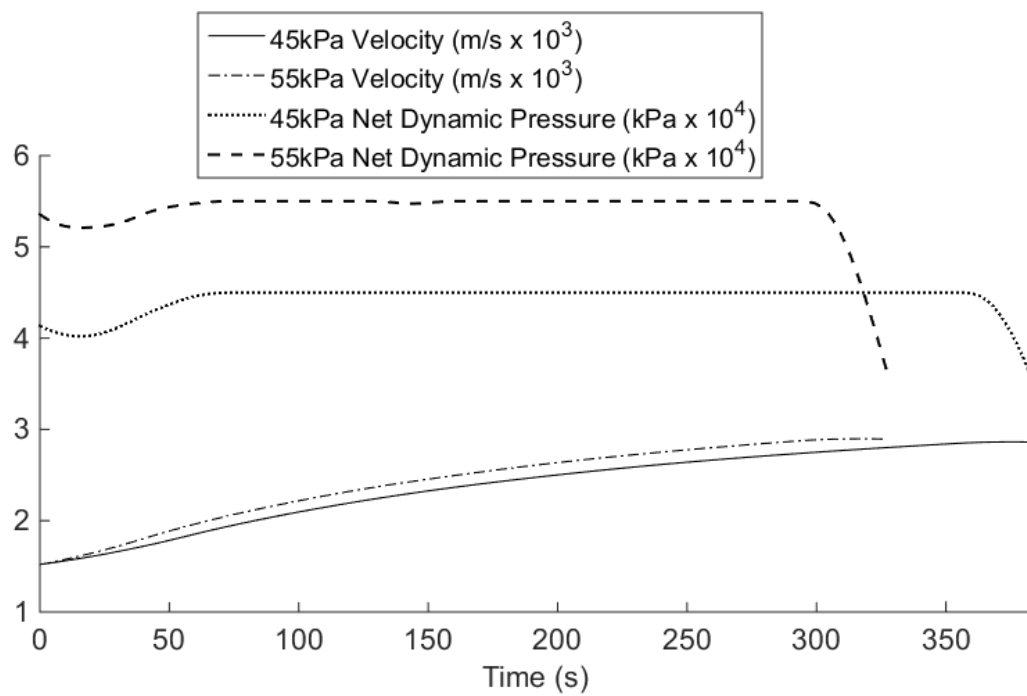


Figure 5.11

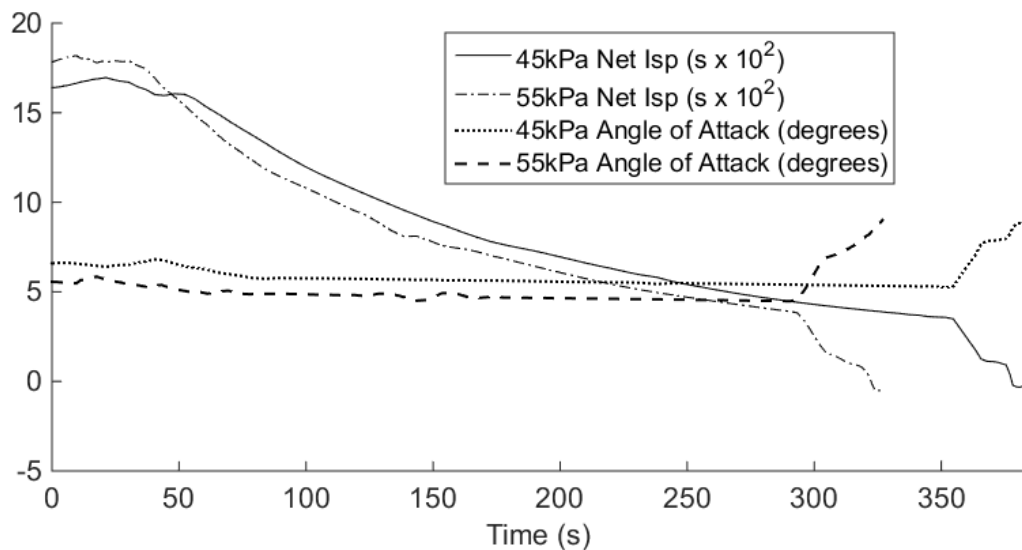


Figure 5.12

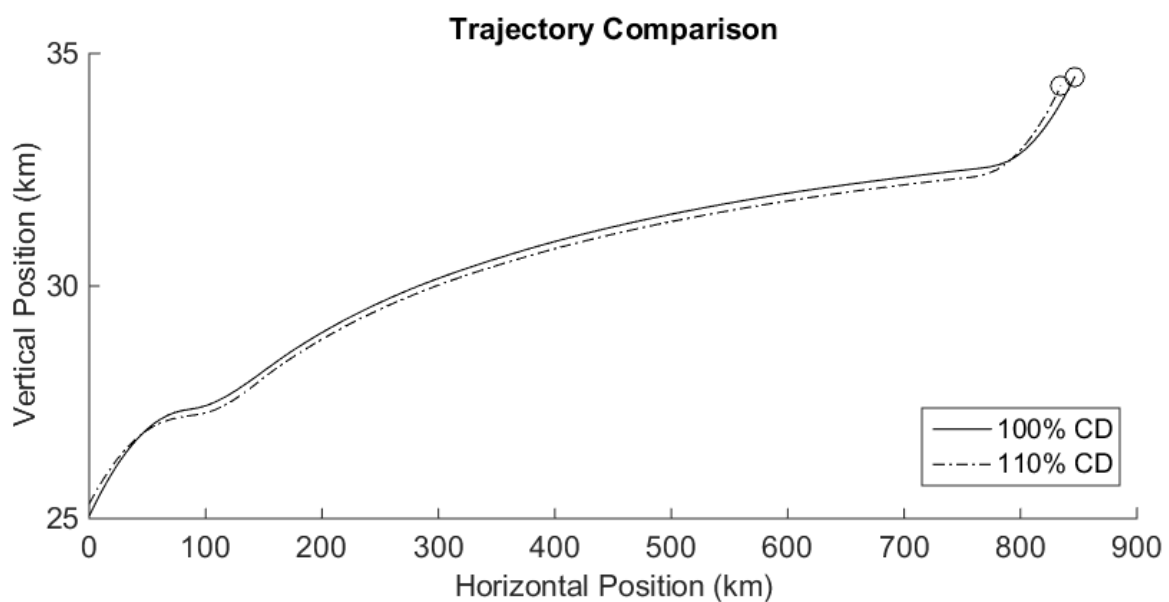


Figure 5.13

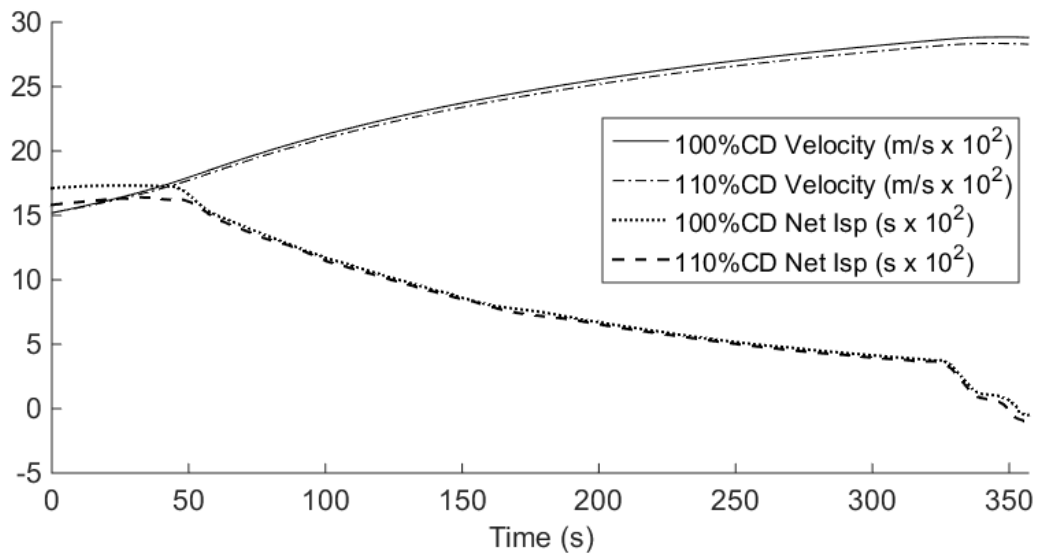


Figure 5.14

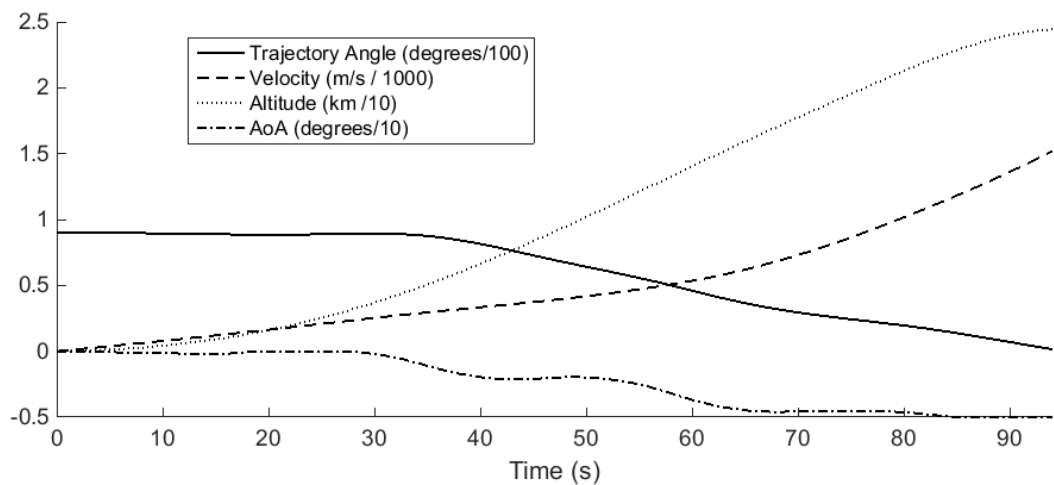


Figure 5.15

CHAPTER 6

TRAJECTORIES INVOLVING FLYBACK

6.1 Flyback trajectories

- Details of bounds & guesses, with reasoning.
- Fuel optimised fly-back of the SPARTAN.

6.2 Sensitivity Analysis

- Details of bounds & guesses, with reasoning.
- Variation of L/D & ISP.
- Heat flux analysis

CHAPTER 7

FULL TRAJECTORY OPTIMISATION

- Details of bounds & guesses, with reasoning.
- Optimisation of the combined ascent and fly-back trajectories of the SPARTAN.
- Potential Abort Analysis

CHAPTER 8

THIRD STAGE SIZING STUDY

- I need to frame this well, so that it does not seem to invalidate my previous work
 - Variation of third stage design, changing width, length, thrust, CL and CD of the third stage, and recalculating optimised trajectories.
 - Determine the optimal sizing of the third stage
 - Analyse the variation in the optimal trajectory with variation in third stage design

CHAPTER 9

CONCLUSIONS

- The optimal ascent trajectory for the rocket-scramjet-rocket three stage launch system involves a pull-up before third stage release.
- The optimal fly-back of the SPARTAN involves several distinct stages, including a boost phase, skip phase and glide phase.
- Description of conclusions from the combined ascent/fly-back trajectory. The combined ascent and fly-back trajectory involves the SPARTAN banking during ascent, to mitigate the distance flown during the ascent trajectory.
- Summary of conclusions from third stage sizing analysis.

9.1 Recommendations for future work

- Design optimisation incorporating trajectory optimisation.
- Sizing of entire system for optimal cost efficiency.

REFERENCES

- [1] Xcor Aerospace. *Lynx Sspacecraft*. 2017. URL: <https://xcor.com/launch/lynx-spacecraft/> (visited on 11/30/2017).
- [2] Michael J. Aftosmis, Marian Nemec, and Susan E. Cliff. “Adjoint-based low-boom design with Cart3D”. In: *29th AIAA Applied Aerodynamics Conference 2011*. June. 2011, pp. 1–17. ISBN: 9781624101458. DOI: [10.2514/6.2011-3500](https://doi.org/10.2514/6.2011-3500). URL: <http://www.scopus.com/inward/record.url?eid=2-s2.0-84872373928&partnerID=tZ0tx3y1>.
- [3] ARCA. *Haas2CA*. 2017. URL: <http://www.arcaspace.com/en/haas2c.htm> (visited on 12/01/2017).
- [4] Mokhtar S. Bazaraa, Hanif D. Sherali, and C. M. Shetty. *Nonlinear Programming: Theory and Algorithms*. John Wiley & Sons, 2013.
- [5] Nazareth Bedrossian, Bastion Technologies, and Louis Nguyen Nasa. “Zero Propellant Maneuvre Flight Results For 180 Degree ISS Rotation”. In: *20th International Symposium on Space Flight Dynamics*. Annapolis, MD, 2007.
- [6] F. S. Billig. “Research on supersonic combustion”. In: *Journal of Propulsion and Power* 9.4 (1993), pp. 499–514. ISSN: 0748-4658. DOI: [10.2514/3.23652](https://doi.org/10.2514/3.23652).
- [7] Pt Boggs and Jw Tolle. “Sequential quadratic programming for large-scale nonlinear optimization”. In: *Journal of Computational and Applied Mathematics* 124.1-2 (2000), pp. 123–137. ISSN: 03770427. DOI: [10.1016/S0377-0427\(00\)00429-5](https://doi.org/10.1016/S0377-0427(00)00429-5). URL: <http://linkinghub.elsevier.com/retrieve/pii/S0377042700004295> \$ \backslash \text{newline} \$ <http://www.sciencedirect.com/science/article/pii/S0377042700004295>.
- [8] R Bulirsch et al. “Combining direct and indirect methods in optimal control: Range maximization of a hang glider”. In: *Optimal Control (Calculus of Variations, Optimal Control Theory and Numerical Methods)* 111 (1993), pp. 273–288.

REFERENCES

- [9] Dong Chai et al. “Boost-skipping trajectory optimization for air-breathing hypersonic missile”. In: *Aerospace Science and Technology* 46 (2015), pp. 506–513. ISSN: 12709638. DOI: [10.1016/j.ast.2015.09.004](https://doi.org/10.1016/j.ast.2015.09.004). URL: <http://dx.doi.org/10.1016/j.ast.2015.09.004>.
- [10] Stephen Cook and Uwe Hueter. “NASA’s Integrated Space Transportation Plan 3rd generation reusable launch vehicle technology update”. In: *Acta Astronautica* 53.4-10 (2003), pp. 719–728. ISSN: 00945765. DOI: [10.1016/S0094-5765\(03\)00113-9](https://doi.org/10.1016/S0094-5765(03)00113-9).
- [11] Edward T. Curran. “Scramjet Engines: The First Forty Years”. In: *Journal of Propulsion and Power* 17.6 (2001), pp. 1138–1148. ISSN: 0748-4658. DOI: [10.2514/2.5875](https://doi.org/10.2514/2.5875).
- [12] Christopher L. Darby, William W. Hager, and Anil V. Rao. “Direct Trajectory Optimization Using a Variable Low-Order Adaptive Pseudospectral Method”. In: *Journal of Spacecraft and Rockets* 48.3 (2011), pp. 433–445. ISSN: 0022-4650. DOI: [10.2514/1.52136](https://doi.org/10.2514/1.52136).
- [13] M. Diehl et al. “Fast direct multiple shooting algorithms for optimal robot control”. In: *Lecture Notes in Control and Information Sciences* 340 (2006), pp. 65–93. ISSN: 01708643. DOI: [10.1007/978-3-540-36119-0_4](https://doi.org/10.1007/978-3-540-36119-0_4).
- [14] F. Fahroo and I.M. Ross. “Direct trajectory optimization by a Chebyshev pseudospectral method”. In: *Proceedings of the 2000 American Control Conference*. Vol. 6. Chicago, IL, 2000, pp. 3860–3864. ISBN: 0-7803-5519-9. DOI: [10.1109/ACC.2000.876945](https://doi.org/10.1109/ACC.2000.876945).
- [15] Fariba Fahroo and I. Michael Ross. “Costate Estimation by a Legendre Pseudospectral Method”. In: *Journal of Guidance, Control, and Dynamics* 24.2 (2001), pp. 270–277. ISSN: 0731-5090. DOI: [10.2514/2.4709](https://doi.org/10.2514/2.4709).
- [16] I. Fahroo F. & Ross. “Computational Optimal Control By Spectral Collocation With Differential Inclusion ..” In: *1999 Flight Mechanics Symposium*. May. 1999, pp. 185–200.
- [17] Giorgio Fasano and Janos Pinter. *Modelling and Optimisation in Space Engineering*. New York, NY: Springer, 2013. DOI: [10.1007/978-1-4614-4469-5](https://doi.org/10.1007/978-1-4614-4469-5).
- [18] Kevin W. Flaherty, Katherine M. Andrews, and Glenn W. Liston. “Operability Benefits of Airbreathing Hypersonic Propulsion for Flexible Access to Space”. In: *Journal of Spacecraft and Rockets* 47.2 (2010), pp. 280–287. ISSN: 0022-4650. DOI: [10.2514/1.43750](https://doi.org/10.2514/1.43750). URL: <http://arc.aiaa.org/doi/abs/10.2514/1.43750>.
- [19] Sholto O. Forbes-Spyratos et al. “Trajectory Design of a Rocket-Scramjet-Rocket Multi-Stage Launch System”. In: *Journal of Spacecraft and Rockets - Under Consideration* TBD (2018).
- [20] S.O. Forbes-Spyratos et al. “Trajectory design of a rocket-scramjet-rocket multi-stage launch system”. In: *21st AIAA International Space Planes and Hypersonics Technologies Conference, Hypersonics 2017*. Xiamen, China, 2017. ISBN: 9781624104633.

- [21] Adam Gilmour. *ROCKET STARTUP SHOOTS FOR THE STARS WITH AUD 5 MILLION (USD 3 . 7 MILLION) SERIES A FUNDING*. 2017.
- [22] Qi Gong, I. Michael Ross, and Friba Fahroo. “Costate Computation by a Chebyshev Pseudospectral Method”. In: *Journal of Guidance, Control, and Dynamics* 33.2 (2010), pp. 623–628. ISSN: 0731-5090. DOI: [10.2514/1.45154](https://doi.org/10.2514/1.45154).
- [23] Barry Mark Hellman. *Comparison of Return to Launch Site Options for a Reusable Booster Stage*. Tech. rep. Space Systems Design Lab, Georgia Institute of technology, 2005, pp. 1–18.
- [24] Mark Hempsell. *SKYLON Users Manual*. Reaction Engines Limited, 2014.
- [25] Horizon. *Black Arrow 2*. 2017. URL: <http://www.horizonsas.com/products/> (visited on 12/01/2017).
- [26] Thomas Jazra, Dawid Preller, and Michael K. Smart. “Design of an Airbreathing Second Stage for a Rocket-Scramjet-Rocket Launch Vehicle”. In: *Journal of Spacecraft and Rockets* 50.2 (2013), pp. 411–422. ISSN: 0022-4650. DOI: [10.2514/1.A32381](https://doi.org/10.2514/1.A32381). URL: <http://arc.aiaa.org/doi/abs/10.2514/1.A32381>.
- [27] D. Jezewski. “An Optimal, Analytic Solution to the Linear-Gravity, Constant-Thrust Trajectory Problem”. In: *Journal of Spacecraft and Rockets* July (1971), pp. 793–796.
- [28] Scott Josselyn and I Michael Ross. “Rapid Verification Method for the Trajectory Optimization of Reentry Vehicles”. In: *Notes* 26.3 (2002), pp. 505–508. ISSN: 0731-5090. DOI: [10.2514/2.5074](https://doi.org/10.2514/2.5074).
- [29] Rl Kimmel et al. “HIFiRE-5 flight vehicle design”. In: *AIAA paper* July (2010), pp. 1–17. DOI: [10.2514/6.2010-4985](https://doi.org/10.2514/6.2010-4985). URL: <http://arc.aiaa.org/doi/pdf/10.2514/6.2010-4985>.
- [30] Heinz-Otto Kreiss and Joseph Oliger. “Comparison of accurate methods for the integration of hyperbolic equations”. In: *Tellus A* 1971 (1972). ISSN: 0280-6495. DOI: [10.3402/tellusa.v24i3.10634](https://doi.org/10.3402/tellusa.v24i3.10634).
- [31] *Kuai Zhou (Fast Vessel)*. URL: <https://chinaspacereport.com/launch-vehicles/kuaizhou/> (visited on 12/01/2017).
- [32] Markus Kuhn et al. “Innovative European Launcher Concept SMILE”. In: *21st AIAA International Space Planes and Hypersonics Technologies Conference* March (2017), pp. 1–14. DOI: [10.2514/6.2017-2441](https://doi.org/10.2514/6.2017-2441). URL: <https://arc.aiaa.org/doi/10.2514/6.2017-2441>.
- [33] Huifeng Li et al. “Footprint problem with angle of attack optimization for high lifting reentry vehicle”. In: *Chinese Journal of Aeronautics* 25.2 (2012), pp. 243–251. ISSN: 10009361. DOI: [10.1016/S1000-9361\(11\)60384-1](https://doi.org/10.1016/S1000-9361(11)60384-1). URL: [http://dx.doi.org/10.1016/S1000-9361\(11\)60384-1](http://dx.doi.org/10.1016/S1000-9361(11)60384-1).

REFERENCES

- [34] Ping Lu. “Inverse dynamics approach to trajectory optimization for an aerospace plane”. In: *Journal of Guidance, Control, and Dynamics* 16.4 (1993), pp. 726–732. ISSN: 0731-5090. DOI: [10.2514/3.21073](https://doi.org/10.2514/3.21073). URL: <http://arc.aiaa.org/doi/abs/10.2514/3.21073>.
- [35] J W Magee Bruno, T.J., Friend, D. G., Huber, M.L., Laesecke, A., Lemmon, E.W., McLinden, M.O., Perkins, R.A., Baranski, J., Widegren, J.A. *Thermophysical Properties Measurements and Models for Rocket Propellant RP-1: Phase I, NIST- IR 6644, National Institute of Standards and Technology (U.S.)* Tech. rep. 2006.
- [36] Unmeel Mehta et al. “Skylon Aerospace Plane and Its Aerodynamics and Plumes”. In: *Journal of Spacecraft and Rockets* 53.2 (2016), pp. 340–353. ISSN: 0022-4650. DOI: [10.2514/1.A33408](https://doi.org/10.2514/1.A33408). URL: <http://arc.aiaa.org/doi/10.2514/1.A33408>.
- [37] Unmeel B. Mehta and Jeffrey V. Bowles. “Two-Stage-to-Orbit Spaceplane Concept with Growth Potential”. In: *Journal of Propulsion and Power* 17.6 (2001), pp. 1149–1161. ISSN: 0748-4658. DOI: [10.2514/2.5886](https://doi.org/10.2514/2.5886).
- [38] Claas Michalik, Ralf Hannemann, and Wolfgang Marquardt. “Incremental single shooting - A robust method for the estimation of parameters in dynamical systems”. In: *Computers & Chemical Engineering* 33.7 (2009), pp. 1298–1305. ISSN: 00981354. DOI: [10.1016/j.compchemeng.2009.02.002](https://doi.org/10.1016/j.compchemeng.2009.02.002). URL: <http://linkinghub.elsevier.com/retrieve/pii/S0098135409000544>.
- [39] Nathan D. Moshman and Ronald J. Proulx. “Range Improvements in Gliding Reentry Vehicles from Thrust Capability”. In: *Journal of Spacecraft and Rockets* 51.5 (2014), pp. 1681–1694. ISSN: 0022-4650. DOI: [10.2514/1.A32764](https://doi.org/10.2514/1.A32764). URL: <http://arc.aiaa.org/doi/10.2514/1.A32764>.
- [40] J.R. Olds and I.a. Budianto. “Constant Dynamic Pressure Trajectory Simulation with POST”. In: *Aerospace Sciences Meeting & Exhibit*. Reno, NV, 1998, pp. 1–13. DOI: [10.2514/6.1998-302](https://doi.org/10.2514/6.1998-302). URL: <http://citeseerx.ist.psu.edu/viewdoc/download?doi=10.1.1.25.6506&rep=rep1&type=pdf>.
- [41] Orbital Access. *The Orbital 500R*. 2017. URL: <http://www.orbital-access.com/the-orbital-500/> (visited on 12/01/2017).
- [42] DARPA Outreach. *DARPA Picks Design for Next-Generation Spaceplane*. 2017. URL: <https://www.darpa.mil/news-events/2017-05-24> (visited on 11/16/2017).
- [43] A Paull, R.J Stalker, and D Mee. “Thrust Measurements of a Complete Axisymmetric Scramjet in an Impulse Facility”. In: *5TH INTERNATIONAL AEROSPACE PLANES AND HYPERSONICS TECHNOLOGIES CONFERENCE*. 1993.
- [44] Pointwise. *www.pointwise.com*. 2017. URL: <http://www.pointwise.com/> (visited on 02/01/2017).

- [45] Richard W. Powell et al. “Ascent performance of an air-breathing horizontal-takeoff launch vehicle”. In: 14.4 (1991), pp. 834–839. ISSN: 0731-5090. DOI: [10.2514/3.20719](https://doi.org/10.2514/3.20719).
- [46] Dawid Preller and Michael K Smart. “Longitudinal Control Strategy for Hypersonic Accelerating Vehicles”. In: *Journal of Spacecraft and Rockets* 52.3 (2015), pp. 1–6. ISSN: 0022-4650. DOI: [10.2514/1.A32934](https://doi.org/10.2514/1.A32934). URL: <http://dx.doi.org/10.2514/1.A32934>.
- [47] Dawid Preller and Michael K Smart. “Scramjets for Reusable Launch of Small Satellites”. In: *20th AIAA International Space Planes and Hypersonic Systems and Technologies Conference*. July. Glasgow, Scotland, 2015, pp. 1–23. DOI: [10.2514/6.2015-3586](https://doi.org/10.2514/6.2015-3586).
- [48] Dawid Preller and Michael K. Smart. “Scramjets for Reusable Launch of Small Satellites”. In: *Journal of Spacecraft and Rockets Advance On* (2017), pp. 1–13. ISSN: 0022-4650. DOI: [10.2514/6.2015-3586](https://doi.org/10.2514/6.2015-3586). URL: <http://arc.aiaa.org/doi/10.2514/6.2015-3586>.
- [49] Anil V. Rao et al. “Algorithm 902”. In: *ACM Transactions on Mathematical Software* 37.2 (2010), pp. 1–39. ISSN: 00983500. DOI: [10.1145/1731022.1731032](https://doi.org/10.1145/1731022.1731032).
- [50] S. Tauqueer Ul Islam Rizvi, Lin Shu He, and Da Jun Xu. “Optimal trajectory and heat load analysis of different shape lifting reentry vehicles for medium range application”. In: *Defence Technology* 11.4 (2015), pp. 350–361. ISSN: 22149147. DOI: [10.1016/j.dt.2015.06.003](https://doi.org/10.1016/j.dt.2015.06.003). URL: <http://dx.doi.org/10.1016/j.dt.2015.06.003>.
- [51] Rocket Lab. *Electron*. 2016. URL: <https://www.rocketlabusa.com/electron/> (visited on 11/30/2017).
- [52] RocketCrafters. *Intrepid-1*. 2017. URL: <http://rocketcrafters.space/products-services/intrepid-launcher-family/intrepid-1/> (visited on 12/01/2017).
- [53] Paul O Romere, David B Kanipe, and James C Youngt. “Space Shuttle Entry Aerodynamic Comparisons of Flight 1 with Preflight Predictions”. In: *Journal of Spacecraft and Rockets* (1983).
- [54] I M Ross and F Fahroo. “A direct method for solving nonsmooth optimal control problems”. In: *Proceedings of the 2002 {IFAC World Congress}* (2002).
- [55] I. Michael Ross and Fariba Fahroo. “Pseudospectral Knotting Methods for Solving Nonsmooth Optimal Control Problems”. In: *Journal of Guidance, Control, and Dynamics* 27.3 (2004), pp. 397–405. ISSN: 0731-5090. DOI: [10.2514/1.3426](https://doi.org/10.2514/1.3426).
- [56] P E Rutquist and M M Edvall. “PROPT - Matlab Optimal Control Software”. In: *Tomlab Optimization Inc* 260 (2010), pp. –.
- [57] Michael Smart. *Scramjet Inlets*. Tech. rep. 9. The University of Queensland, 2010, pp. 1–24. DOI: [10.2514/5.9781600866609.0447.0511](https://doi.org/10.2514/5.9781600866609.0447.0511).

REFERENCES

- [58] Michael K Smart and Edward G Ruf. “Free-jet testing of a {REST} scramjet at off-design conditions”. In: *Collection of Technical Papers - 25th AIAA Aerodynamic Measurement Technology and Ground Testing Conference* AIAA 2006-2955 (2006), pp. 190–201. DOI: [doi : 10.2514/6.2006-2955](https://doi.org/10.2514/6.2006-2955).
- [59] Michael K. Smart and Matthew R. Tetlow. “Orbital Delivery of Small Payloads Using Hypersonic Airbreathing Propulsion”. In: *Journal of Spacecraft and Rockets* 46.1 (2009), pp. 117–125. ISSN: 0022-4650. DOI: [10.2514/1.38784](https://doi.org/10.2514/1.38784). URL: <http://arc.aiaa.org/doi/abs/10.2514/1.38784>.
- [60] Thomas J. Sooy and Rebecca Z. Schmidt. “Aerodynamic Predictions, Comparisons, and Validations Using Missile DATCOM (97) and Aeroprediction 98 (AP98)”. In: *Journal of Spacecraft and Rockets* 42.2 (2005), pp. 257–265. ISSN: 0022-4650. DOI: [10.2514/1.7814](https://doi.org/10.2514/1.7814).
- [61] Space Exploration technologies. *Falcon 1 Launch Vehicle Payload Users Guide*. Tech. rep. Hawthorne, CA: Space Exploration Technologies, 2008, p. 65.
- [62] O. Stryk and R. Bulirsch. “Direct and indirect methods for trajectory optimization”. In: *Annals of Operations Research* 37 (1992), pp. 357–373. ISSN: 0254-5330. DOI: [10.1007 / BF02071065](https://doi.org/10.1007/BF02071065).
- [63] S. Subchan. “A Direct Multiple Shooting for the Optimal Trajectory of Missile Guidance”. In: *Proceedings of the IEEE International Conference on Control Applications* 2.4 (2008), pp. 268–273. ISSN: 1085-1992. DOI: [10.1109/CCA.2008.4629675](https://doi.org/10.1109/CCA.2008.4629675).
- [64] George Sutton and Oscar Biblarz. *Rocket propulsion Elements*. 8th. John Wiley & Sons, 2010, p. 67.
- [65] M R Tetlow et al. “Comparison of Glideback and Flyback Boosters”. In: *Journal of Spacecraft and Rockets* 38.5 (1992), pp. 752–758. ISSN: 0022-4650. DOI: [10.2514/2.3742](https://doi.org/10.2514/2.3742). URL: <http://dx.doi.org/10.2514/2.3742>.
- [66] Bailing Tian and Qun Zong. “Optimal guidance for reentry vehicles based on indirect Legendre pseudospectral method”. In: *Acta Astronautica* 68.7-8 (2011), pp. 1176–1184. ISSN: 00945765. DOI: [10.1016/j.actaastro.2010.10.010](https://doi.org/10.1016/j.actaastro.2010.10.010). URL: <http://linkinghub.elsevier.com/retrieve/pii/S0094576510003899>.
- [67] Charles Trefny. “An Air-Breathing Concept Launch Vehicle for Single-Stage-to-Orbit”. In: *35th Joing Propulsion Conference and Exhibit*. May. Los Angeles, CA, 1999.
- [68] Takeshi Tsuchiya and Takashige Mori. “Optimal Design of Two-Stage-To-Orbit Space Planes with Airbreathing Engines”. In: *Journal of Spacecraft and Rockets* 42.1 (2005), pp. 90–97. ISSN: 0022-4650. DOI: [10.2514/1.8012](https://doi.org/10.2514/1.8012).

- [69] Richard Varvill and Alan Bond. “The SKYLON Spaceplane”. In: *Journal of the British Interplanetary Society* 57.October 1995 (2004), pp. 22–32. ISSN: 0007084X.
- [70] Richard Varvill and Alan Bond. “THE SKYLON SPACEPLANE : PROGRESS TO REALISATION”. In: *Journal of the British Interplanetary Society* 61 (2008), pp. 412–418.
- [71] Vector Space. *Vector Launch Vehicle Family*. 2017. URL: <https://vectorspacesystems.com/technology/> (visited on 12/01/2017).
- [72] VirginOrbit. *LauncherOne*. 2017. URL: <https://virginorbit.com/> (visited on 11/30/2017).
- [73] Alan W. Wilhite et al. “Technology and staging effects on two-stage-to-orbit systems”. In: *Journal of Spacecraft and Rockets* 31.1 (1991), pp. 31–39. ISSN: 0022-4650. DOI: [10.2514/3.26399](https://doi.org/10.2514/3.26399).
- [74] Zero2Infinity. *Bloostar*. 2016. URL: <http://www.zero2infinity.space/bloostar/> (visited on 11/30/2017).
- [75] Jiang Zhao and Rui Zhou. “Reentry trajectory optimization for hypersonic vehicle satisfying complex constraints”. In: *Chinese Journal of Aeronautics* 26.6 (2013), pp. 1544–1553. ISSN: 10009361. DOI: [10.1016/j.cja.2013.10.009](https://doi.org/10.1016/j.cja.2013.10.009). URL: <http://dx.doi.org/10.1016/j.cja.2013.10.009>.

APPENDIX A

CART3D RESULTS

A.1 Engine-On Plume Check

-simulate engine-on conditions to check that the plumes do not adversely affect the tail of the vehicle
(justify that I can just remove engines/boattail)

-Mach 5,7,9 at 50kPa

A.2 CART3D Results

-include mesh here

APPENDIX A. CART3D RESULTS

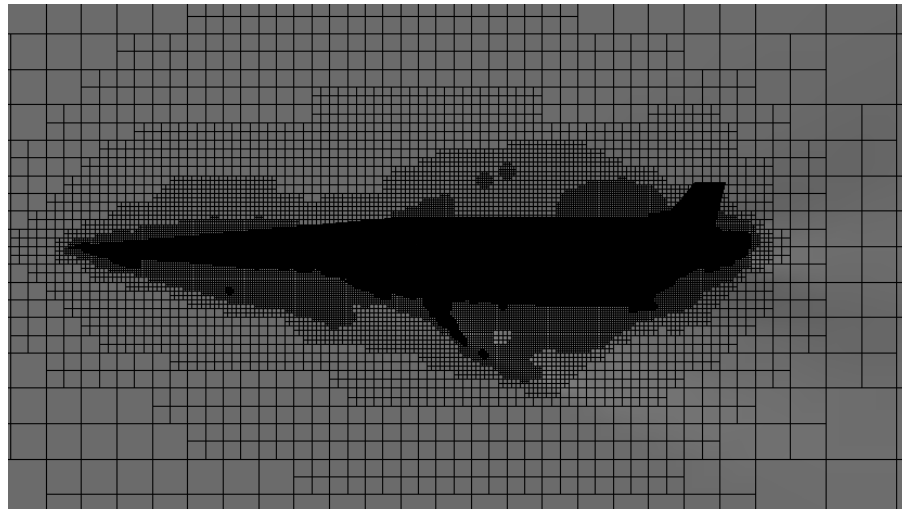


Figure A.1

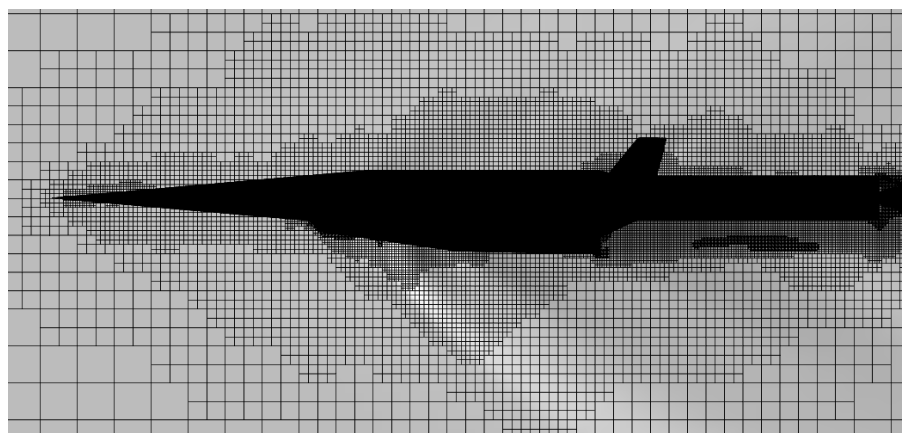


Figure A.2: Mesh generated by CART3D around the SPARTAN and first stage vehicles.